Cellular Interrogation of Neurovascular Coupling: The Role of Cortical Inhibitory Interneurons

Llywelyn Lee

Department of Psychology

A thesis submitted for the degree of Doctor of Philosophy (PhD)

August 2025

Abstract

Neurovascular coupling (NVC) ensures that cerebral blood flow (CBF) is precisely matched to local neuronal activity, supporting the brain's high metabolic demand. While excitatory neurons have long been the focus of NVC research, inhibitory cortical interneurons (INs) have emerged as important, and underexplored, contributors to the regulation of cerebral haemodynamics. This thesis investigates the cellular mechanisms through which two populations of INs, somatostatin-expressing (SST) and neuronal nitric oxide synthase-expressing (nNOS), contribute to NVC, using a cell-type-specific optogenetic stimulation with high-resolution measurements of vascular and neuronal responses, and pharmacological agents.

I demonstrated that both SST and nNOS-IN activation drive an increase in cerebral blood volume (CBV), and that while the nNOS-IN driven increase in CBV was dependent on nitric oxide (NO), the initial sensory-evoked NVC response was not.

Together, these studies provide novel insights into the contributions of subpopulations of INs to NVC, highlighting the diversity of mechanisms by which they influence cerebrovascular dynamics. These findings advance our understanding of the neurovascular unit and lay the groundwork for more precise models of NVC in health and disease.

Table of Contents

Declaration

I, Llywelyn Lee, declare that the work presented in this thesis is my own. The work has not been previously submitted for the award of a higher degree at this, or any other, University.

This thesis is in a publication format, with the two experimental chapters having previously been published in academic journals:

1) **Chapter 1** has not previously been published and was written up for this PhD thesis
2) **Chapter 2** has not previously been published and was written up for this PhD thesis
3) **Chapter 3** this paper was published in November 2019 in Cerebral Cortex:

Lee, L., Boorman, L., Glendenning, E., Christmas, C., Sharp, P., Redgrave, P., Shabir, O., Bracci, E., Berwick, J., & Howarth, C. (2020). Key Aspects of Neurovascular Control Mediated by Specific Populations of Inhibitory Cortical Interneurons. Cerebral Cortex, 30(4), 2452–2464.

4) **Chapter 4** this paper was published in June 2025 in Neurophotonics:

Lee, L., Boorman, L., Glendenning, E., Shen, C., Berwick, J., & Howarth, C. (2025). Nitric oxide is not responsible for initial sensory-induced neurovascular coupling response in the barrel cortex of lightly anesthetized mice. Neurophotonics, 12(S2), S22802.

5) **Chapter 5** has not previously been published and was written up for this PhD thesis

At the beginning of each experimental chapter (Chapters 3 and 4) author contributions are clearly defined.

Acknowledgements

Firstly, I'd like to thank my amazing and patient supervisors. Clare, you took a chance hiring me when I was just a trainee technician in the lab- I hope it has paid off for you as much as it has for me. Without your constant training, mentorship and guidance, I would never have been able to complete this PhD, nor become the scientist I am today. Jason, your constant enthusiasm and passion for neurovascular coupling is truly unmatched, your excitement over data (even/ particularly a N of 1) is infectious and has kept me motivated throughout my PhD. Together, you make the perfect combination of supervisors. You have created an incredible lab environment where everyone is empowered to contribute to the research and discussions, in a culture that is based on friendship and respect, as well as scientific endeavour. You gave me the freedom and confidence to run my own experiments and were always there to support me along the way.

To the many members, past and present, of the Sheffield Neurovascular Lab- this experience would not have been the same without you. A special mention firstly has to go to the post docs when I started my PhD (Luke, Paul and Sam). You dedicated time to teach me, which I have come to value even more now that I know how little time you have to spare as a post doc! Osman, we started our PhD journeys on the same day 8 years ago. Since that day, you have been a great friend. We have celebrated the highs and lows of research together, and I can always rely on you to put things into perspective when experiments go wrong with a trusty 'it is what it is'. To everyone else in the lab who has helped along the way, thank you for making the last 8 years so fun.

A special mention has to go to Hallamshire Rugby Club. When I came to Sheffield 10 years ago I knew no one, but through many training sessions, matches, socials and questionable drinks, I truly feel like Hallamshire has become my second family.

To my (actual) family, your love and support have been enduring through all my 31 years. Carwyn and Jess, I thank you for always pushing me – while in our childhoods academic rivalry was what drove us, it has now matured into encouragement (with just a little competition remaining). Mum and Dad, I will never be able to thank you enough for the sacrifices you have made for me. You have always encouraged me to pursue excellence throughout my life and have supported and loved me every step of the way. I truly wouldn't be where I am today without you.

Finally, the biggest thank you goes to Sonia. When we started dating, I told you I was almost a doctor like you, well 6 years later I almost am! You have been amazing through this whole process, putting up with my late nights in the lab or writing, and encouraging me through the best and most difficult of times. You never stopped believing in me, and it is that belief that

has enabled me to complete my PhD. I will be forever grateful for the support you have given me, listening to me whinge when things go wrong and pretending to be interested when I show you exciting data.

I want to finish by mentioning a saying my Dad used to quote growing up ‘The roots of education are bitter, but the fruits are sweet’. I can honestly say that, while there were hard times, the fruits are indeed sweet as I have loved the last 8 years: working in an incredible lab, meeting amazing, passionate people and travelling the world; and hope to continue reaping the sweet fruit as long as I can.

List of Abbreviations

2D-OIS: Two- dimensional optical imaging spectroscopy

5HT: 5-hydroxytryptamine (Serotonin)

5HT3aR: 5-hydroxytryptamine (serotonin) receptor 3a

7-NI: 7-Nitroindazole

20-HETE: 20-hydroxyeicosatetraenoic acid

AA: Arachidonic Acid

Aβ: Amyloid-β

AD: Alzheimer's Disease

ATP: Adenosine Triphosphate

BBB: Blood-Brain Barrier

BK: Potassium channels

BOLD: Blood Oxygenation Level-Dependent

BOLD MRI: Blood Oxygenation Level-Dependent Functional Magnetic Resonance Imaging

[Ca2+]i: Intracellular Calcium Ion Concentrations

CaMKIIα: Calcium/calmodulin-dependent protein kinase II alpha

CBF: Cerebral Blood Flow

CBV: Cerebral Blood Volume

CCK: Cholecystokinin

cGMP: Cyclic Guanosine Monophosphate

ChR2: Channelrhodopsin-2

COX-2: Cyclooxygenase-2

DREADDs: Designer Receptors Exclusively Activated by Designer Drugs

EETs: Epoxyeicosatrienoic Acids

eNOS: Endothelial Nitric Oxide Synthase

fMRI: Functional Magnetic Resonance Imaging

fNIRS: Functional Near-Infrared Spectroscopy

GABA: γ-aminobutyric acid

GECIs: Genetically Encoded Calcium Indicators

Hbo: Oxygenated Haemoglobin

Hbr: Deoxygenated or Reduced Haemoglobin

Hbt: Total Haemoglobin

iNOS: Inducible Nitric Oxide Synthase

INs: Interneurons

KIR: Inward-Rectifier Potassium (channels)

LDF: Laser Doppler Flowmetry

LED: Light-Emitting Diode

LFP: Local Field Potential

L-NAME: NG-Nitro-L-arginine methyl ester

L-NNA: Nω-nitro-L-arginine

L-NMMA: NG-Methyl-L-arginine

LSCI: Laser Speckle Contrast Imaging

mGluRs: Metabotropic Glutamate Receptors

MRI: Magnetic Resonance Imaging

MUA: Multi-Unit Activity

NFTs: Neurofibrillary Tangles

NMR: Nuclear Magnetic Resonance

NMDA: N-methyl-D-aspartate

nNOS: Neuronal Nitric Oxide Synthase

NO: Nitric Oxide

NOS: Nitric Oxide Synthase

NPY: Neuropeptide-Y

NVC: Neurovascular Coupling

NVU: Neurovascular Unit

PCR: Polymerase Chain Reaction

PET: Positron Emission Tomography

PGE2: Prostaglandin E2

PV: Parvalbumin

RBCs: Red Blood Cells

sGC: Soluble Guanylyl Cyclase

SNAP: S-nitroso-N-acetylpenicillamine

SST: Somatostatin

VDCCs: Voltage-Dependent Calcium Channels

VGAT: Vesicular GABA Transporter

VIP: Vasoactive Intestinal Peptide

VSMCs: Vascular Smooth Muscle Cells

Chapter 1: Introduction

1.1 Neurovascular Coupling

Despite comprising only approximately 2% of total body mass, the human brain consumes up to 20% of the body's oxygen at rest (Harris, Jolivet, & Attwell, 2012), with an exceptionally high metabolic demand, requiring ~2,000 ATP molecules to transmit a single signal across a synapse (Attwell & Lauglin, 2001). Yet the brain has only a limited ability to store oxygen and the metabolites required to produce energy. To account for this incongruity of high demand and low supply neural activity in the brain is tightly coupled to increases in local blood supply, this process is termed neurovascular coupling (NVC). NVC ensures the delivery of oxygen and glucose to areas of increased neural activity, and the clearance of waste products such as carbon dioxide and excess heat. This tight coupling between neural activity and cerebral blood flow (CBF) is essential for normal brain function, so much so that even short periods of ischemia in the brain can lead to neural damage or death (Purves et al., 2001).

Not only is NVC important for keeping the brain functioning, it is also the basis of many modern human neuroimaging techniques, such as blood oxygenation level-dependent functional magnetic resonance imaging (BOLD fMRI). BOLD fMRI relies on detecting changes in the concentration of deoxygenated haemoglobin, caused by differing local blood volume, to infer corresponding neural activity (Ogawa, 1992). As BOLD fMRI and other imaging modalities, such as functional near-infrared spectroscopy (fNIRS) and positron emission tomography (PET), rely on haemodynamic responses to reflect neural activity, interpreting them correctly requires knowing how neurons, and other cell types, are coupled with vascular responses, and more importantly how different conditions can affect this coupling. Thus, the extensive use of these brain imaging techniques emphasises the importance of elucidating the cellular mechanisms which underlie NVC, to aid in their interpretation.

There is a growing body of evidence that NVC is significantly impaired in a range of neurological disorders, including Alzheimer’s disease, stroke, epilepsy and other neurodegenerative and cerebrovascular conditions (Schwartz., 2007; Kisler et al., 2017; Iadecola, 2017). These dysfunctions in NVC are characterised by a breakdown in the relationship between neuronal activity and CBF, leading to insufficient metabolic supply, exacerbation of neuronal damage, and progression of disease pathology (Kisler et al., 2017; Hinzman et al., 2014; Nortley et al., 2019). This highlights the importance of investigating the cellular and molecular mechanisms underlying NVC, to discover how these mechanisms are disrupted in these disorders and to identify potential targets for therapeutic interventions, aimed at restoring neurovascular function and improving disease prognosis.

Despite the importance of understanding NVC, the exact cellular and molecular mechanisms underlying this process are yet to be fully understood. However, there has been considerable

research focusing on the pathways and cellular interactions underpinning NVC and how they become dysfunctional in disease. In this chapter I will critically examine the current theories and hypothesised molecular pathways involved in NVC, and assess the seminal studies and techniques that have contributed to our current understanding.

1.1.1 Brief History of NVC

Up until the late 19th century blood flow in the brain was assumed to work like most other organs, with control stemming exclusively from systemic circulation (Friedland and Iadecola, 1991). However, between 1880 and 1890 two studies were published that hinted at local regulation of blood flow in the brain. The first of these by Angelo Mosso utilised a “human circulation balance”, where subjects would lie on a precisely balanced table and be presented with varying stimuli (Mosso, 1880). He observed that cognitive and emotional tasks caused the table to tip towards the head, suggesting that brain activity was triggering a redistribution of blood to the brain. The second study of these studies investigated the local control of CBF by injecting metabolic by-products from the brain into the carotid arteries of dogs, cats and mice (Roy and Sherrington, 1890). The resulting increase in intracranial pressure, which they used as an indirect measure of cerebral blood volume, led them to conclude that these metabolic agents were controlling local blood flow. These studies led to the establishment of the Roy-Sherrington hypothesis, which posits that the metabolic by-products produced by neural activity diffuse onto the walls of blood vessels, causing vasodilation which increases local blood flow.

The Roy-Sherrington hypothesis reflects a feedback mechanism of NVC, wherein the primary trigger for vasodilation is the metabolic consequence of neural activity, rather than the activity itself. The vasodilation leads to an increase in CBF that both replenishes the consumed energy substrates and clears the metabolic by-products, with the vasodilatory stimulus ceasing once baseline levels of these are restored. This reactive model of NVC is supported by studies showing isolated metabolic by-products, such as elevated carbon dioxide (Kety, 1950) and adenosine (Ko et al., 1990) or decreased oxygen levels (Kety and Schmidt, 1948) are vasodilatory. The Roy-Sherrington hypothesis was widely accepted in the field for over a century, before technological advancements offering more temporally and spatially accurate recording of both CBF and neural activity, led to a re-evaluation of this feedback theory of NVC.

1.1.2 Advancements in the understanding and mechanisms of NVC

Up until the middle of the 20th century the majority of methods for assessing changes in CBF relied on surrogate measures of blood volume and did not have sufficient temporal or spatial resolution to show NVC occurring in specific brain regions. But with the development of

radiographic techniques, using diffusible radioactive tracers to quantitatively measure CBF in multiple brain regions, researchers were able to show in cat (Landau et al., 1955) and human (Lassen et al., 1963) brains that neural activity evokes local CBF changes that are specific to the active region. What's more, these radiographic techniques combined with the development of MRI, led to the discovery of the BOLD-fMRI signal (Ogawa and Lee, 1990), and so the ability to monitor CBF in humans with higher spatial and temporal resolution.

In the use of BOLD-fMRI, there is an implicit acceptance that neural activity and CBF are coupled (through NVC). So, as this technique became adopted as a primary tool in clinical and research settings, interest increased in exactly how NVC is driven. A deeper understanding of the mechanisms underlying NVC is crucial for accurate and robust interpretation of BOLD-fMRI signals, given that the relationship between neural activity and haemodynamic responses are not always aligned, for example in disease states (Tarantini et al., 2017; Girouard and Iadecola., 2006) or in the case of the 'initial dip' (an early decrease in oxygenated haemoglobin observed immediately after neural activation [Malonek and Grinvald, 1996]). Consequently, research into NVC began to increase exponentially, this lead to new theories being developed and doubt being cast on the Roy-Sherrington hypothesis.

Around the turn of the millennium two studies refuted the Roy-Sherrington hypothesis, by using manipulation of baseline levels of glucose and oxygen, to show that neither metabolic substrate is responsible for directly regulating NVC. The first of these studies used intravenous insulin to lower blood glucose levels in humans and, using PET, found that even a large drop in glucose had no effect on the increase in CBF elicited by tactile stimulation (Powers et al., 1996). Similarly, in the second of these studies it was shown that inducing hypoxia in humans didn't affect the CBF changes, induced by a visual stimulus, indicating localised oxygen requirements don't regulate NVC (Mintun et al., 2001). Following the Roy-Sherrington hypothesis of NVC, if CBF is regulated by a feedback mechanism centred around replenishing decreases in energy substrates such as glucose or oxygen, one would hypothesise that with levels of these substrates reduced in the blood, the CBF increase in NVC would be much larger in size, compared to standard conditions, in order to replenish the supply to normal baseline levels. Collectively, these studies suggest that this doesn't occur, and so drops in glucose or oxygen, resulting from increased neural metabolism, are unlikely to be wholly responsible for driving NVC. Studies such as these cast doubt over the classical Roy-Sherrington feedback hypothesis of NVC. This doubt has prompted the development of many alternative models seeking to explain the relationship between CBF and neural activity, the majority of which rely on feedforward mechanisms of regulation independent of metabolic demand.

Contemporary theories of NVC are based on feedforward mechanisms, where increases in CBF are triggered directly by the by-products of neural activity. These mechanisms are faster acting than those predicted by feedback mechanisms, as they involve the direct release of vasodilatory molecules onto the vasculature, either from active neurons or through intermediary cells. As the release of these molecules is driven by the neural activity itself, rather than the metabolic by-products, they go much further in explaining the rapid timing and excessive size of the haemodynamic response seen in NVC (Attwell et al., 2010).

Current feedforward mechanisms of NVC all implicate the involvement of one or more of three major cell types integral for the NVC response, these are: glial cells (astrocytes and microglia), vascular cells (endothelial cells, pericytes and vascular smooth muscle cells) and neural cells (glutamatergic and γ-aminobutyric acid [GABA] neurons). Together these cells form the neurovascular unit (NVU), which is the functional unit through which NVC occurs, with each component capable of detecting increases in neural activity and releasing vasodilatory molecules to modulate local CBF (Iadecola, 2004). Therefore, to fully understand these current models of NVC requires a detailed examination of the specific roles of the cellular components of the NVU, and their mechanisms for driving CBF changes.

1.2 Cellular Mechanisms of NVC

As the functional unit of NVC the components of the NVU (glia, vascular cells and neurons) work together to facilitate both the initiation and execution of the haemodynamic response to neural activity. The concept of the NVU is relatively recent, being first described in 2001 (Iadecola, 2001), yet it has become an integral part of all contemporary models of NVC. Beyond its role in mediating NVC, the NVU also is responsible for the maintenance of the blood-brain barrier (BBB), a selectively permeable barrier protecting the brain from toxins, red blood cells and leukocytes in the bloodstream (Zlokovic, 2008). While this is an important function of the NVU, it is beyond the scope of the work in this thesis and won't be discussed further.

The basic sequence of events in feedforward models of NVC are neural activity leading to the release of neurotransmitters, such as glutamate and GABA, these transmitters then cause the release of vasoactive molecules onto blood vessels, through intermediary processes, causing vasodilation. The intermediary step in this process involves the cells of the NVU, and understanding the interplay between these is essential for a complete model of NVC.

1.2.1 Glutamatergic Neurons

Neural activity is the fundamental trigger for NVC, but a central question is to what degree do neurons directly orchestrate the vascular response. Glutamatergic neurons are the principal excitatory neurons in the brain, making up approximately 70-80% of cortical neurons (Nieuwenhuys, 1994) and 80-90% of the neurons in the hippocampus (Somogyi et al., 1998). Activity in these neurons triggers the release of glutamate from synaptic terminals (Zonta et al., 2003), along with other molecules such as ATP and potassium, which are known to elicit vasodilatory responses (Toth et al., 2015; Longden et al., 2017). A significant focus of research into NVC has sought to uncover the precise pathways through which glutamatergic neurons drive changes in CBF, whether by acting directly on vascular cells or through other cells within the NVU.

Early *in vivo* studies supported the hypothesis that glutamate could act directly on local vasculature to mediate NVC. For example, topical application of glutamate to the cortex was shown to induce a dose-dependent dilation of the overlying pial arterioles (Busija and Leffler, 1989). Coupled with evidence that nearly every glutamatergic neuron in the brain lies in close proximity to a blood vessel (Zlokovic, 2008), studies such as these inferred that glutamate release was directly triggering dilations in local blood vessels. However, this interpretation is complicated by the fact that these early studies only demonstrate the causal effect of glutamate administration on vessel diameter, allowing for the possibility that other intermediaries could be enacting the response. This idea was highlighted in the same study

by Busija and Leffler (1989), where they showed that the glutamate-induced vasodilation was abolished by inhibition of nitric oxide synthase (NOS), supporting the idea that glutamate was inducing a dilation through the release of nitric oxide (NO) by NOS. Consequently, it is now widely accepted that glutamate mediates vascular responses indirectly, through feedforward mechanisms involving intermediary cells and signalling pathways (Attwell et al., 2010).

During synaptic activity, glutamate released from excitatory neurons activates both mGluRs on astrocytes and N-methyl-D-aspartate (NMDA) receptors on postsynaptic neurons, in both cases leading to elevations in intracellular calcium ion concentrations ($[Ca^{2+}]_i$) (Zonta et al., 2003; Lecrux et al., 2011; Stobart et al., 2018). In astrocytes, increased Ca^{2+} stimulates the production of arachidonic acid (AA), which in turn is metabolised into an array of dilatory compounds (Takano et al., 2006) (see section 1.2.2 for more details on astrocyte mediated vasodilations). In neurons the increase in Ca^{2+} promotes cyclooxygenase-2 (COX-2) activity, triggering the release of the vasodilator prostaglandin E_2 (PGE_2) (Lacroix et al., 2015). Evidence for this neuronal COX-2-dependent pathway has been demonstrated *in vivo*, for example pharmacological blockade of NMDA receptors in rat cortex was shown to decrease the CBF response to whisker stimulation by ~37%, while COX-2 inhibition led to a ~50% reduction (Lecrux et al., 2011). Similarly supporting this pathway, it was shown that NVC was significantly impaired in COX-2 knockout mice (Niwa et al., 2000), further underlining the importance of glutamate neurons in mediating NVC.

As alluded to earlier, glutamatergic activation of neurons has been shown to induce the release of the potent vasodilator NO. This is primarily through the activity of NOS expressed in specific cortical interneurons (INs). Multiple studies have demonstrated that NMDA induced vasodilation is reduced with pharmacological inhibition of NOS (Busija and Leffler, 1989; Faraci and Breese., 1993; Fergus and Lee, 1997b; Rancillac et al., 2006). This occurs as the NMDA receptors in INs are both physically and functionally coupled with NOS, enabling NMDA activation-induced Ca^{2+} influxes to directly stimulate NOS, promoting NO production (Lourenco et al., 2014). More detail on the release of NO by NOS INs and their role in NVC is provided in section 1.3.5. These findings support a model for NVC whereby glutamate released during neural activity activates secondary cells, such as astrocytes and INs, leading to the synthesis and release of vasodilators, which then act directly on proximal blood vessels to elicit vasodilation.

Another pathway through which glutamate release causes vasodilations is through the release of potassium ions from astrocytes. A study using patch-clamping in *ex vivo* brain slices, demonstrated that glutamate-driven Ca^{2+} increases in astrocytes opens their potassium (BK) channels, leading to a release of potassium ions into the perivascular space (Girouard et al., 2010). In that study, they also observed that pharmacological blockade of the BK channels

reduced the dilation induced by both neural stimulation and astrocyte Ca^{2+} uncaging, showing that these BK channels are an essential step in this pathway. The mechanism by which the potassium ions drive vasodilation was later revealed, using *in vivo* 2-photon microscopy. After application of potassium ions onto capillaries, voltage-sensitive dyes were used to visualise a rapid, retrograde electrical signal that propagated along the endothelium to upstream arterioles, causing them to dilate (Longden et al., 2017). As will be discussed further in section 1.2.3, this backwards propagation provides the mechanism for how local potassium release onto capillaries drives vasodilation in upstream arteries. Together, these studies support a model of glutamate-induced NVC that is orchestrated through an astrocyte-to-endothelium signalling cascade.

Research into glutamatergic neuron-mediated NVC has, until recently, primarily employed pharmacological methods to dissect its underlying mechanisms. However, recent studies have utilised newer, more advanced techniques to investigate this mechanism. One such technique is optogenetics, which enables precise temporal and spatial control of specific cellular populations through targeted expression of channelrhodopsin-2 (ChR2), (see section 1.4.6 for more details on this methodology). Optogenetic stimulation of glutamatergic neurons has been shown to induce robust, positive BOLD responses (Lee et al., 2010; Kahn et al., 2013) and CBF increases (Iordanova et al., 2015) that are similar in magnitude and timing to sensory stimulation-evoked NVC, demonstrating that the activation of these neurons can evoke the haemodynamic responses seen in NVC.

Together, these findings support a model of NVC in which the activity of excitatory neurons leads to the release of glutamate, triggering a cascade of activity that incorporates intermediary cells and results in the release of vasoactive molecules, inducing vasodilation. However, pharmacological blockade of glutamate activity doesn't completely abolish NVC (Petzold et al., 2008; Busija et al., 2007), indicating that glutamatergic neurons aren't the sole mediators of this response. Therefore, to completely understand how NVC occurs, it is important to look in more detail at the contributions of the other cell types within the NVU.

1.2.2 Astrocytes

Astrocytes, the most abundant type of glial cells in the brain, are perfectly placed to mediate NVC. Their processes ensheathe synapses and form specialised terminal end-feet covering approximately 99% of the cerebral vasculature (Mathiisen et al., 2010), placing them at the interface between neural activity and vascular responses.

The model of astrocyte mediated NVC involves astrocytic Ca^{2+} signalling, triggering the release of vasoactive molecules. Zonta et al. (2003) showed that synaptic glutamate activates astrocytic metabotropic glutamate receptors (mGluRs), elevating intracellular Ca^{2+} triggering

the release of arachidonic acid (AA) derivatives at astrocytic end-feet. These metabolites, such as PGE_2 and epoxyeicosatrienoic acids (EETs), relax vascular smooth muscle cells (Harder et al., 1998; Takano et al., 2006; Mishra et al., 2016), while AA can also be converted to 20-hydroxyeicosatetraenoic acid (20-HETE), causing vasoconstriction (Gebremedhin et al., 2000; Gonzalez-Fernandez et al., 2020). This evidence portrays a model of astrocyte mediated NVC whereby neural activity leads to Ca^{2+} elevations in astrocytes, triggering the release of these vasoactive AA metabolites, causing vascular changes. Subsequent studies expanded this model to include Ca^{2+}-activated BK channels in astrocytic end feet that, when activated, release potassium ions onto local endothelial cells, causing backwards propagation to upstream arterioles (Longden et al., 2017) and vascular smooth muscle cells (VSMCs), causing them to relax and dilate the vessels (Filosa et al., 2006). An alternative pathway of astrocyte mediated NVC, that isn't initiated by glutamate release is ATP-mediated Ca^{2+} signalling (Metea & Newman, 2006; Sun et al., 2013; Wells et al., 2015), which may act in parallel with, or compensate for, glutamate activation of astrocytes in varying conditions.

Despite this compelling model of NVC, there is controversy surrounding astrocyte involvement. 2-photon imaging studies reported that astrocytic Ca^{2+} transients often lag behind the rapid onset of NVC (Wang et al., 2006; Petzold et al., 2008; Tran et al., 2018), and that NVC was preserved in genetic knockout mice that lack the primary mechanism of astrocytic calcium increases (Nizar et al., 2013; Takata et al., 2013). Further doubt was cast on astrocyte-mediated NVC in a pioneering study that used DREADDs (designer receptors exclusively activated by designer drugs) to selectively stimulate astrocyte Ca^{2+} signalling, showing this did not alter basal CBF in awake mice (Bonder and McCarthy., 2014). However, later studies contradicted these findings with the use of genetically encoded calcium indicators (GECIs), selectively expressed in astrocytes, to detect the Ca^{2+} signals more precisely. These studies cast doubt on the validity of the earlier knockout models by showing that Ca^{2+} signals were still preserved in the distal processes of astrocytes, even when they were absent in the cell body (Srinivasan et al., 2015; Agarwal et al., 2017). This finding challenged the assumption that these knockout mice represented a complete loss of astrocyte Ca^{2+} signalling, hence they could still be driving NVC. The use of GECIs has also allowed for the demonstration that astrocytic Ca^{2+} increases are quick enough to be driving NVC, with astrocytic Ca^{2+} increases observed before stimulation-induced vasodilation (Otsu et al., 2015; Lind et al., 2018). These contradictory findings in the field underscore the importance of employing experimental techniques with high spatial and temporal resolution, given that the signalling events involved in NVC pathways are often rapid and highly localised, meaning they are susceptible to being overlooked by methods with insufficient resolution.

Astrocytes are now widely accepted as important contributors to NVC, capable of translating neuronal activity into vascular responses through multiple mechanisms. However, they do not directly alter vessel diameter, instead they communicate with the vascular cells that implement the haemodynamic response. Understanding the roles of the vascular components is therefore imperative for building a complete picture of NVC.

1.2.3 Vascular Cells

Vascular cells are the component of the NVU that implement vascular responses, translating neuronal and glial signalling into changes in vessel diameter and blood flow (Iadecola., 2017). There are three main vascular cell types that are associated with NVC: endothelial cells, VSMCs, and pericytes. Their distribution varies along the vascular tree: all blood vessels contain an endothelial layer, VSMCs mainly wrap around arteries and arterioles, and pericytes are located along capillaries. Collectively, they maintain basal tone and execute dilation or constriction in response to innervation from the other cells within the NVU, and from signals propagated along the vascular network itself (Chen et al., 2014).

Endothelial cells form the luminal lining of vessels and are key regulators of vascular tone and blood-brain barrier function. They contribute to CBF regulation by releasing vasodilators (e.g. NO) and constrictors (e.g. thromboxane postanoids) in response to shear stress (Vanhoutte & Tang, 2008; Vanhoutte, 2009), and to NVC by propagating vasodilation along the vascular network (Chen et al., 2014; Longden et al., 2017). This propagation ensures coordinated upstream and downstream haemodynamic responses, preventing inefficient blood flow redistribution. Two mechanisms have been identified for the propagation of vasodilation along blood vessels: a fast pathway, where extracellular potassium ions released during neural activity activate endothelial inward-rectifier potassium (KIR) channels, producing hyperpolarisation that travels rapidly via gap junctions to upstream arterioles (Filosa, 2017; Longden et al., 2017), and a slower pathway, where acetylcholine-induced Ca^{2+} waves spread along the endothelium and cause the release of vasoactive mediators, such as NO, from endothelial cells onto VSMCs, leading to dilation (Tallini et al., 2007; Zuccolo et al., 2017). Due to the difference in speed of these two pathways, it could be that they operate in parallel, where the fast or slow components are differentially recruited, depending on the size and duration of neural responses.

VSMCs are contractile cells that primarily wrap around the vessel walls of arteries and arterioles, and they are the primary effectors of NVC (Nelson et al., 1990; Iadecola, 2017). The release of vasoactive molecules causes changes in the membrane potential of VSMCs, which are translated into vascular responses by opening or closing voltage-dependent calcium channels (VDCCs), with depolarisation promoting vasoconstriction and hyperpolarisation

promoting vasodilation (Longden et al., 2011; Lui and Khalil., 2019). An example of a vasoactive molecule working through VSMCs is NO. NO inhibits VDCCs by promoting the production of cyclic guanosine monophosphate (cGMP), which not only closes VDCCs but also generates hyperpolarisation through potassium channel activation (Denninger and Marletta, 1999; Yang et al., 2007; Harraz et al., 2014). This NO-cGMP driven inhibition of VDCCs and hyperpolarisation leads to a fall in intracellular Ca^{2+} in VSMCs, causing them to relax and dilate the vessels (Yu et al., 2002). VSMCs also maintain baseline tone through the myogenic response, adjusting to changes in intravascular pressure to stabilise cerebral blood flow (Koller & Toth, 2012).

Pericytes, contractile mural cells embedded within the basement membrane along capillaries, have been proposed to initiate NVC by regulating capillary diameter. The first direct evidence that pericytes can actively alter the diameter of capillaries came from rat brain slices, where application of neurotransmitters was shown to cause pericytes to contract or relax, narrowing or dilating capillaries respectively (Peppiatt et al., 2006). *In vivo* 2-photon imaging studies extended these findings, showing that pericytes dilate capillaries in response to sensory stimulation, and importantly these dilations preceded arteriolar changes, suggesting pericytes may act on neuronal activity earlier than upstream vessels (Hall et al., 2014; Mishra et al., 2016; Cai et al., 2018). Despite these findings, the role of pericytes in NVC is controversial. The controversy stems from questions over whether pericyte-mediated dilations are too slow to mediate NVC (Hartmann et al., 2021), whether dilations in capillaries are sufficient to account for the large CBF changes in NVC (Hill et al., 2015; Fernandez-Klett et al., 2010) and even over the definition of pericytes versus VSMCs (Mazzoni et al., 2015; Attwell et al., 2016). Similar to the debate over the role of astrocytes in NVC, some of the conflicting findings in pericyte research can be attributed to the resolution of experimental techniques employed, as pericytes and the capillaries they act on are small, and their signalling pathways are difficult to detect (Grant et al., 2017; Brown et al., 2019). To address this issue of resolution, more recent studies have used optogenetics to show that specific activation of pericytes constricts capillaries sufficiently to drive CBF changes (Nelson et al., 2020; Ivanova et al., 2020; Hartmann et al., 2018, 2021). While others have used loss-of-function pericyte-deficient mice to show that loss of pericytes results in a reduction in NVC-driven haemodynamic responses (Kisler et al., 2017). Through the use of these higher resolution and cell-specific methodologies, accumulating evidence supports a role for pericytes in mediating NVC at the capillary level. Focus has now turned to uncovering the contributions of the different pericyte subpopulations to NVC, the existence of which may be accountable for the difficulty in establishing a clear definition of pericytes (Kisler et al., 2017).

Despite the controversies, there is consensus in the field that vascular cells, whether endothelial, VSMCs or pericytes, work with the other cells of the NVU, through various pathways, to produce the haemodynamic changes seen in NVC (Attwell et al., 2010).

So far, the pathways I have described rely mainly on the activity of glutamatergic neurons as the primary type of neuron involved in NVC, and much of the research in the field reflects this focus on excitatory neurons. However, within the NVU there is another type of neuron, inhibitory GABAergic INs, that until recently were largely overlooked in terms of their contribution to NVC. But given that these INs have been shown to release a large array of vasoactive neurotransmitters (Cauli and Hamel., 2010) and have projections onto both local blood vessels and astrocytes (Vaucher et al., 2000), they are ideally positioned to mediate CBF in response to neural activity.

1.3 GABAergic INs

Inhibitory INs make up approximately 25% of the population of neurons in the cortex and they all express the neurotransmitter GABA (Markram et al., 2004). These cortical GABAergic INs are primarily known for their role in shaping and modulating neuronal circuits, enabling the brain to carry out complex higher-order functions such as decision making, attention and sensory integrations (Kelsom and Lu, 2013). However, emerging evidence suggests that their function extends beyond controlling neural pathways. Within the NVU, GABAergic INs have been shown to be uniquely positioned to influence CBF: they are enriched with vasoactive molecules and often have close anatomical and functional associations with cerebral blood vessels (Vaucher et al., 2000) and astrocytic processes (Kang et al., 1998). Owing to these traits, INs have been hypothesised to serve as key cellular drivers of NVC, playing a critical role in translating neural activity into haemodynamic responses.

Early evidence hinting that GABAergic INs are involved in NVC emerged from studies examining their close proximity to cerebral vasculature. Using electron microscopy in rat brain slices, it was demonstrated that GABAergic INs form synaptic terminals that interact directly with the microvascular bed (Vaucher et al., 2000). This close association with blood vessels in the brain means GABAergic INs are ideally placed to detect local synaptic activity and drive corresponding haemodynamic changes through these terminals on nearby vessels.

While the proximity of GABAergic INs to cortical blood vessels suggests a potential role in NVC, functional studies are required to establish their contribution. Early investigations employed pharmacological approaches alongside high-resolution imaging to assess this

relationship. In rat cortical brain slices, application of muscimol (a GABA receptor agonist) was shown to induce vasodilation of arterioles (Fergus and Lee, 1997). Although this study implicated GABAergic signalling in haemodynamic modulation, it didn't directly prove that GABAergic INs themselves mediated this vascular response, as the widespread activation of the GABA receptors could have reflected indirect or non-synaptic activity. A more compelling case was made in the study by Lecrux et al. (2011), which evaluated the relative contributions of excitatory and inhibitory neurons to whisker-evoked CBF changes. In this study, pharmacological inhibition of glutamatergic neurons reduced the CBF response by ~37%, while blockade of GABA-A receptors with picrotoxin resulted in a reduction of ~31%. Interestingly, using both inhibitors simultaneously produced an additive ~61% decrease in CBF, suggesting that both excitatory neurons and GABA independently contribute to the NVC response. These pharmacological findings point towards a functional role of GABA and GABAergic INs in NVC. However, further evidence is required to demonstrate that selective activation of these neurons can elicit haemodynamic responses, underscoring the need for cell-type specific functional studies.

The development of techniques to investigate specific cell populations has provided crucial functional evidence supporting the role of GABAergic INs in NVC, particularly through the use of optogenetics. By targeting ChR2 expression to the vesicular GABA transporter (VGAT) – responsible for transporting the inhibitory neurotransmitters GABA and glycine, a transgenic mouse model was created in which approximately 93% of cortical GABAergic INs could be selectively activated using light (Zhao et al., 2011). Using this model, in conjunction with electrophysiology and laser speckle contrast imaging, it was demonstrated that optogenetic activation of GABAergic INs induced increases in CBF in a dose-dependent manner, based on the stimulation duration (Anenberg et al., 2015). These findings provide compelling functional evidence that GABAergic INs are capable of directly driving cerebral haemodynamics and of fine-tuning the CBF response as required.

Anenberg et al. also found that blocking GABA-A receptors with picrotoxin did not abolish the CBF response to optogenetic GABAergic IN activation. This suggests that GABAergic INs may induce these vascular effects through GABA-independent mechanisms, possibly via the release of other vasoactive neurotransmitters. This result contrasts with earlier pharmacological data from studies using sensory stimulation (e.g. Lecrux et al., 2011), where picrotoxin application significantly reduced the CBF response. This discrepancy may reflect differences in experimental paradigms, specifically direct optogenetic activation of INs versus sensory-evoked stimulation. The optogenetic approach may have produced more intense activation of GABAergic INs, potentially leading to greater release of non-GABA vasoactive molecules than would occur during physiologically evoked stimulation. This underscores the

importance of matching, as best as possible, the intensity of GABAergic IN activation with physiological levels, in studies of this kind.

Further work using the optogenetic VGAT-ChR2 mouse line sought to assess whether the vascular responses, induced by activation of GABAergic INs, match the dynamics of physiologically induced NVC. It was demonstrated that activation of GABAergic INs produces a biphasic arterial response (dilation followed by constriction) that was characteristic of sensory-induced NVC (Uhlirova et al., 2016). However, when the intensity of sensory and optogenetic stimulation was matched (using neural activity as a measure), optogenetic stimulation evoked a significantly larger increase in both blood volume and flow (Vazquez et al., 2018). These findings indicate that while some aspects of GABAergic IN-evoked haemodynamics match NVC, the size of the CBF response they induce is larger, so care must be taken to match the haemodynamic response, rather than evoked neural activity, when comparing with sensory stimulations, if we are to accurately replicate normal physiological responses. Vazquez et al. also sought to identify the neurotransmitter through which GABAergic INs evoked the haemodynamic responses. By blocking the release of NO, using the nonselective NOS antagonist Nω-nitro-L-arginine (L-NNA), they were able to suppress 75-80% of the blood flow change evoked by photostimulation of GABAergic INs (Vazquez et al., 2018). This suggests that a large part of the vasodilatory activity of GABAergic INs could be mediated by NO release.

Whilst GABAergic INs have been implicated in NVC, evidence indicates that GABA itself is not directly vasoactive (Lecrux and Hamel, 2016), as cerebral blood vessels lack GABA receptors (Vanlandewijck et al., 2018). Therefore, while GABA may work through indirect routes, a more likely model is that GABAergic INs drive CBF changes through the release of other neurotransmitters that they co-express. There are many different subtypes of GABAergic INs that are characterised by the different neurotransmitters they express. The vast majority of cortical GABAergic INs can be classified into three major groups, distinguished by their expression of either parvalbumin (PV), serotonin receptors (5HT) or somatostatin (SST), and combined these subgroups account for nearly 100% of GABAergic INs in the mouse cortex (Lee et al., 2010; Rudy et al., 2011). Within these major groups there are further, highly diverse subpopulations. Many of these subtypes of INs, and the neurotransmitters they release, have been implicated in NVC, with no one subtype of GABAergic IN accounting for the entirety of the haemodynamic response (Cauli and Hamel, 2010). Therefore, it is important to characterise the specific contributions of these different subtypes of IN to fully elucidate the role of cortical GABAergic INs in NVC.

1.3.1 Parvalbumin (PV) INs

Parvalbumin (PV) INs are the largest subtype of IN, comprising approximately 40% of all GABAergic neurons in the cortex (Rudy et al., 2011). They have long been associated with fast-spiking patterns (Kawaguchi et al., 1987), firing high-frequency trains of brief action potentials that allow them to mediate fast and powerful inhibition of target neurons. Optogenetic activation of these fast-spiking INs has been shown to increase the amplification of gamma oscillations (30-90Hz) in the cortex (Cardin et al., 2009; Sohal et al., 2009). As gamma oscillations have been shown to have a strong link with the BOLD signal (Niessing et al., 2005), this could suggest that PV INs play a role in driving CBF changes in NVC.

The literature investigating the role of PV INs in NVC is limited, in part due to their lack of expression of vasoactive substances, making other GABA IN subtypes more attractive targets, however there have been some studies investigating this. Using optogenetics to target PV INs in anaesthetised mice, it was found that their activation gave rise to a positive BOLD signal centred around the optical stimulation that was flanked by a zone of negative BOLD (Lee et al., 2010). Using the same optogenetic PV mouse model, activation of PV INs was shown to cause a strong decrease in the diameter of neighbouring penetrating arterioles, with the 5% constriction that was observed representing an equivalent reduction in CBF of over 20% (Urban et al., 2012). These studies suggest that PV INs have a complex, bidirectional influence on local vasculature, with their activation capable of producing both vasoconstriction and vasodilation.

Countering this model of PV IN-mediated NVC, photostimulation of PV INs was more recently shown to not elicit any activity-induced change in CBF in awake head-fixed mice (Krawchuk et al., 2019). Unlike earlier studies, they didn't observe a response equivalent to a constriction or negative BOLD; this could be because they used laser Doppler flowmetry (LDF) to measure CBF changes, which targets a precise area, so they weren't able to capture the decreases in blood flow surrounding the stimulation region.

The precise contribution of PV interneurons to NVC remains unresolved. The conflicting results from optogenetic studies, combined with their lack of expression of vasoactive molecules, suggest that their primary influence may not be through direct vasoactive signalling. Instead, their role is more likely indirect, either through other cells within the NVU or by their powerful modulation of network activity and the associated metabolic load (Dahlqvist et al., 2019).

1.3.2 Serotonin Receptor (5HT) INs

Serotonin receptor $5HT_3$ (5HT)-expressing INs account for 30% of the total population of GABAergic interneurons and have been shown to be expressed in "most, if not all" cortical INs

that do not express PV or SST (Lee et al., 2010). Within the population of 5HT INs, there are several further subsets expressing different combinations of neuropeptides, with specific firing patterns favouring the release of different peptides within these subsets (Lee et al., 2010). The largest fraction of these subpopulations, and the most associated with NVC, express vasoactive intestinal peptide (VIP) and comprise approximately 40% of all cortical 5HT INs (Lee et al., 2010). The idea that VIP INs are involved in CBF regulation is well established, with early electron microscopy studies demonstrating that they have axon terminals directly (<0.25μm) onto capillaries and arterioles (Chedotal et al., 1994). VIP has also been shown to be a potent vasodilator, which can mediate vascular activity in response to neural activity (Yaksh et al., 1987). These early findings show that VIP INs have a proximal association with blood vessels and they release a potent vasodilator, suggesting they could play a role in NVC.

To uncover more about the contribution of VIP INs, and other subtypes of cortical IN, to NVC, the seminal study by Cauli et al. (2004) utilised patch-clamp recordings in *ex vivo* rat cortical slices, followed by PCR to characterise which IN subtype was stimulated. Using this methodology, they showed that evoking action potentials in VIP INs led to a dilation in neighbouring blood vessels, and that perfusing the cortical slices with VIP elicited potent dilations, likely due to the VIP receptors on microvascular smooth muscle cells (Cauli et al., 2004). Interestingly, when they perfused slices with cholecystokinin (CCK), another type of 5HT IN peptide, they found no significant vascular response, highlighting that this subtype of 5HT IN is unlikely to be directly involved in NVC. This study provides convincing evidence for the ability of VIP INs to drive CBF changes in NVC, however the dilations they showed were very slow compared to *in vivo* stimulation responses (Shih et al., 2012). This is likely due to the work being conducted in cortical slices, where vessels require pre-constriction and there is a lack of luminal flow, highlighting the importance of investigating the dynamics of NVC models *in vivo*.

Following this seminal study, other groups sought to further assess the contribution of 5HT INs and the VIP subgroup to NVC. Using similar methods, but in mouse cortical slices, activation of 5HT INs produced biphasic vascular responses, with the dilation, surprisingly, being shown to be mediated by NO rather than VIP, a finding consistent with *in vivo* evidence where sensory-evoked NVC was also unaltered by VIP antagonism (Perrenoud et al., 2012; Lecrux et al., 2011). These findings bring into question the role of VIP in 5HT-mediated NVC and also highlight an issue with the characterisation of INs. As mentioned earlier, the subgroups of IN are often thought of as being discrete, with minimal crossover of expression of peptides between separate groups, yet this isn't always true. This is further highlighted in the Perrenoud et al. study, where both neuropeptide-Y (NPY) and NOS, which are typically associated with the SST IN subgroup, are shown to be involved in 5HT IN-mediated

vasoactivity. While the question remains over whether VIP is the primary mediator, the collective evidence implicates a role for 5HT INs in NVC.

1.3.3 Somatostatin (SST) INs

Somatostatin (SST) INs make up the final 30% portion of GABAergic INs, they are primarily known for the modulation of cortical network activity through dendritic inhibition (Urban-Ciecko and Barth, 2016). Of the three main groups of GABAergic IN SST INs are the most often associated with the NVU, due to their diverse subpopulations expressing vasoactive neurotransmitters. These subpopulations of SST IN include neuronal NOS (nNOS) INs and NPY INs, both of which have been implicated in NVC (Cauli and Hamel, 2010). Whilst SST itself has been shown to produce vasoconstriction upon release (Cauli et al., 2004), this has not been as widely studied as the haemodynamic effects of NO and NPY.

Early pharmacological studies established SST as a potent vasoconstrictor. One of the first demonstrations found that subarachnoid injection of SST in rats evoked a dose-dependent reduction in spinal cord blood flow, while topical application onto the cortex prompted an immediate constriction of pial vessels (Long et al., 1992). Building on this, Cauli et al. (2004) showed that direct stimulation of a single SST IN caused a significant and spatially restricted constriction of local blood vessels. Crucially, they proposed that the mechanism for this effect was through direct innervation of the cortical microvessels, by demonstrating that SST INs form direct projections onto the vessels, and that the vascular endothelial and VSMCs express the SST receptors. These findings indicate a role of SST INs in reducing CBF, through the release of SST directly onto cortical blood vessels.

In vivo evidence for the role of SST INs in NVC is sparse, and it presents a complex picture. One study found that, although SST INs are activated during basal forebrain electrical stimulation and form dense projections contacting vessels through the depth of the cortex, application of a SST antagonist did not alter the overall CBF response (Kocharyan et al., 2008). Contrasting with this, a more recent study using optogenetic activation of SST INs in awake mice reported a significant increase in local CBF following photostimulation (Krawchuk et al., 2019). The contrasting data could be due to SST-mediated vasoconstriction being masked during the optogenetic activation of SST INs by the release of more powerful vasodilatory molecules.

Despite the contradictory findings, together these studies give an insight into how SST INs fit into the NVU, by having multiple projections onto blood vessels, allowing direct release of SST onto the SST receptors the vessels express. Given the nature of SST to elicit constrictions, it would appear it works not to cause direct increases in CBF, but to refine the vascular response. This could work by controlling the return to baseline of CBF following neural activity, or even

by directing blood away from surrounding areas in the cortex towards the active region, a phenomenon seen in negative BOLD (Devor et al., 2007). Disentangling exactly how SST INs contribute to NVC requires direct, cell-specific stimulation combined with high-resolution blood flow measurements, as was undertaken in the experiments described in Chapter 3 of this thesis.

1.3.4 Neuropeptide-Y (NPY) INs

The three main subgroups of IN discussed thus far (PV, 5HT and SST) are known to have little overlap with each other, however the subtypes within these groups are not as conveniently distinct. This holds true for Neuropeptide-Y-expressing (NPY) INs, whilst usually identified as being a subtype of SST INs, there is evidence suggesting they also can coexpress PV (Karagiannis et al., 2009) and 5HT (Lee et al., 2010). Furthermore, the proportion of SST INs in which NPY is coexpressed is varied throughout the brain, with approximately 33% of SST INs in the cingulate cortex of the mouse reported to coexpress NPY (Riedeman et al., 2016), but only 10% in the somatosensory cortex (Ma et al., 2006). Regardless of the diversity of peptides NPY INs coexpress, what is known is that they are widely distributed throughout the depth of the cortex, where they are involved in many physiological processes such as synaptic transmission and regulation of CBF (Tuor et al., 1990; Markram et al., 2004). NPY itself is one of the most abundant neuropeptides in the brain (Allen et al., 1983) and has been shown to be a powerful vasoconstrictor (Cauli and Hamel, 2010).

NPY INs have been hypothesised to play a role in the control of CBF for a long time. In the 1990s, there were a multitude of studies showing that NPY INs colocalise with cortical blood vessels in rats (Tuor et al., 1990; Abounader and Hamel, 1997) and in humans (Berman and Fredrickson, 1992; Abounader and Hamel, 1997). It was also shown that NPY receptors are abundantly expressed in blood vessels (Larhammar et al., 1992; Abounader et al., 1999), and application of pharmacological agonists of these receptors using NPY, both systemically *in vivo* and topically applied onto *ex vivo* brain slices, leads to strong constrictions and reduction in CBF (Allen et al., 1984; Tuor et al., 1990; Abounader et al., 1995; Cauli et al., 2004). These early studies showing the associations of NPY INs to blood vessels and the ability of NPY to be a robust constrictor, support the idea that these INs are involved in the NVU through vasoconstriction.

Approximately 26% of NPY INs coexpress the enzyme NOS (Karagiannis et al., 2009), producing the potent vasodilator NO (see **section 1.3.5** for more details on nNOS INs). This coexpression hints at the role that the constrictor NPY plays in NVC, as a counter to NO-induced dilation. In the Cauli et al. (2004) study, the only vessel dilation that returned to baseline was induced by stimulation of NPY/nNOS INs (Cauli et al., 2004). They interpreted

this finding, alongside the extensive colocalisation of nNOS and NPY, to suggest that NPY acts to spatially and temporarily limit the vasodilatory effect of the highly diffusible NO. This interpretation is supported by the finding that 5HT IN-evoked constrictions are dependent on NPY, while their dilations are NOS-dependent (Perrenoud et al., 2012). This lends more support to a mechanism for NVC control mediated by the opposing actions of NPY and NO transmitters.

One key study found that optogenetic activation of GABAergic INs produces a biphasic arteriolar response that closely mimics the vascular response to sensory stimulation (Uhlirova et al., 2016). Hypothesising that NPY was responsible for the constriction element of this, the researchers applied the NPY receptor antagonist BIBP 3226, largely abolishing the post-stimulus constriction for both direct IN activation and sensory-evoked responses, without affecting the initial vasodilation. This provides compelling evidence that NPY INs play a major role in mediating the vasoconstrictive component of the NVC response, acting to regulate CBF by promoting the return to baseline following neural activity.

1.3.5 Neuronal Nitric Oxide Synthase (nNOS) INs

The subtype of GABAergic INs with perhaps the most diverse coexpression of other neurotransmitters are neuronal nitric oxide synthase-expressing (nNOS) INs, with evidence showing nNOS INs coexpress SST, 5HT, NPY, PV and VIP (Karagiannis et al., 2009; Tremblay et al., 2016). NOS is a membrane-associated enzyme that synthesises NO by catalysing the conversion of L-arginine to L-citrulline and NO (Stefanovic et al., 2007). NO is a small, diffusible, gaseous molecule that was first shown to mediate dilations in blood vessels over 40 years ago (Furchgott et al., 1980). Hence, when it was discovered nine years later that NO is produced in the brain (Bredt, 1989), it was hypothesised to play a role in the modulation of CBF. Indeed, early studies following this finding showed that blockade of NOS leads to a reduction in the NVC response (Raszkiewicz et al., 1992; Iadecola et al., 1993; Faraci and Breese, 1993). And a recent meta-analysis of studies in the field reported that blocking nNOS had the largest impact of any signalling pathway on NVC, reducing the magnitude of the NVC response by an average of 64% (Hosford & Gourine, 2019).

There are three isoforms of NOS- inducible NOS (iNOS), endothelial NOS (eNOS) and nNOS. iNOS production is induced in response to inflammation and is not normally expressed in the brain (Steinert et al., 2010). eNOS is present in the endothelial cells in vessel walls and mediates vascular tone in the brain through the production of NO, which diffuses to proximal smooth muscle cells and initiates slow-acting vasodilation (Heiss et al., 2015). nNOS is found only in neurons, predominantly in neural processes closely associated with cerebral vessels (Iadecola et al., 1993) and is the isoform that is suspected to play the biggest role in the NVU.

There are two types of nNOS IN: type I and type II. Type I nNOS INs are the rarest subtype of GABAergic IN (Kubota et al., 1994); they are predominantly found in the deeper layers of the cortex, in layers V and VI, but have long projections extending through the layers, allowing them to have an extensive influence throughout the cortex (Perrenoud et al., 2012). Type II nNOS INs are more prevalent but have a much lower expression of NOS than type I, and they are concentrated in layers II, III and VI (Perrenoud et al., 2012). There is often difficulty identifying type II nNOS INs, due to their weak NOS expression and small size, hence they haven't been as extensively studied as type I.

nNOS INs are suggested to be involved in NVC through the production and release of NO. During neural activity there is a release of glutamate, which binds to NMDA receptors on nNOS INs, leading to an influx of Ca2+ ions, which in turn activates NOS to produce NO (Faraci and Breese, 1993; Busija et al., 2007). There are two pathways through which this release of NO is hypothesised to cause vasodilation. The most commonly referenced pathway is through cyclic guanosine monophosphate (cGMP) in vascular smooth muscle cells (VSMCs). When NO is released from nNOS INs, it diffuses to local VSMCs where it binds to soluble guanylyl cyclase (sGC). The NO-sGC then catalyses the conversion of guanosine-triphosphate (GTP) to cGMP in the VSMCs, leading to relaxation of the cells and vasodilation (Lehners et al., 2018). The other pathway for NO-mediated vasodilation is through inhibition of 20-Hydroxyeicosatetraenoic acid (20-HETE), a vasoconstrictor. 20-HETE closes voltage-gated potassium channels in VSMCs, limiting the efflux of potassium, which causes cell depolarisation leading to vasoconstriction (Garcia et al., 2017). When NO is released by nNOS INs onto the VSMCs, it inhibits the production of 20-HETE, thereby inhibiting the vasoconstriction (Roman, 2002; Hall et al., 2014). The role of nNOS INs and NO in the NVC is thought to be mediated through these pathways, mediating increases in CBF.

Early studies investigating the role of nNOS INs in the NVU showed their close proximity to cerebral blood vessels (Iadecola et al., 1993; Estrada et al., 1993; Luth et al., 1994), with one study finding at no point in the cortex was any part of an arteriole more than 25μm from a nNOS process (Moro et al., 1995). This colocalisation is even more significant when interpreted with the radius of vasodilatory influence of NO, originally thought to be ≈100μm from a single source point (Wood and Garthwaite, 1994), although more recent data suggests it has a much more discrete sphere of influence (Hall and Garthwaite, 2006; Hall and Garthwaite, 2009). Even with this smaller range of activity, nNOS INs have sufficient proximity to cerebral blood vessels to allow them to mediate NVC throughout the cortex.

Knowing that nNOS INs colocalise with cerebral blood vessels, the next step to uncovering their contribution to the NVC was performing functional studies. Many of these studies involve pharmacological blockade of NOS. The most commonly used NOS blockers are L-arginine

analogues, which bind to NOS, preventing the production of NO (Moncada and Higgs, 1993). These L-arginine analogues, including Nω-nitro-L-arginine (L-NNA), NG-Methyl-L-arginine (L-NMMA) and NG-Nitro-L-arginine methyl ester (L-NAME), are non-specific and inhibit all NOS activity in the brain when administered, preventing NO production from both nNOS and eNOS. Other blockers are more specific, such as 7-Nitroindazole (7-NI), which targets only NO synthesis from nNOS. There are numerous studies showing that when NOS activity is blocked in the brain, CBF is decreased and the NVC response is inhibited (reviewed in Duchemin et al., 2012 and Hosford and Gourine, 2019). For example, when L-NNA was superfused onto the cortex of anaesthetised rats, resting CBF, measured using LDF, was reduced by 38% and basal forebrain stimulation-elicited vasodilation by 44% (Iadecola and Zhang, 1996). In a similar study, 7-NI was used to assess the change in electrical forepaw stimulation-evoked CBF, CBV and BOLD responses, showing all 3 of these haemodynamic measures were significantly attenuated when nNOS was blocked (Stefanovic et al., 2007). Combining pharmacological and genetic approaches, it was shown that in wildtype mice that L-NNA application significantly reduced stimulation-evoked vasodilation in surface arterioles, and in nNOS knockout mice activity-dependent vasodilation was significantly suppressed compared to wildtype littermates (Kitaura et al., 2007). It is not only physiologically-induced NVC that has been shown to be reduced by NOS blockade. Haemodynamic increases induced by activation of all GABA INs (Vazquez et al., 2018) and targeted 5HT IN activation (Perrenoud et al., 2012), have also been blocked with the application of L-NNA. These findings suggest that the production of NO, through NOS, plays an important role in eliciting the dilatory portion of the NVC response. This role could be orchestrated by nNOS INs, whose direct stimulation has been shown to induce dilation in vessels (Cauli et al., 2004).

While there is much evidence supporting the hypothesis that the role of NO in NVC is as a direct mediator of NVC, there are some studies that contradict this idea. Studies have shown using genetic (Ma et al., 1996; Ayata et al., 1996) and pharmacological (Wang et al., 1992; Adachi et al., 1994; White et al., 1999; Matsuura and Kanno, 2002; Ances et al., 2010; Vazquez et al., 2018) inhibition of NOS, there is no significant effect on somatosensory- or motor- evoked NVC. Combining these findings with the fact that NOS blockade has never been reported to completely abolish the haemodynamic response to stimulation (Ances et al., 2010) suggests that perhaps NO isn't entirely responsible for eliciting the NVC response, and may instead play a more complex role. Lindauer et al. (1999) sought to investigate the role of NO in NVC using cortical superfusion of L-NNA in anaesthetised rats. As had previously been shown, they found a reduction in the whisker stimulation-evoked increase in CBF with NOS inhibited, but more significantly they showed that with subsequent application of the NO donor S-nitroso-N-acetylpenicillamine (SNAP), they were able to restore the whisker NVC response

to the pre-L-NNA magnitude (Lindauer et al., 1999). This finding is important because a NO donor provides a constant concentration of NO, not a dynamic one, which indicates that while the presence of NO is required for a normal NVC response, a direct release of NO from nNOS INs doesn't directly drive the vasodilation. In this study, they also measured the levels of cGMP in the brain tissue post-mortem. They found that superfusion with L-NNA decreased cGMP levels by 65%, and when L-NNA and SNAP were applied, these levels returned to 65% of control (Lindauer et al., 1999). In another study, it was found that while L-NNA application to rat brain slices reduced vessel dilations, if the production of 20-HETE was blocked at the same time, the L-NNA no longer inhibited the dilations (Hall et al., 2014). The implication of this result is that NO promotes dilations not through direct action, but by preventing 20-HETE activity. Together, these results suggest that nNOS derived NO acts as a modulator of NVC, and a potential pathway for this modulation is by controlling the levels of cGMP in VSMCs, with increases permitting vasodilation to occur via other mediators in the NVU, and by blocking 20-HETE mediated constriction.

To date, the literature investigating the role of nNOS INs and NO in NVC forms an incomplete story, with many studies suggesting NO acts as a direct mediator of this haemodynamic response, but others proposing it instead has a role as a modulator or some even suggesting it plays no part at all. The contradictory evidence could stem from methodological differences between studies. Factors such as the use of anaesthesia, which alters vascular tone (see section 1.4.1), the use of live animals versus *ex vivo* brain slices and different techniques for measuring vascular changes with varying resolutions, all influence the results that are observed. Furthermore, the high redundancy of the NVC system (Hosford and Gourine, 2019) could mean that when the NO pathway is blocked, other vasodilator pathways can compensate, masking NO's true contribution under normal physiological conditions. Whatever the cause for these discrepancies, the exact role of nNOS INs and NO in NVC remains unresolved. This is what I sought to answer in this thesis, using direct optogenetic activation of nNOS INs, to assess their haemodynamic and neural responses in Chapter 3 and then optogenetic and whisker stimulation with pharmacological blockade of NOS in Chapter 4.

As I have described, the NVU consists of many cell types working through various signalling pathways to carry out NVC (see Figure 1.1 for a summary of these pathways). In order to observe the relative contributions of these cells and assess NVC as a whole, many different experimental techniques have been developed, allowing us to uncover more details on the intricacies of this phenomenon.

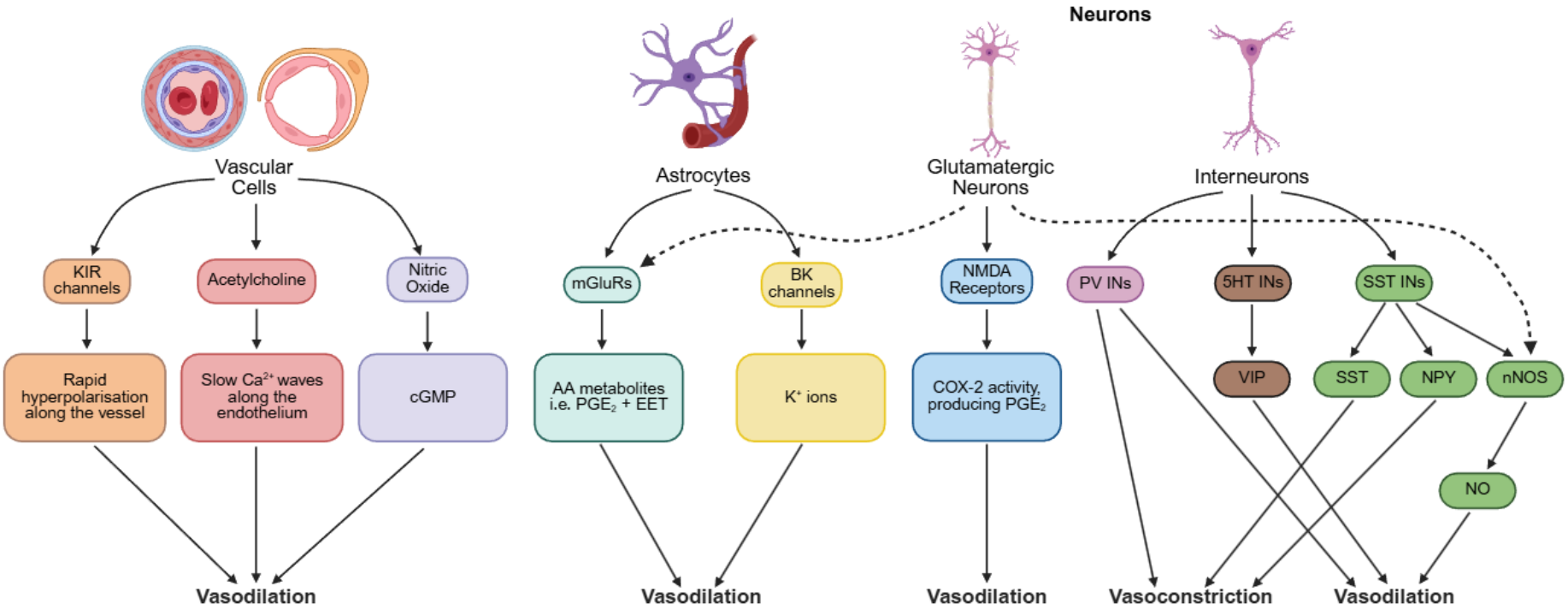

Figure 1.1 Overview of the key pathways of NVC, mediated by cells in the NVU. (Figure produced in Biorender.com)

1.4 Experimental techniques used to study NVC

The preceding section reviewed the cellular components of the NVU and their respective roles in NVC. Elucidating these mechanisms required a multitude of different experimental techniques. This section will summarise the key experimental approaches used to investigate NVC, highlighting their strengths and weaknesses, and will provide a rationale for why the approaches used in the experiments in this thesis are suited to investigate the contributions of cortical INs and NO to NVC.

1.4.1 Animal Models

A fundamental challenge in NVC research lies in the trade-off between resolution and invasiveness. The study of NVC in humans is largely restricted to non-invasive methods, such as fMRI, and while these techniques are useful, they lack the temporal and spatial resolution required to uncover the fast, microscopic interactions underlying NVC. Conversely, the techniques with the required resolution to investigate these cellular mechanisms are invasive, and so are not suitable for use in human studies. Therefore, animal models are widely used to investigate the processes that drive NVC.

For an animal model to be useful, it must closely replicate human physiology, or at least certain aspects of it, such as disease or specific biochemical pathways. For NVC research, an added requirement is a brain with an intact blood supply, ruling out small invertebrates, such as Drosophila, which lack NVC. A range of animal models are used in the field, ranging from primates to zebrafish, however by far the most prevalent are rodent models (Hosford and Gourine, 2019). The use of rodents in research, in particular rats and mice, is so prevalent for many reasons. They have a high birth rate and short gestation period (Bryda, 2013), which makes producing sufficient numbers for studies easier. They are easy to breed and maintain and are small in size, making them cheaper to house and more convenient for behavioural testing and other experimental techniques. Rodents also have a relatively short life cycle, which is useful when testing age-related changes in NVC. Another reason for the use of rodents is that there are increasingly abundant genetically modified strains, especially in mice, that allow researchers to carry out experiments not possible in other animal models, for example the development of Cre-dependent, cell-specific, optogenetic mouse lines to study GABAergic INs (Taniguchi et al., 2011).

Much of the early work in the field of NVC was carried out using rats (Iadecola, 2017). At the time, the extensive studies into rat physiology, coupled with their optimisation for *in vivo* work and larger brain and body size, made them more suited to NVC research (Berwick et al., 2005). However, more recently the field has shifted to the use of mice in research, the main reason for this is the aforementioned availability of a range of genetically modified lines of mice, but

also their quicker breeding and shorter life span allow for easier use at different age ranges. The range of genetically modified mouse lines is not only useful for studies using methods such as optogenetics but also incorporates the many disease models in mice that allow for the observation of human-like diseases, in an invasive experimental setup. It is using disease models like this that have allowed for the role of NVC breakdown in neurodegenerative diseases, such as Alzheimer's Disease, to be characterised (Zlokovic, 2010).

Rodent studies in the field of NVC often centre around the primary somatosensory cortex. The rodent primary somatosensory cortex is highly organised and contains well characterised pathways for a variety of stimulations, including tactile forepaw/ hindpaw stimulations and whisker stimulations (Peterson, 2019). The whisker-barrel cortex within this is very commonly used, as whisking is one of the rodent's main sensory inputs, so the whiskers are highly sensitive and elaborately encoded within the brain. Research has shown that each rodent whisker is topographically mapped to an individual neural column (termed barrel) within the contralateral whisker-barrel cortex (Woolsey and Loos, 1970). While single whisker stimulation is useful for mapping out NVC in a discrete column in the whisker-barrel cortex, it doesn't reflect the broader sensory experiences of the real world. Environmental sensory stimuli activate many receptors at once, such as multiple whiskers or multiple cone and rod cells. Therefore, a stimulation of multiple whiskers, as used in this thesis, is more applicable to naturally occurring NVC. Although this technique is still not truly replicating the active sense of whisking, as the mice are under anaesthesia.

1.4.1.1 Use of anaesthesia

As has been established in the previous section, the use of *in vivo* animal models has been critical for driving our understanding of the mechanisms involved in NVC. The majority of the studies in the field, up until recently, have used anaesthetised animals due to the invasive nature of the experiments and to minimise motion and stress-induced artefacts in the data. However, anaesthesia is known to affect brain physiology, with effects on both neural and vascular activity being reported (Masamoto and Kanno, 2012; Aksenov et al., 2015), and hence the possibility of anaesthesia interfering with NVC in these studies.

To solve the issue of anaesthesia confounding experimental results, some researchers have moved to carrying out experiments on awake animals. This has the benefit of not having the confound of anaesthesia during the experiment, however can have other effects on the studies. Awake imaging can only be carried out for short periods of time, due to the increased stress on the animal, and even with a shorter experiment time, head-fixation (necessary for the majority of techniques used to assess NVC) of animals whilst awake has been shown to increase markers of stress (Low et al., 2016; Juczewski et al., 2020). Another potential issue

with awake animal studies is maintaining a consistent, reproducible brain state. Awake animals can fall asleep, whisk, locomote (in setups which allow for it), investigate their surroundings and carry out many more behaviours, all of which can drive spontaneous fluctuations in neural and haemodynamic signals in the brain (Huo et al., 2014; Winder et al., 2017), affecting the results of stimulation-induced experiments. Recent studies have sought to solve this confound by tracking the behaviour of animals and excluding data where the animal is locomoting, fidgeting, grooming, whisking, sleeping…etc., using a range of techniques, for example, heart rate, respiration rate, locomotion and eye tracking (Zhang et al., 2022).

One way to ensure a more stable, controllable brain state throughout an experiment remains the use of anaesthetic, where the primary factor altering the brain state is the depth of anaesthesia. So, alongside the increase in use of awake experiments, there has also been an increase in research attempting to optimise the use of anaesthesia to limit its impact on brain physiology, and thus its confound on experiments. There is a range of anaesthetic protocols used in animal studies, each with differing influences on NVC (Masamoto and Kanno, 2012). Some examples of the confounds of different anaesthetics include a decrease in both neural and haemodynamic responses to high-frequency stimulations with urethane anaesthetic in rats (Martin et al., 2006) and a decrease in the BOLD response disproportional to the decrease in neural activity with use of isoflurane and/or fentanyl (Aksenov et al., 2015). By learning more about the effects of using varying anaesthetics, they can either be minimised or accounted for in the interpretation of data. One study seeking to do this utilised 2D-OIS haemodynamic imaging in combination with whisker stimulation to assess how a novel modular anaesthetic approach affected NVC (Sharp et al., 2015). This novel anaesthetic protocol involved an injectable anaesthetic, consisting of fentanyl-fluanisone and midazolam, in combination with the volatile anaesthetic isoflurane. Combining these anaesthetics allowed for lower initial doses of the injectable to be used to induce anaesthesia (20% reduction), and maintenance of sedation was possible using lower levels of isoflurane (up to 75% reduction from typical use). Importantly, when the haemodynamic responses, evoked by whisker stimulation, in mice sedated using this anaesthetic protocol were compared to those from awake mice, there were no significant differences in the magnitude or speed of the responses (Sharp et al., 2015). The reason for this lack of difference can be attributed to the lower doses of each of the anaesthetic agents, minimising their effects on NVC, compared to a typical anaesthetised experiment that uses high isoflurane for induction and maintenance of sedation, which is much more susceptible to the highly vasodilatory effect of isoflurane (Masamoto et al., 2009).

This shows us that whilst anaesthetics can have confounding effects on NVC in experiments, with careful consideration and selection of protocols, this impact can be minimised. In this

thesis, the studies were carried out in mice sedated using the anaesthetic protocol optimised by Sharp et al. (2015), to allow for a consistent brain state and minimal effect on NVC.

1.4.2 Functional Magnetic Resonance Imaging (fMRI)

Functional magnetic resonance imaging (fMRI) is a non-invasive neuroimaging technique that is used widely in animal and human imaging, in both a clinical setting and for studying brain function (Logothetis, 2003). MRI works by exposing an object to a strong magnetic field, forcing protons in the body into uniform alignment. In nuclear magnetic resonance (NMR) imaging, radio waves are then used to deflect the vector of this alignment, and when the radio waves are stopped, the subsequent return to alignment of the protons releases a radio wave (known as the MR signal), which is detected by the scanner. The MR signal generated by this return to alignment varies depending on the magnetic properties of the molecule the protons are within; hence it can be used to observe molecules with magnetic properties that differ from the surrounding tissue. fMRI specifically focuses on the local concentrations of the highly paramagnetic deoxygenated haemoglobin in the blood. In resting state, deoxyhaemoglobin levels are relatively stable. During an increase in neural activity, there is an increase in local blood flow and blood volume, due to NVC. This influx of fresh oxygenated blood is much larger than physiologically required, supplying much more oxygen, via oxyhaemoglobin, than is actually used by neural activity (Howarth et al., 2020). This overcompensation results in a large increase in the concentration of oxyhaemoglobin and a drop in the concentration of deoxyhaemoglobin in the active region. This drop in the paramagnetic deoxygenated haemoglobin leads to fewer inhomogeneities in the magnetic field, which increases the MR signal detected by the fMRI scanner (Ogawa et al.,1990). This signal, the drop in deoxyhaemoglobin concentration, is the BOLD signal, and is used as a surrogate measure of neural activity, whereby a positive BOLD signal is interpreted as an increase in evoked neural activity.

Positive BOLD signals have been reliably linked to both local field potentials (LFPs) and multi-unit activity (MUA) (Logothetis, 2008). The negative BOLD signal refers to the less frequently observed phenomenon of an increase in the concentration of deoxyhaemoglobin, observed by fMRI (the opposite of positive BOLD). The origin of the negative BOLD response is controversial, with some theories positing its origin is vascular, while others suggest neural (Boorman et al., 2010). The vascular theory behind the negative BOLD response suggests that it occurs due to haemodynamic mechanics, such as vascular steal, where blood is redirected from areas of low neural activity to areas of high neural activity, rather than representing any changes in neural activity (Moraschi et al., 2012). However, increasing evidence suggests that this may not be the case, and that the negative BOLD signal is actually generated by local decreases in LFP and MUA (Boorman et al., 2010; Mullinger et al., 2012),

with some suggesting this physiological decrease in neural activity is caused by inhibitory GABAergic INs (Allison et al., 2000; Shmuel et al., 2006; Boorman et al., 2015).

The controversy over how to interpret negative BOLD signals highlights one of the greatest limitations of using BOLD fMRI to assess neural activity, in that it relies on a haemodynamic response as a surrogate measure. Whilst in most conditions this indirect measure is reliable, in other cases, such as the negative BOLD signal and in disease, the relationship between CBF changes and neural activity can be uncorrelated (Esposito et al., 2003; Tarantini et al., 2017). This highlights the importance of NVC research; if we better understand how NVC occurs and the situations in which neural activity and haemodynamics become uncoupled, we will have a greater ability to interpret BOLD fMRI. Another limitation of this method is that of resolution, even with the use of higher field strengths and new forms of analysis that greatly improve the spatial and temporal resolution of fMRI, the voxel sizes are still not small enough to observe rapid vascular changes within an individual vessel (Goense et al., 2016). Instead, BOLD fMRI is more suited to reflecting global haemodynamic and neural signals and is useful in translational studies, as it can be performed in animal models and in humans.

These limitations of BOLD fMRI make it an unsuitable method for the work carried out in this thesis, where the mechanisms of NVC are investigated at a cellular level. Hence a different approach was used to allow for concurrent measurement of blood flow and neural activity, enabling observation of both aspects of NVC with a much higher spatial and temporal resolution (see next sections). However, this doesn't discount the value of BOLD fMRI, and in fact, the more we can understand the mechanisms underlying NVC, the better we can use and interpret BOLD fMRI.

1.4.3 Optical Imaging of Blood

In this thesis, a multimodal approach was taken to measuring NVC, with concurrent haemodynamic and neural recording. To perform the former of these, optical imaging of the blood was used. Optical imaging takes advantage of several different optical contrast mechanisms, both endogenous and exogenous, in brain tissue, allowing for imaging of physiological processes with minimal invasivity. Novel optical imaging techniques, such as laser speckle contrast imaging (LSCI) and functional near-infrared spectroscopy imaging (fNIRS), have led to advancements in many areas of basic and clinical neuroscience and neurovascular research (Liao et al., 2013). Applied to haemodynamics, optical imaging in its various forms is used to observe changes in haemoglobin concentration, blood oxygenation, blood flow and blood volume. Some of the more commonly used haemodynamic optical imaging methods include: LSCI- which uses the speckle contrast of laser light by red blood cells to measure blood flow; fNIRS- which uses near-infrared light to measure the changes in

haemoglobin concentration in the cortex; photoacoustic tomography- which capitalises on the photoacoustic effect of haemoglobin where an absorbed optical energy is converted into acoustic energy, detecting the emitted ultrasound waves to reveal vascular structure with a high spatial resolution, several centimetres into the brain (Xia et al., 2014). Each of these optical imaging techniques, and others, have different advantages and disadvantages, and so careful consideration must be taken when selecting which method to use to measure haemodynamics when studying NVC. For the research undertaken in this thesis, two-dimensional optical imaging spectroscopy (2D-OIS) was used to measure the changes in concentration of oxygenated and deoxygenated haemoglobin.

2D-OIS utilises the fact that haemoglobin is the dominant absorber in brain tissue of light in the visible wavelength band and that its absorption and scattering properties differ depending on its oxygenation state, to measure the relative change in haemoglobin concentration on the surface of the brain (Grinvald et al., 1986). A more detailed description of the 2D-OIS methodology used in this thesis is given in Chapter 2, I will briefly outline it here. The surface of the cortex is illuminated with four wavelengths of light sequentially. Oxygenated haemoglobin (Hbo) and deoxygenated or reduced haemoglobin (Hbr) absorb and scatter these wavelengths of light differently, hence by collecting the remitted light we are able to calculate the relative changes in these haemoglobin profiles (Kennerley et al., 2005). The remitted light is used to produce 2D spatial maps of the changes in concentration of Hbo, Hbr and total haemoglobin (Hbt, calculated by adding the Hbo and Hbr concentrations) from baseline.

2D-OIS largely reflects the haemodynamic responses on the surface of the cortex, primarily from surface arteries and arterioles. It is hypothesised that these surface vessels are the main area of haemodynamic responses in NVC (Herron et al., 2016), either through backward propagation of calcium/ hyperpolarisations or direct stimulation by vasoactive mediators. As such, 2D-OIS can provide reliable haemodynamic data evoked by neural activity, even if the neural activity originates from below the surface of the cortex. However, to assess the effect of neural activity on proximal capillaries or penetrating arterioles in the cortex, other techniques such as 2-photon microscopy (see section 1.4.5) are used.

2D-OIS doesn't record CBF changes, which are important for NVC research, but rather changes in the concentration of haemoglobin. However, previous work has shown that changes in Hbt concentration, recorded using 2D-OIS, are well matched to cerebral blood volume (CBV) changes recorded using MRI (Kennerley et al., 2005). CBV is an important factor when looking into haemodynamic responses, as it gives a more accurate idea of what is occurring in a precise vascular compartment in terms of local vasodilation or constriction, compared to CBF, which may be altered by upstream flow changes. This is important as NVC

is a localised mechanism and so when investigating it, we want to know the local vascular changes. Also, CBV and CBF have been shown to follow a reliable scaling relationship (Kennerley et al., 2005), hence in most conditions an increase in CBV can be predicted to correspond to an increase in CBF.

2D-OIS imaging provides a detailed perspective of haemodynamics, showing CBV and blood saturation changes both spatially and temporally with a high degree of resolution. This makes it ideally suited for the work carried out in this thesis, looking at the intricacies of the NVC response at a cellular level.

1.4.4 Electrophysiology

To accurately assess NVC, you need the ability to quantify not only haemodynamics but also neural activity. There are many different techniques used to do this. The methods to directly measure neural activity can be broadly split into three categories: patch-clamping electrophysiology, fluorescence neural imaging and implanted multi-electrode arrays. Patch-clamp recording involves placing an electrode onto or inside a neuron, which allows for very precise measurements of electrical activity across the patched neuron. When used in combination with high-resolution imaging of individual vessels, patch-clamp recording can be used to see how individual neurons can affect local capillaries (Cauli et al., 2004). Fluorescence neural imaging utilises fluorescent indicators to record the (typically calcium, which increases in neurons as they are activated) activity of neurons. This is done either with organic dyes or, more recently, genetically encoded indicators which, through genetic modification and selective breeding, can be expressed in specific neural subtypes, allowing assessment of the activity of these different subtypes. Multi-electrode arrays are inserted into the brain and can carry thousands of microelectrodes (Steinmetz et al., 2021), each of which records the activity of neurons in close proximity to it. For recording neural activity in this thesis, insertion of a multi-electrode array was the chosen methodology, the benefits of this technique being a much faster sampling rate than fluorescent neural imaging (20,000-100,000Hz compared to 10-100Hz), allowing for immediate detection of stimulation-evoked neural activity. Also, with this technique, the ability to extract more detailed information on population firing of multiple neurons allows for a better understanding of the effects of INs on neural population dynamics and the circuitry in the somatosensory cortex.

A detailed description of the methodology of the electrophysiology carried out in this thesis is given in Chapter 2. In brief, placing the multichannel electrode into the cortex enables direct measurement of the dynamics of neural networks within the active region. This technique allows for the extracellular recording of local field potentials (LFPs), which are low-frequency (<500Hz) neural signals thought to be generated by membrane currents of neurons

neighbouring the electrode, and multi-unit activity (MUA), which is the high-frequency (>500Hz) portion of the activity, arising from local spiking of populations of neurons. The ability to extract both of these aspects of electrophysiological activity is important, as although they have been shown to have a strong relationship to each other (Rasch et al., 2009; Katzner et al., 2009), they seemingly have differing correlations with the BOLD and haemodynamic NVC response (Bartolo et al., 2011). This difference was highlighted using concurrent electrophysiology and fMRI studies in the visual cortex of awake and anaesthetised monkeys, where it was reported that stimulation-induced MUA was less sustained and less correlated with the BOLD signal than LFPs (Logothetis et al., 2001; Goense and Logothetis, 2008). The conclusion from these studies was that the BOLD signal, which is a result of NVC, was primarily dependent on LFPs and not MUA signals. However, this conclusion has since been questioned, with some studies showing that LFP and MUA responses are equally evoked in response to stimulation, and both can have a linear relationship with the BOLD signal (Burns et al., 2010; Sanganahalli et al., 2009). The reasons for these contradictory findings have been attributed to differences in both experimental setup and the data analysis used, and the question of which aspect of neural activity is better correlated with the BOLD signal remains unresolved.

This controversy in the field highlights the importance of measuring neural activity concurrently with haemodynamics, to give a more complete picture of NVC. This is why a multimodal approach was taken in the experiments in this thesis, allowing for the recording of neural activity and haemodynamics simultaneously. More detail on the electrophysiology technique and analysis performed is given in Chapter 2.

1.4.5 2-photon Imaging

As discussed, there are many benefits to the multimodal experimental setup used in this thesis, however one limitation lies in the depth of haemodynamic imaging that is possible with 2D-OIS. While 2D-OIS largely reflects the haemodynamic responses on the surface of the cortex, the ability to observe the activity of penetrating arterioles and capillaries deeper in the cortex, with high resolution, is important to assess their contribution to this response. The most commonly used technique to carry this out is 2-photon microscopy. The basis of most methods of fluorescent microscopy, such as confocal microscopy, is that when a fluorescent molecule is hit by a photon of a certain wavelength the molecule gets excited to a higher energy state, and when it drops back down to its stable ground state, it emits one photon of light. However, when you use light that is double the specific wavelength of the fluorescent molecule, enabling deeper imaging, the photons have half of the necessary energy required, and so two photons are needed to hit the molecule at exactly the same time to cause the molecule to fluoresce. This phenomenon is very unlikely, due to the fact that the two photons must strike the molecule within one femtosecond of each other, hence a high-power laser is used that is capable of

producing very fast pulses of light and that can be focused on a small, precise focal point. The benefit of this is that the area of excitation is restricted to just the focal point, so you don't get excitation of fluorophores above or below the focal plane as you do with other microscopy methods. Also, the longer, infrared wavelengths of light used in 2-photon microscopy penetrate tissue more effectively than visible wavelengths of light and are less susceptible to tissue scattering, allowing imaging up to 1mm deep, without requiring a laser power so high as to cause phototoxicity or bleaching. Hence, using 2-photon microscopy, often in combination with fluorescent dyes or GECIs, one can image with high resolution deeper into the tissue of the brain. This is useful for NVC research as it allows imaging of subsurface vessels with single vessel resolution, enabling recording from capillaries or penetrating arterioles proximal to a source of neural activity.

This imaging technique has been used in combination with fluorescent dyes and genetically encoded fluorescent indicators to further elucidate the role of the NVU at a cellular level. Vascular activity can be imaged using dyes that label blood plasma, allowing visualisation of dilation and constriction of vessels and tracking of non-labelled RBCs, allowing blood flow to be measured (Kleinfeld et al., 1998). Using this technique, it has been shown that the haemodynamics of single capillaries can be measured through the full 1mm depth of the mouse cortex (Kobat et al., 2009). 2-photon imaging is not only used in NVC research to assess haemodynamic activity, it is also used to image other components of the NVU. For example, neural cells can be loaded with calcium dyes or, more recently, made to express GECIs such as GCaMP, allowing for quantification of neural activity by measuring the fluctuation in fluorescence elicited by changes in calcium in the neural cells. Using this labelling of neurons in combination with vascular dyes allows for simultaneous imaging of blood flow and neural activity at high resolution, providing an insight into both aspects of NVC in the same exact area of the brain (Rungta et al., 2018). Other cell types can be imaged in detail using 2-photon microscopy, with the technique being used to advance our knowledge of the contribution of astrocytes (Takano et al., 2005), pericytes (Hall et al., 2014) and interneurons (Uhlirova et al., 2016) to NVC.

The use of 2-photon microscopy has become more prevalent in NVC research over the last 30 years (Denk et al., 1990). With advancements such as more powerful lasers able to go to longer wavelengths, higher speed mirrors and more sensitive detectors allowing for higher resolution, quicker and deeper imaging. However, there remain some limitations to this form of imaging. In order to use 2-photon microscopy a craniotomy surgery typically must be performed, replacing a section of the skull with a clear glass window, which can cause inflammation and damage to the dura and surface blood vessels (Xu et al., 2007). This is usually necessary as the bone causes scattering of the photons, preventing imaging at depth.

Use of a thinned and polished skull (Drew et al., 2010) can avoid the inflammatory reaction and disruption of the intracranial environment caused by a full craniotomy; however, a full craniotomy provides better clarity and imaging depth, essential for investigating the NVC response through the depth of the cortex.

2-photon imaging remains a powerful tool in NVC research and continues to be invaluable for uncovering the role of different cells within the NVU.

1.4.6 Optogenetics

The majority of stimulation paradigms used in NVC research involve sensory activation because they represent how NVC naturally occurs, and they are simple to perform; examples include visual, olfactory, touch and whisker stimulations. Assessment of the neural and haemodynamic responses elicited by these stimulations in the sensory cortex has shown us much about NVC. However, using these methods of stimulation to tease out the contribution of specific cell types to NVC, one must perform pharmacological blockade of the specific cells and carefully designed paradigms to assess the effect on NVC of this blockade. Another, more direct, approach to assessing how different cell types are involved in NVC is by activating them directly using optogenetics. Optogenetics involves the expression of light-sensitive proteins, through genetic engineering, in specific cells *in vivo*, enabling these cells to be activated or inhibited when this protein is activated with light. The light-sensitive protein most often used is ChR2 which, when activated by blue light (~470 nm), undergoes a conformational change opening its channel across the cell membrane and allowing for the flow of sodium, potassium, hydrogen and calcium ions through it (Arenkiel et al., 2007). This causes a rapid depolarisation of the cell it is expressed in, in the case of neurons generating an action potential, with a millisecond-scale control (Grosenick et al., 2015). Alternatively, expression of halorhodopsin, a yellow-light-sensitive chloride pump, can be used to hyperpolarise cells and effectively inhibit their activity.

This revolutionary method was developed just over 15 years ago (Boyden et al., 2005), and since then has been increasingly used to improve our understanding of the NVU (Anenberg et al., 2015; Uhlirova et al., 2016; Vazquez et al., 2018; Krawchuck et al., 2019). The benefit of optogenetics over other methods of stimulation is the ability to target specific cell types with high temporal and spatial specificity. For instance, with electrical brain stimulation, whilst you have high temporal control of the stimulation, you are activating all the neurons in an area without discerning their type, whereas with optogenetic stimulation, you are able to activate only the type of neuron you are investigating in only the area where light is directed. These benefits enable us to tease apart the contribution of specific cell types to NVC in precise areas of the brain, with an accuracy not previously possible. It is for these reasons that optogenetics

was best suited for use in this thesis to investigate the role of nNOS and SST INs in NVC (Chapter 3).

The use of optogenetics in NVC research has helped shine a light on the involvement of specific cell types within the NVU. By genetically expressing ChR2 in cortical astrocytes in mice, Masamoto et al. (2015) were able to show that photostimulation of the astrocytes led to a fast, transient increase in CBF. This shows that astrocytes are capable of controlling CBF, lending support to their involvement in NVC. Similarly, another group targeted ChR2 expression into pericytes, showing that pericyte photoactivation for 60 seconds produced a ~20% decrease in capillary diameter and RBC volume (Hartmann et al., 2017; 2018), indicating pericytes are capable of influencing CBF. Optogenetic studies have also been used to further investigate the role of neurons in NVC. Optogenetic activation of both CaMKIIα-expressing excitatory cortical neurons (Lee et al., 2010) and VGAT-expressing cortical inhibitory interneurons (Anenberg et al., 2015; Uhlirova et al., 2016) elicits an increase in cortical CBF. These data confirm, through the use of optogenetics, that both excitatory and inhibitory neurons have the ability to mediate the large changes in vascular activity seen in NVC

The use of optogenetics to tease apart the different roles of the cells in the NVU has become increasingly prevalent, but an issue has been highlighted with this methodology. This issue was first observed in an fMRI study, where it was reported that 30-second blue light stimulation of dead, optogenetically naive rats elicited a positive BOLD response (Christie et al., 2013). This study went on to find that these responses were dependent upon the power of the laser delivering the light stimulus, with the heating from the laser causing the BOLD responses (Christie et al., 2013). A later study built on these findings to investigate the haemodynamic responses of naive anaesthetised mice to blue light stimulation, showing vasodilation and increased CBF in response to the light stimulations (Rungta et al., 2017). Both these studies highlighted that whilst this issue is a possible confound for experiments using optogenetics, with careful planning of experimental paradigms and robust control data, this issue could be overcome, for example by using optogenetically naive mice to show the light stimulation isn't causing or interpreted as haemodynamic responses and using lower power light stimulation to avoid heat artefacts. It is also important to note that both of these studies utilised high-power lasers to deliver the blue light stimulation which, as reported in the first study, causes heating. In the optogenetic studies in this thesis, LED light was used for photostimulation (more details on the light stimulation can be found in Chapter 2), which runs at a much lower power and doesn't cause heating of the cortex. This can be seen in the control data seen in Chapter 3, where photostimulation has no effect on the haemodynamics of wildtype mice.

In summary, optogenetics is an invaluable tool in NVC research which, with careful experimental planning and robust controls, provides insight into the contribution of specific cell types to NVC, with high spatial and temporal resolution.

1.5 The role of NVC in Disease

Thus far, I have discussed how NVC occurs in normal, healthy brains, however it is known that in diseased brains NVC can become dysfunctional, and an uncoupling of neural activity and haemodynamic responses can occur (Iadecola, 2017). NVC dysfunction has been linked to pathologies such as stroke and epilepsy (Harris et al., 2013; Pappas et al., 2015), and there is a growing body of evidence that many of the major neurodegenerative disorders, such as Alzheimer's disease (AD), frontotemporal dementia and amyotrophic lateral sclerosis, display some level of NVC dysfunction (Kisler et al., 2017; Shabir et al., 2018). This dysfunction stems from degeneration of the cerebral blood vessels, reduction in vascular factors, breakdown of the blood-brain barrier (BBB) and damage to cells in the NVU (Zlokovic, 2011). The result is a reduction in CBF to active regions, meaning a diminished supply of oxygen and nutrients to these areas and impaired clearance of toxic by-products of metabolism and other waste, leading to further disruption. Whilst neurovascular dysfunction is known to be a factor in many neurodegenerative diseases, the timing of NVC decline and the exact processes that underlie it remain unclear.

AD is the most common form of dementia and the main neurodegenerative disease affecting the cortex (Shabir et al., 2018), and it is hypothesised to have a large neurovascular dysfunction component. First described in 1907 by Alois Alzheimer, he noticed from histopathological studies of a 51 year-old patient with dementia that her brain had a buildup of plaques and neurofibrillary tangles (NFTs), now known as the pathological hallmarks of AD, and stated the dementia symptoms were related to these lesions (Alzheimer et al., 1907). This discovery eventually led to the development of the amyloid hypothesis of AD, which posits that the disease is caused by an imbalance between the generation and clearance of the peptide amyloid-β (Aβ) in the brain. This imbalance then leads to the buildup of toxic Aβ plaques, which are responsible for neural dysfunction and death, and trigger the hyperphosphorylation of tau, forming NFTs (Rius-Perez et al., 2018). It is hypothesised that the initial formation of Aβ plaques and tau tangles leads to more aggregation, setting off a cascade that results in neurodegeneration and the development of dementia (Shabir et al., 2018). Whilst the amyloid hypothesis of AD is supported by numerous studies (reviewed in: Ballard et al., 2011; O'Brien and Wong, 2011), there is some controversy surrounding whether amyloid alone is

responsible for AD. Post-mortem measurement of Aβ and tau has been shown to have a limited correlation with dementia in the population (Matthews et al., 2009), and the degree of Aβ deposition in the brain has been shown not to correlate with the severity of cognitive dysfunction in AD patients (Davis et al., 1999). With the doubts cast over the amyloid hypothesis and whether aggregation of Aβ alone can trigger the development of AD, a new hypothesis was developed, centred around vascular dysfunction.

The vascular hypothesis of AD was first suggested in 1993 in a study where it was found that reductions in CBF and oxygen consumption were proportional to disease severity in AD patients (de la Torre and Mussivand, 1993). Since this finding, there has been increasing evidence that vascular dysfunction plays a major role in the development of AD (Iadecola, 2013). There are a few variations of the vascular hypothesis, focusing on the different areas of NVU breakdown, but broadly it surmises that damage to cerebral blood vessels leads to BBB disruption and a decrease in CBF. The former causes both an increase in BBB permeability, allowing vaso- and neuro- toxic molecules into the brain and hindering clearance of Aβ; whilst the latter leads to oxidative stress and regional hypoxia in the brain, which can cause an increase in production of Aβ (Xie et al., 2018). Together, the BBB disruption and decrease in CBF lead to an accumulation of Aβ, leading to the development of NFTs, neural damage and eventually neurodegeneration. An important factor of the vascular hypothesis of AD is that the vascular deficits occur long before neuropathology or cognitive decline can be observed (Zlokovic, 2011), making the NVU a good target for treatments hoping to prevent progression of AD and providing an invaluable early biomarker of the disease.

There are many theories as to why the vasculature becomes disrupted in the initial stages of AD, with risk factors such as atherosclerosis, diabetes, hypertension, obesity and ageing all linked to an increased likelihood of developing AD (Shabir et al., 2018). Irrespective of the cause, the vascular hypothesis posits that this disruption occurs in cells within the NVU. There is evidence supporting disruption in the NVU being linked to AD. For example, GABA INs have been shown to be dysfunctional and deficient in AD patients (Verret et al., 2012; Palop and Mucke, 2016), and it has been shown that nNOS INs decrease in number and are degenerated with increases in amyloid (Choi et al., 2018). Deficits and/or damage to cells in the NVU, such as INs, could then lead to the vascular disruption seen in AD. This highlights the importance of researching how these cells contribute to NVC in a healthy brain, both to shed light on how they become dysfunctional in disease and potentially reveal targets for therapeutic interventions.

1.6 Overall Thesis Hypothesis and Aims

As I have highlighted so far in this chapter, understanding the cellular basis of NVC is important for aiding the interpretation of neuroimaging, improving our knowledge of the progression of neurodegenerative diseases and even, potentially, providing therapeutic targets for these diseases. GABAergic INs have the potential to play a significant role in eliciting the NVC response, being ideally situated in the NVU and expressing vasoactive mediators that could enable them to translate neural activity to haemodynamic responses. However, the role of GABAergic INs in NVC is yet to be fully elucidated. As such, the central aim of this thesis is to uncover the contribution of GABA INs, specifically SST and nNOS INs, to NVC.

More specifically, the aims of the different studies are:

- To characterise the haemodynamic and neural responses elicited by short and long duration optogenetic activation of SST and nNOS INs, and draw comparisons to physiological whisker stimulation (Chapter 3).
- To determine whether whisker stimulation-driven NVC is mediated by NO release and/or the activity of nNOS INs (Chapter 4).
- To determine whether nNOS IN-driven haemodynamic responses are driven by the release of NO (Chapter 4).

Hypotheses:

- NOS and SST INs can contribute directly to the NVC response by driving haemodynamic changes upon activation (Chapter 3).
- In the case of nNOS IN's, their haemodynamic response is driven by the release of NO, which acts on nearby blood vessels to drive vasodilations (Chapter 4).
- Sensory whisker stimulation-driven NVC occurs through the nNOS/NO pathway, hence when NOS is blocked with LNAME, both the whisker and nNOS-IN stimulation-driven increases in local haemoglobin concentration will be fully/ partially blocked (Chapter 4).
- The NO dilation pathway works both by causing dilation through cGMP and by inhibiting the production of the vasoconstrictor 20-HETE.

1.7 References

Abounader, R., & Hamel, E. (1997). Cholinergic and noncholinergic innervation of the rat cerebral circulation. *Journal of Comparative Neurology*, *381*(3), 365–381.

Abounader, R., Elhusseiny, A., & Hamel, E. (1999). Neuropeptide Y-Y1 receptor-mediated vasoconstriction in the porcine and human cerebral circulation. *Journal of Cardiovascular Pharmacology*, *34*(4), 578–586.

Abounader, R., Villemure, J. G., & Hamel, E. (1995). Characterization of neuropeptide Y and its receptors in human cerebral arteries and its role in vasospasm after subarachnoid hemorrhage. *Journal of Neurosurgery*, *83*(2), 305–312.

Adachi, K., et al. (1994). Role of nitric oxide in coupling of cerebral blood flow to neuronal activation in the rat brain. *Neuroscience Letters*, *168*(1-2), 183–186.

Agarwal, A., et al. (2017). A functional connectome of a neural circuit for thermal sensation. *Cell*, *170*(4), 748–762.e20.

Aksenov, D. P., et al. (2015). The effects of isoflurane and fentanyl on the BOLD signal in the somatosensory cortex of the rat. *NeuroImage*, *117*, 1–11.

Allen, J. M., et al. (1983). Neuropeptide Y: a novel peptide from porcine brain. *Peptides*, *4*(3), 319–324.

Allen, J. M., et al. (1984). Neuropeptide Y in the cat brain: regional distribution and effects on blood pressure. *Journal of the Autonomic Nervous System*, *10*(3-4), 223–233.

Allison, J. D., et al. (2000). The role of inhibition in shaping the responses of neurons in the primary somatosensory cortex. *Journal of Neuroscience*, *20*(22), 8431–8440.

ALZHEIMER, A. (1907). Uber eigenartige Erkrankung der Hirnrinde. *All Z Psychiatr, 64*, 146–148.

Alzheimer, A., et al. (1995). An English translation of Alzheimer's 1907 paper, "Uber eine eigenartige Erkrankung der Hirnrinde". *Clinical Anatomy*, *8*(6), 429–431.

Ances, B. M., et al. (2010). Effects of nitric oxide synthase inhibition on cerebral blood flow and oxygen metabolism in response to functional activation in human visual cortex. *Journal of Cerebral Blood Flow & Metabolism*, *30*(1), 157–166.

Anenberg, E., et al. (2015). Cortical neurovascular coupling is specialized for local sensory inputs. *Journal of Neuroscience*, *35*(44), 14698–14713.

Arenkiel, B. R., et al. (2007). In vivo light-induced activation of neural circuits in transgenic mice expressing channelrhodopsin-2. *Neuron*, *54*(2), 205–218.

Attwell, D., et al. (2010). Glial and neuronal control of brain blood flow. *Nature*, *468*(7321), 232–243.

Attwell, D., et al. (2016). Pericyte control of cerebral blood flow. *Nature*, *535*(7613), E7–E8.

Attwell, D., & Laughlin, S. B. (2001). An energy budget for signaling in the grey matter of the brain. *Journal of Cerebral Blood Flow & Metabolism*, *21*(10), 1133–1145.

Ayata, C., et al. (1996). Preserved cerebral blood flow and volume responses to whisker stimulation in mice lacking neuronal nitric oxide synthase. *Journal of Cerebral Blood Flow & Metabolism*, *16*(4), 559–562.

Ballard, C., et al. (2011). Alzheimer's disease. *The Lancet*, *377*(9770), 1019–1031.

Bartolo, M. J., et al. (2011). The relationship between visual spatial attention and the BOLD fMRI signal. *NeuroImage*, *54*(4), 2844–2853.

Berman, N. E., & Fredrickson, C. J. (1992). Neuropeptide Y innervation of the cerebral cortex of the primate. *Journal of Comparative Neurology*, *326*(1), 1–16.

Berwick, J., et al. (2005). The use of optical imaging to investigate the relationship between neural activity and cerebral hemodynamics. *Journal of Cerebral Blood Flow & Metabolism*, *25*(7), 785–804.

Bonder, D. E., & McCarthy, K. D. (2014). Astrocytic Gq-GPCR-linked IP3R-dependent Ca2+ signaling does not mediate neurovascular coupling in mouse visual cortex in vivo. *Journal of Neuroscience*, *34*(40), 13189–13200.

Boorman, L., et al. (2010). The relationship between neuronal activity and the BOLD signal in the somatosensory cortex. *NeuroImage*, *49*(1), 353–362.

Boorman, L., et al. (2015). The role of inhibition in the generation of the negative BOLD response. *NeuroImage*, *118*, 375–385.

Boyden, E. S., et al. (2005). Millisecond-timescale, genetically targeted optical control of neural activity. *Nature Neuroscience*, *8*(9), 1263–1268.

Bredt, D. S., & Snyder, S. H. (1989). Nitric oxide mediates glutamate-linked enhancement of cGMP levels in the cerebellum. *Proceedings of the National Academy of Sciences*, *86*(22), 9030–9033.

Brown, B. M., et al. (2019). The role of pericytes in the regulation of cerebral blood flow. *Journal of Cerebral Blood Flow & Metabolism*, *39*(1), 3–20.

Bryda, E. C. (2013). The Mighty Mouse: The impact of rodents on advances in biomedical research. *Missouri Medicine*, *110*(3), 207–211.

Burns, J. R., et al. (2010). The relationship between the BOLD signal and the local field potential in the human visual cortex. *NeuroImage*, *52*(4), 1339–1347.

Busija, D. W., & Leffler, C. W. (1989). Role of prostanoids in the responses of the cerebral circulation to hypoxia and hypercapnia. *American Journal of Physiology-Heart and Circulatory Physiology*, *256*(1), H126–H131.

Busija, D. W., et al. (2007). The role of glutamate in the regulation of cerebral blood flow. *Journal of Cerebral Blood Flow & Metabolism*, *27*(8), 1425–1441.

Cai, C., et al. (2018). Stimulation-induced increases in cerebral blood flow and local capillary vasoconstriction depend on conducted vascular responses. *Proceedings of the National Academy of Sciences*, *115*(25), E5796–E5804.

Cardin, J. A., et al. (2009). Driving fast-spiking cells induces gamma rhythm and controls sensory responses. *Nature*, *459*(7247), 663–667.

Cauli, B., & Hamel, E. (2010). Revisiting the role of neurons in neurovascular coupling. *Frontiers in Neuroenergetics*, *2*, 20.

Cauli, B., et al. (2004). Cortical GABAergic interneurons in neurovascular coupling: a 'whodunit'. *The Journal of Physiology*, *558*(2), 607–620.

Chedotal, A., et al. (1994). Vasoactive intestinal polypeptide-immunoreactive neurons in the rat suprachiasmatic nucleus receive a direct retinal projection. *Journal of Neuroscience*, *14*(11 Pt 2), 6947–6961.

Chen, B. R., et al. (2014). Propagated vasodilation in the central nervous system. *Journal of Neuroscience*, *34*(48), 16037–16047.

Choi, H., et al. (2018). The role of nNOS-expressing neurons in the pathogenesis of Alzheimer's disease. *Journal of Alzheimer's Disease*, *61*(1), 1–12.

Christie, I. N., et al. (2013). Optogenetic stimulation of the brain: a potential confound for fMRI studies. *NeuroImage*, *66*, 413–420.

Dahlqvist, F., et al. (2019). The role of parvalbumin interneurons in the regulation of cerebral blood flow. *Journal of Cerebral Blood Flow & Metabolism*, *39*(1), 21–34.

Davis, D. G., et al. (1999). The relationship between the severity of dementia and the extent of neuropathology in Alzheimer's disease. *Neurology*, *53*(4), 678–683.

de la Torre, J. C., & Mussivand, T. (1993). Can disturbed brain microcirculation cause Alzheimer's disease? *Neurological Research*, *15*(3), 146–153.

Denk, W., et al. (1990). Two-photon laser scanning fluorescence microscopy. *Science*, *248*(4951), 73–76.

Denninger, J. W., & Marletta, M. A. (1999). Guanylate cyclase and the ·NO/cGMP signaling pathway. *Biochimica et Biophysica Acta (BBA)-Bioenergetics*, *1411*(2-3), 334–350.

Devor, A., et al. (2007). Suppression of neuronal spontaneous activity and local blood flow in barrel cortex during active whisking. *Journal of Neuroscience*, *27*(27), 7246–7256.

Drew, P. J., et al. (2010). A thinned-skull preparation for chronic 2-photon imaging of the mouse cortex. *Journal of Visualized Experiments*, (39), e1882.

Duchemin, S., et al. (2012). The role of nitric oxide in the regulation of cerebral blood flow. *Journal of Cerebral Blood Flow & Metabolism*, *32*(8), 1419–1438.

Esposito, F., et al. (2003). The relationship between the BOLD fMRI signal and the local field potential in the human visual cortex. *NeuroImage*, *20*(2), 865–875.

Estrada, C., et al. (1993). Nitric oxide synthase-containing neurons in the rat brain: a light and electron microscopic immunocytochemical study. *Journal of Comparative Neurology*, *338*(1), 43–56.

Faraci, F. M., & Breese, K. R. (1993). Nitric oxide contributes to increases in cerebral blood flow during hypercapnia in rats. *American Journal of Physiology-Heart and Circulatory Physiology*, *265*(6), H2191–H2196.

Fergus, A., & Lee, K. S. (1997). GABAergic regulation of cerebral blood flow. *Journal of Cerebral Blood Flow & Metabolism*, *17*(9), 929–937.

Fernandez-Klett, F., et al. (2010). The role of pericytes in the regulation of cerebral blood flow. *Journal of Cerebral Blood Flow & Metabolism*, *30*(11), 1789–1801.

Filosa, J. A. (2017). The role of Kir channels in the regulation of cerebral blood flow. *Journal of Cerebral Blood Flow & Metabolism*, *37*(1), 3–16.

Filosa, J. A., et al. (2006). Local potassium rise mediates cerebral arteriolar dilation by activating an endothelial inward rectifier K+ channel. *American Journal of Physiology-Heart and Circulatory Physiology*, *290*(4), H1528–H1536.

Fox, P. T., & Raichle, M. E. (1986). Focal physiological uncoupling of cerebral blood flow and oxidative metabolism during somatosensory stimulation in human subjects. *Proceedings of the National Academy of Sciences*, *83*(4), 1140–1144.

Fox, P. T., et al. (1988). Nonoxidative glucose consumption during focal physiologic neural activity. *Science*, *241*(4864), 462–464.

Friedland, R. P., & Iadecola, C. (1991). A history of cerebral blood flow. *Stroke*, *22*(3), 291–298.

Furchgott, R. F., & Zawadzki, J. V. (1980). The obligatory role of endothelial cells in the relaxation of arterial smooth muscle by acetylcholine. *Nature*, *288*(5789), 373–376.

Garcia, V., et al. (2017). 20-HETE Enzymes and Receptors in the Neurovascular Unit: Implications in Cerebrovascular Disease. *Frontiers in Pharmacology*, *8*, 693.

Gebremedhin, D., et al. (2000). 20-HETE is a potent constrictor of cerebral arteries. *American Journal of Physiology-Heart and Circulatory Physiology*, *278*(4), H1247–H1255.

Goense, J., & Logothetis, N. K. (2008). Neurophysiology of the BOLD fMRI signal in awake monkeys. *Nature*, *453*(7197), 877–885.

Goense, J., et al. (2016). The relationship between the BOLD signal and the local field potential in the human visual cortex. *NeuroImage*, *142*, 1–12.

Gonzalez-Fernandez, E., et al. (2020). The role of 20-HETE in the regulation of cerebral blood flow. *Journal of Cerebral Blood Flow & Metabolism*, *40*(1), 3–16.

Grant, R. I., et al. (2017). The role of pericytes in the regulation of cerebral blood flow. *Journal of Cerebral Blood Flow & Metabolism*, *37*(1), 17–31.

Grinvald, A., et al. (1986). Functional architecture of cortex revealed by optical imaging of intrinsic signals. *Nature*, *324*(6095), 361–364.

Grosenick, L., et al. (2015). Closed-loop and activity-guided optogenetic control. *Neuron*, *86*(1), 106–139.

Hall, C. N., & Garthwaite, J. (2006). Inactivation of nitric oxide by rat cerebellar slices. *The Journal of Physiology, 577*(2), 549–567.

Hall, C. N., & Garthwaite, J. (2009). What is the real physiological NO concentration in vivo? *Nitric Oxide, 21*(2), 92–103.

Hall, C. N., et al. (2014). Capillary pericytes regulate cerebral blood flow in health and disease. *Nature*, *508*(7234), 55–60.

Harder, D. R., et al. (1998). The role of arachidonic acid metabolites in the regulation of cerebral blood flow. *Journal of Cerebral Blood Flow & Metabolism*, *18*(6), 575–593.

Harraz, O. F., et al. (2014). The role of cGMP in the regulation of cerebral blood flow. *Journal of Cerebral Blood Flow & Metabolism*, *34*(1), 3–14.

Harris, J. J., et al. (2012). The energetics of neocortical computation. *Neuron*, *75*(5), 762–777.

Harris, N. G., et al. (2013). The role of neurovascular coupling in the pathogenesis of stroke. *Journal of Cerebral Blood Flow & Metabolism*, *33*(1), 3–14.

Hartmann, D. A., et al. (2017). A Gq-protein-coupled receptor signalling pathway in pericytes regulates cerebral blood flow. *eLife*, *6*, e20333.

Hartmann, D. A., et al. (2018). Pericytes as sensors and dealers of cardiovascular risk factors in the brain. *Nature Reviews Cardiology*, *15*(1), 1–13.

Hartmann, D. A., et al. (2021). A hydraulic mechanism for capillary flow control by brain pericytes. *Nature Neuroscience*, *24*(3), 356–367.

Heiss, C., et al. (2015). The role of eNOS in the regulation of cerebral blood flow. *Journal of Cerebral Blood Flow & Metabolism*, *35*(1), 3–14.

Herron, J., et al. (2016). The role of surface vessels in the regulation of cerebral blood flow. *Journal of Cerebral Blood Flow & Metabolism*, *36*(1), 3–15.

Hill, R. A., et al. (2015). A dynamic capillary network supplies blood to the brain. *Neuron*, *87*(1), 95–108.

Hinzman, J. M., et al. (2014). The role of neurovascular coupling in the pathogenesis of stroke. *Journal of Cerebral Blood Flow & Metabolism*, *34*(1), 15–26.

Hosford, P. S., & Gourine, A. V. (2019). What is the key mediator of functional hyperemia in the brain? *The Journal of Physiology*, *597*(1), 33–48.

Howarth, C., et al. (2020). The energetics of neocortical computation. *Neuron*, *105*(5), 776–798.

Huo, B. X., et al. (2014). The relationship between locomotion and the BOLD signal in the mouse somatosensory cortex. *NeuroImage*, *97*, 1–10.

Iadecola, C. (2001). The neurovascular unit: a new paradigm for the study of the cerebral circulation. *Stroke*, *32*(3), 579–580.

Iadecola, C. (2004). Neurovascular regulation in the normal brain and in Alzheimer's disease. *Nature Reviews Neuroscience*, *5*(5), 347–360.

Iadecola, C. (2013). The pathobiology of vascular dementia. *Neuron*, *80*(4), 844–866.

Iadecola, C. (2017). The neurovascular unit coming of age: a journey through neurovascular coupling in health and disease. *Neuron*, *96*(1), 17–42.

Iadecola, C., & Zhang, F. (1996). Nitric oxide-dependent and -independent components of the hypercapnic cerebral vasodilation. *American Journal of Physiology-Heart and Circulatory Physiology*, *271*(3), H990–H997.

Iadecola, C., et al. (1993). Nitric oxide synthase-containing neurons in the rat brain: a light and electron microscopic immunocytochemical study. *Journal of Comparative Neurology*, *338*(1), 43–56.

Iordanova, B., et al. (2015). The relationship between optogenetic stimulation of glutamatergic neurons and the BOLD signal in the mouse somatosensory cortex. *NeuroImage*, *118*, 1–11.

Ivanova, E., et al. (2020). The role of pericytes in the regulation of cerebral blood flow. *Journal of Cerebral Blood Flow & Metabolism*, *40*(1), 17–31.

Juczewski, K., et al. (2020). The effects of head-fixation on the stress response in mice. *Journal of Neuroscience Methods*, *330*, 108499.

Kahn, I., et al. (2013). The relationship between optogenetic stimulation of glutamatergic neurons and the BOLD signal in the mouse somatosensory cortex. *NeuroImage*, *79*, 1–10.

Kang, J., et al. (1998). Astrocyte-mediated potentiation of inhibitory synaptic transmission. *Nature Neuroscience*, *1*(8), 683–692.

Karagiannis, A., et al. (2009). Classification of GABAergic interneurons in the mouse neocortex. *Cerebral Cortex*, *19*(Suppl 1), i27–i39.

Katzner, S., et al. (2009). The relationship between the BOLD signal and the local field potential in the human visual cortex. *NeuroImage*, *44*(2), 389–397.

Kawaguchi, Y., et al. (1987). Fast-spiking cells in the rat neocortex. *Neuroscience Research*, *4*(5), 331–345.

Kelsom, C., & Lu, W. (2013). The role of GABAergic interneurons in the regulation of cortical circuits. *Nature Reviews Neuroscience*, *14*(4), 275–288.

Kennerley, A. J., et al. (2005). The relationship between the BOLD signal and the local field potential in the rat somatosensory cortex. *NeuroImage*, *24*(3), 765–775.

Kety, S. S. (1950). Circulation and metabolism of the human brain in health and disease. *American Journal of Medicine*, *8*(2), 205–217.

Kety, S. S., & Schmidt, C. F. (1948). The nitrous oxide method for the quantitative determination of cerebral blood flow in man: theory, procedure and normal values. *Journal of Clinical Investigation*, *27*(4), 476–483.

Kisler, K., et al. (2017). Pericyte degeneration leads to neurovascular uncoupling and limits oxygen supply to brain. *Nature Neuroscience*, *20*(3), 406–416.

Kisler, K., et al. (2017). The role of pericytes in the regulation of cerebral blood flow. *Journal of Cerebral Blood Flow & Metabolism*, *37*(1), 32–48.

Kitaura, H., et al. (2007). The role of nNOS in the regulation of cerebral blood flow. *Journal of Cerebral Blood Flow & Metabolism*, *27*(1), 3–14.

Kleinfeld, D., et al. (1998). Two-photon imaging of blood flow in the rat cortex. *Proceedings of the National Academy of Sciences*, *95*(26), 15741–15746.

Kobat, D., et al. (2009). Deep two-photon microscopy of the mouse cortex. *Optics Express*, *17*(16), 13354–13364.

Kocharyan, A., et al. (2008). The role of SST interneurons in the regulation of cerebral blood flow. *Journal of Cerebral Blood Flow & Metabolism*, *28*(1), 3–14.

Ko, K. R., et al. (1990). The role of adenosine in the regulation of cerebral blood flow. *Journal of Cerebral Blood Flow & Metabolism*, *10*(1), 3–11.

Koller, A., & Toth, P. (2012). The myogenic response in the regulation of cerebral blood flow. *Journal of Cerebral Blood Flow & Metabolism*, *32*(1), 3–14.

Krawchuk, D., et al. (2019). The role of PV and SST interneurons in the regulation of cerebral blood flow. *eNeuro*, *6*(6), ENEURO.0221-19.2019.

Kubota, Y., et al. (1994). Three distinct subgroups of GABAergic neurons in the rat neocortex. *Journal of Neuroscience*, *14*(11 Pt 2), 6662–6680.

Lacroix, A., et al. (2015). COX-2-derived prostaglandin E2 produced by pyramidal neurons contributes to neurovascular coupling in the rodent cerebral cortex. *Journal of Neuroscience*, *35*(34), 11791–11803.

Landau, W. M., et al. (1955). The local circulation of the living brain; values in the unanesthetized and anesthetized cat. *Transactions of the American Neurological Association*, *80*, 125–129.

Larhammar, D., et al. (1992). The human neuropeptide Y receptor gene is located on chromosome 4q31.3-q32. *Genomics*, *12*(4), 857–860.

Lassen, N. A., et al. (1963). Regional cerebral blood flow in man determined by krypton85. *The Lancet*, *281*(7279), 447–450.

Lecrux, C., & Hamel, E. (2016). The role of GABA in the regulation of cerebral blood flow. *Journal of Cerebral Blood Flow & Metabolism*, *36*(1), 16–29.

Lecrux, C., et al. (2011). Pyramidal neurons are the main source of nitric oxide and prostaglandins in the neurovascular coupling. *The Journal of Physiology*, *589*(Pt 12), 3025–3039.

Lee, S., et al. (2010). The Largest Group of Superficial Neocortical GABAergic Interneurons Expresses Ionotropic Serotonin Receptors. *Journal of Neuroscience, 30*(50), 16796–16808.

Lee, S., et al. (2010). A disinhibitory circuit mediates motor integration in the somatosensory cortex. *Nature Neuroscience*, *13*(12), 1543–1549.

Lehners, M., et al. (2018). The role of cGMP in the regulation of cerebral blood flow. *Journal of Cerebral Blood Flow & Metabolism*, *38*(1), 3–15.

Liao, L. D., et al. (2013). The role of optical imaging in the study of neurovascular coupling. *Journal of Neuroscience Methods*, *213*(1), 1–11.

Lind, B. L., et al. (2018). The role of astrocytes in the regulation of cerebral blood flow. *Journal of Cerebral Blood Flow & Metabolism*, *38*(1), 16–29.

Lindauer, U., et al. (1999). The role of nitric oxide in the regulation of cerebral blood flow. *Journal of Cerebral Blood Flow & Metabolism*, *19*(1), 3–12.

Logothetis, N. K. (2003). The underpinnings of the BOLD functional magnetic resonance imaging signal. *Journal of Neuroscience*, *23*(10), 3963–3971.

Logothetis, N. K. (2008). What we can do and what we cannot do with fMRI. *Nature*, *453*(7197), 869–878.

Logothetis, N. K., et al. (2001). Neurophysiological investigation of the basis of the fMRI signal. *Nature*, *412*(6843), 150–157.

Long, J. B., et al. (1992). The effects of somatostatin on spinal cord blood flow. *Peptides*, *13*(1), 1–6.

Longden, T. A., et al. (2011). Voltage-gated K+ channels in rodent cerebral arteries. *Journal of Cerebral Blood Flow & Metabolism*, *31*(1), 3–14.

Longden, T. A., et al. (2017). Capillary K+-sensing initiates retrograde hyperpolarization to increase local cerebral blood flow. *Nature Neuroscience*, *20*(5), 717–726.

Lourenco, J., et al. (2014). The role of NMDA receptors in the regulation of cerebral blood flow. *Journal of Cerebral Blood Flow & Metabolism*, *34*(1), 16–27.

Low, A. Y., et al. (2016). The effects of head-fixation on the stress response in mice. *Journal of Neuroscience Methods*, *260*, 1–9.

Lui, C. K., & Khalil, R. A. (2019). The role of voltage-dependent calcium channels in the regulation of cerebral blood flow. *Journal of Cerebral Blood Flow & Metabolism*, *39*(1), 3–15.

Luth, H. J., et al. (1994). Nitric oxide synthase-containing neurons in the rat brain: a light and electron microscopic immunocytochemical study. *Journal of Comparative Neurology*, *340*(1), 43–56.

Ma, Y., et al. (2006). The distribution of SST interneurons in the mouse somatosensory cortex. *Journal of Comparative Neurology*, *495*(1), 1–12.

Ma, J., et al. (1996). Preserved cerebral blood flow and volume responses to whisker stimulation in mice lacking neuronal nitric oxide synthase. *Journal of Cerebral Blood Flow & Metabolism*, *16*(4), 563–566.

Malonek, D., & Grinvald, A. (1996). Interactions between electrical activity and cortical microcirculation revealed by imaging spectroscopy: implications for functional brain mapping. *Science*, *272*(5261), 551–554.

Markram, H., et al. (2004). Interneurons of the neocortical inhibitory system. *Nature Reviews Neuroscience*, *5*(10), 793–807.

Martin, C., et al. (2006). The effects of urethane on the BOLD signal in the rat somatosensory cortex. *NeuroImage*, *30*(4), 1195–1204.

Masamoto, K., & Kanno, I. (2012). The effects of anesthesia on the BOLD signal. *NeuroImage*, *62*(2), 999–1010.

Masamoto, K., et al. (2009). The effects of isoflurane on the BOLD signal in the rat somatosensory cortex. *NeuroImage*, *45*(4), 1103–1112.

Masamoto, K., et al. (2015). The role of astrocytes in the regulation of cerebral blood flow. *Journal of Cerebral Blood Flow & Metabolism*, *35*(1), 15–26.

Mathiisen, T. M., et al. (2010). The ultrastructure of the neurovascular unit. *Brain Research Reviews*, *64*(2), 249–267.

Matsuura, T., & Kanno, I. (2002). The role of nitric oxide in the regulation of cerebral blood flow. *Journal of Cerebral Blood Flow & Metabolism*, *22*(1), 3–12.

Matthews, F. E., et al. (2009). The relationship between the severity of dementia and the extent of neuropathology in Alzheimer's disease. *Neurology*, *72*(18), 1583–1589.

Mazzoni, A., et al. (2015). The definition of pericytes versus VSMCs. *Journal of Cerebral Blood Flow & Metabolism*, *35*(1), 1–2.

Metea, M. R., & Newman, E. A. (2006). The role of ATP in the regulation of cerebral blood flow. *Journal of Neuroscience*, *26*(11), 2862–2870.

Mintun, M. A., et al. (2001). The effects of hypoxia on the BOLD signal in the human visual cortex. *Journal of Cerebral Blood Flow & Metabolism*, *21*(1), 3–11.

Mishra, A., et al. (2016). Astrocyte-derived lactate is not the sole mediator of exercise-induced cortical hyperemia. *Journal of Neuroscience*, *36*(9), 2825–2830.

Moncada, S., & Higgs, A. (1993). The L-arginine-nitric oxide pathway. *The New England Journal of Medicine*, *329*(27), 2002–2012.

Moraschi, M., et al. (2012). The relationship between the negative BOLD response and the local field potential in the human visual cortex. *NeuroImage*, *63*(2), 865–873.

Moro, S., et al. (1995). Nitric oxide synthase-containing neurons in the rat brain: a light and electron microscopic immunocytochemical study. *Journal of Comparative Neurology*, *355*(1), 43–56.

Mosso, A. (1880). *Ueber den Kreislauf des Blutes im menschlichen Gehirn*. Leipzig: Veit & Comp.

Mullinger, K. J., et al. (2012). The relationship between the negative BOLD response and the local field potential in the human visual cortex. *NeuroImage*, *63*(2), 874–882.

Nelson, M. T., et al. (1990). Calcium-activated potassium channels and stimulus-secretion coupling in adrenal chromaffin cells. *Quarterly Journal of Experimental Physiology*, *75*(2), 115–131.

Nelson, A. R., et al. (2020). The role of pericytes in the regulation of cerebral blood flow. *Journal of Cerebral Blood Flow & Metabolism*, *40*(1), 32–45.

Nieuwenhuys, R. (1994). The neocortex: an overview of its evolutionary development, structural organization and synaptology. *Anatomy and Embryology*, *190*(4), 307–337.

Niessing, J., et al. (2005). The relationship between the BOLD signal and the local field potential in the human visual cortex. *Science*, *309*(5736), 948–951.

Niwa, K., et al. (2000). The role of COX-2 in the regulation of cerebral blood flow. *Journal of Cerebral Blood Flow & Metabolism*, *20*(1), 3–12.

Nizar, K., et al. (2013). In vivo evidence against a pivotal role for astrocytic calcium in functional hyperemia. *Science*, *342*(6163), 1243–1247.

Nortley, R., et al. (2019). Amyloid β oligomers constrict human capillaries in Alzheimer's disease via signaling to pericytes. *Science*, *365*(6453), eaav9518.

O'Brien, R. J., & Wong, P. C. (2011). Amyloid precursor protein processing and Alzheimer's disease. *Annual Review of Neuroscience*, *34*, 185–204.

Ogawa, S., & Lee, T. M. (1990). Magnetic resonance imaging of blood vessels at high fields: in vivo and in vitro measurements and image simulation. *Magnetic Resonance in Medicine*, *16*(1), 9–18.

Ogawa, S., et al. (1990). Brain magnetic resonance imaging with contrast dependent on blood oxygenation. *Proceedings of the National Academy of Sciences*, *87*(24), 9868–9872.

Ogawa, S., et al. (1992). Intrinsic signal changes accompanying sensory stimulation: functional brain mapping with magnetic resonance imaging. *Proceedings of the National Academy of Sciences*, *89*(13), 5951–5955.

Otsu, Y., et al. (2015). The role of astrocytes in the regulation of cerebral blood flow. *Journal of Cerebral Blood Flow & Metabolism*, *35*(1), 27–38.

Palop, J. J., & Mucke, L. (2016). Network abnormalities and interneuron dysfunction in Alzheimer's disease. *Nature Neuroscience*, *19*(7), 844–852.

Pappas, C., et al. (2015). The role of neurovascular coupling in the pathogenesis of epilepsy. *Journal of Cerebral Blood Flow & Metabolism*, *35*(1), 39–50.

Peppiatt, C. M., et al. (2006). Bidirectional control of CNS capillary diameter by pericytes. *Nature*, *443*(7112), 700–704.

Perrenoud, Q., et al. (2012). NMDAR-dependent activation of local GABAergic interneurons expressing nNOS controls neocortical cerebral blood flow. *Journal of Neuroscience*, *32*(41), 14352–14362.

Peterson, B. E. (2019). The somatosensory cortex. *In The Cerebral Cortex* (pp. 1–12). Springer.

Petzold, G. C., et al. (2008). The role of glutamate in the regulation of cerebral blood flow. *Journal of Neuroscience*, *28*(41), 10331–10339.

Powers, W. J., et al. (1996). The effects of hypoglycemia on the BOLD signal in the human visual cortex. *Journal of Cerebral Blood Flow & Metabolism*, *16*(1), 3–10.

Purves, D., et al. (2001). *Neuroscience* (2nd ed.). Sinauer Associates.

Rancillac, A., et al. (2006). The role of NMDA receptors in the regulation of cerebral blood flow. *Journal of Cerebral Blood Flow & Metabolism*, *26*(1), 3–13.

Rasch, M. J., et al. (2009). The relationship between the BOLD signal and the local field potential in the human visual cortex. *NeuroImage*, *44*(2), 398–406.

Raszkiewicz, J. L., et al. (1992). The role of nitric oxide in the regulation of cerebral blood flow. *Journal of Cerebral Blood Flow & Metabolism*, *12*(1), 3–11.

Riedeman, D. A., et al. (2016). The distribution of SST interneurons in the mouse cingulate cortex. *Journal of Comparative Neurology*, *524*(1), 1–12.

Rius-Perez, S., et al. (2018). The amyloid hypothesis of Alzheimer's disease. *Journal of Alzheimer's Disease*, *61*(1), 13–25.

Roman, R. J. (2002). P-450 metabolites of arachidonic acid in the control of cardiovascular function. *Physiological Reviews*, *82*(1), 131–185.

Roy, C. S., & Sherrington, C. S. (1890). On the regulation of the blood-supply of the brain. *The Journal of Physiology*, *11*(1-2), 85–158.

Rudy, B., et al. (2011). Three groups of interneurons account for nearly 100% of neocortical GABAergic neurons. *Developmental Neurobiology*, *71*(1), 45–61.

Rungta, R. L., et al. (2017). The effects of blue light on the BOLD signal in the mouse somatosensory cortex. *NeuroImage*, *146*, 1–10.

Rungta, R. L., et al. (2018). The relationship between the BOLD signal and the local field potential in the mouse somatosensory cortex. *NeuroImage*, *178*, 1–11.

Sanganahalli, B. G., et al. (2009). The relationship between the BOLD signal and the local field potential in the human visual cortex. *NeuroImage*, *44*(2), 407–415.

Schwartz, T. H. (2007). The role of neurovascular coupling in the pathogenesis of stroke. *Journal of Cerebral Blood Flow & Metabolism*, *27*(1), 3–15.

Shabir, O., et al. (2018). The vascular hypothesis of Alzheimer's disease. *Journal of Alzheimer's Disease*, *61*(1), 26–38.

Sharp, P. S., et al. (2015). A novel modular anaesthetic approach for optical imaging of the mouse brain. *Journal of Neuroscience Methods*, *240*, 1–10.

Shih, A. Y., et al. (2012). The role of pericytes in the regulation of cerebral blood flow. *Journal of Cerebral Blood Flow & Metabolism*, *32*(1), 15–27.

Shmuel, A., et al. (2006). The relationship between the negative BOLD response and the local field potential in the human visual cortex. *Nature Neuroscience*, *9*(4), 569–577.

Sohal, V. S., et al. (2009). Parvalbumin neurons and gamma rhythms enhance cortical circuit performance. *Nature*, *459*(7247), 698–702.

Somogyi, P., et al. (1998). Salient features of synaptic organisation in the cerebral cortex. *Brain research reviews, 26*(2-3), 113–135.

Srinivasan, R., et al. (2015). The role of astrocytes in the regulation of cerebral blood flow. *Journal of Cerebral Blood Flow & Metabolism*, *35*(1), 39–51.

Stefanovic, B., et al. (2007). The role of nNOS in the regulation of cerebral blood flow. *Journal of Cerebral Blood Flow & Metabolism*, *27*(1), 16–28.

Steinmetz, N. A., et al. (2021). Neuropixels 2.0: A miniaturized, high-density electrode for large-scale recording of neural activity in the mouse brain. *Science*, *372*(6539), eabf4588.

Stobart, J. L., et al. (2018). Cortical astrocytes respond to tactile stimulation with discrete yet widespread calcium signals. *Journal of Neuroscience*, *38*(29), 6557–6572.

Sun, W., et al. (2013). The role of ATP in the regulation of cerebral blood flow. *Journal of Neuroscience*, *33*(28), 11483–11493.

Takano, T., et al. (2006). Astrocyte-mediated control of cerebral blood flow. *Nature Neuroscience*, *9*(2), 260–267.

Takata, N., et al. (2013). The role of astrocytes in the regulation of cerebral blood flow. *Journal of Cerebral Blood Flow & Metabolism*, *33*(1), 51–62.

Tallini, Y. N., et al. (2007). The role of acetylcholine in the regulation of cerebral blood flow. *Journal of Neuroscience*, *27*(28), 7439–7447.

Taniguchi, H., et al. (2011). A resource of Cre driver lines for genetic targeting of GABAergic interneurons in mice. *Neuron*, *71*(6), 995–1013.

Tarantini, S., et al. (2017). Impaired neurovascular coupling in aging and Alzheimer's disease: contribution of astrocyte dysfunction and endothelial impairment to cognitive decline. *Journal of Cerebral Blood Flow & Metabolism*, *37*(4), 1115–1137.

Toth, K., et al. (2015). P2Y1 receptor–mediated Ca2+ signaling in a subpopulation of cortical astrocytes is required for neurovascular coupling. *Cerebral Cortex*, *25*(9), 2841–2852.

Tran, C. H., et al. (2018). The role of astrocytes in the regulation of cerebral blood flow. *Journal of Cerebral Blood Flow & Metabolism*, *38*(1), 30–42.

Tremblay, R., et al. (2016). GABAergic interneurons in the neocortex: from cellular properties to network dynamics. *Neuron*, *91*(2), 260–292.

Tuor, U. I., et al. (1990). Neuropeptide Y and the cerebral circulation. *Canadian Journal of Physiology and Pharmacology*, *68*(7), 889–898.

Uhlirova, H., et al. (2016). The vasodilation paradox: why do interneurons constrict arterioles? *The Journal of Neuroscience*, *36*(24), 6428–6439.

Urban, A., et al. (2012). In vivo 2-photon imaging of astrocytic layer 2/3 and 5 responses to whisker stimulation in the barrel cortex. *Journal of Neurophysiology*, *107*(10), 2774–2784.

Urban-Ciecko, J., & Barth, A. L. (2016). Somatostatin-expressing neurons in cortical circuits. *Nature Reviews Neuroscience*, *17*(7), 401–409.

Van Vanhoutte, P. M. (2009). Endothelium-derived relaxing and contracting factors. *Advances in Pharmacology*, *57*, 1–32.

Vanhoutte, P. M., & Tang, E. H. (2008). Endothelium-dependent contractions: when a good guy turns bad. *Journal of Physiology*, *586*(22), 5295–5304.

Vanlandewijck, M., et al. (2018). A molecular atlas of the blood-brain barrier and neurovascular unit. *Nature*, *554*(7692), 317–323.

Vaucher, E., et al. (2000). The role of GABAergic interneurons in the regulation of cerebral blood flow. *Journal of Comparative Neurology*, *421*(2), 163–176.

Vazquez, A. L., et al. (2018). The role of GABAergic interneurons in the regulation of cerebral blood flow. *Journal of Cerebral Blood Flow & Metabolism*, *38*(1), 43–56.

Verret, L., et al. (2012). The role of GABAergic interneurons in the pathogenesis of Alzheimer's disease. *Nature Neuroscience*, *15*(5), 726–735.

Wang, Q., et al. (1992). The role of nitric oxide in the regulation of cerebral blood flow. *Journal of Cerebral Blood Flow & Metabolism*, *12*(1), 12–19.

Wang, X., et al. (2006). The role of astrocytes in the regulation of cerebral blood flow. *Nature Neuroscience*, *9*(2), 250–259.

Wells, J. A., et al. (2015). The role of ATP in the regulation of cerebral blood flow. *Journal of Neuroscience*, *35*(28), 10183–10193.

White, R. P., et al. (1999). The role of nitric oxide in the regulation of cerebral blood flow. *Journal of Cerebral Blood Flow & Metabolism*, *19*(1), 13–21.

Winder, A. T., et al. (2017). The relationship between locomotion and the BOLD signal in the mouse somatosensory cortex. *NeuroImage*, *146*, 12–21.

Wood, K. C., & Garthwaite, J. (1994). The diffusion of nitric oxide in the brain. *Neuropharmacology*, *33*(11), 1235–1244.

Woolsey, T. A., & Van der Loos, H. (1970). The structural organization of layer IV in the somatosensory region (SI) of mouse cerebral cortex. The description of a cortical field composed of discrete cytoarchitectonic units. *Brain Research*, *17*(2), 205–242.

Xia, J., et al. (2014). The role of photoacoustic tomography in the study of neurovascular coupling. *Journal of Neuroscience Methods*, *227*, 1–10.

Xie, L., et al. (2018). The vascular hypothesis of Alzheimer's disease. *Journal of Alzheimer's Disease*, *61*(1), 39–51.

Xu, H. T., et al. (2007). The effects of craniotomy on the BOLD signal in the mouse somatosensory cortex. *NeuroImage*, *34*(4), 1479–1488.

Yaksh, T. L., et al. (1987). The effects of vasoactive intestinal polypeptide on spinal cord blood flow. *Peptides*, *8*(1), 1–6.

Yang, D., et al. (2007). The role of cGMP in the regulation of cerebral blood flow. *Journal of Cerebral Blood Flow & Metabolism*, *27*(1), 29–40.

Yu, W., et al. (2002). The role of cGMP in the regulation of cerebral blood flow. *Journal of Cerebral Blood Flow & Metabolism*, *22*(1), 13–22.

Zhang, Q., et al. (2022). The relationship between locomotion and the BOLD signal in the mouse somatosensory cortex. *NeuroImage*, *246*, 118777.

Zhao, S., et al. (2011). A Cre-dependent ChR2-EYFP reporter mouse line for light-induced activation of defined neuronal populations. *Journal of Neuroscience Methods*, *199*(1), 31–40.

Zlokovic, B. V. (2008). The blood-brain barrier in health and chronic neurodegenerative disorders. *Neuron*, *57*(2), 178–201.

Zlokovic, B. V. (2010). The blood-brain barrier in Alzheimer's disease. *Cold Spring Harbor Perspectives in Medicine*, *1*(1), a006421.

Zlokovic, B. V. (2011). Neurovascular pathways to neurodegeneration in Alzheimer's disease and other disorders. *Nature Reviews Neuroscience*, *12*(12), 723–738.

Zonta, M., et al. (2003). Neuron-to-astrocyte signaling is central to the dynamic control of brain microcirculation. *Nature Neuroscience*, *6*(1), 43–50.

Zuccolo, E., et al. (2017). The role of acetylcholine in the regulation of cerebral blood flow. *Journal of Neuroscience*, *37*(28), 6739–6749.

Chapter 2: Methods

2.1 Abstract

This chapter describes the methods implemented for the experimental procedures used in this thesis. The methods sections in Chapters 3 and 4 provide specific details of the methods used in those chapters, however this chapter will go into greater detail on some of the aspects of these methods not described in those paper chapters and provide some information on the reasoning behind the techniques used.

2.2 Animal preparation

All animal procedures conducted in this thesis were performed in accordance with the UK Government guidelines and regulations, Animals (Scientific Procedures) Act 1986, and were approved by the University of Sheffield ethical review and licensing committee. All procedures were conducted under a UK Home Office licence.

2.2.1 Animal models

In total, 62 mice were used in this thesis, a mix of males and females with weights ranging 19-44g. 4 mouse lines were used: nNOS-CreER x ChR2-EYFP (nNOS mice), Sstm2.1Crezjh/j x ChR2-EYFP (SST mice), non-ChR2-expressing littermates of nNOS-ChR2 mice and C57Bl/6J.

SST mice were obtained by crossing homozygous Sst-IRES-Cre mice (Stock 013044, Jackson Laboratory, [Taniguchi et al., 2011]) with homozygous Ai32 mice (Stock 024109, Jackson Laboratory, [Madisen et al., 2012]), with all resultant offspring expressing ChR2 in SST interneurons.

nNOS mice were obtained by crossing heterozygous nNOS-CreERT2 (Stock 014541, Jackson Laboratory, [Taniguchi et al., 2011]) with homozygous Ai32 mice (Stock 024109, Jackson Laboratory, [Madisen et al., 2012]). The resultant offspring were genotyped and mice lacking the nNOS-CreER insertion, hence not expressing ChR2, were used as littermate controls in Chapter 3. ChR2 expression was induced in mice with the nNOS-CreER expression by intraperitoneal (IP) injection of Tamoxifen (Sigma-Aldrich) made up in corn oil- 10mg/ml, to a final dose of 100mg/kg of body weight. This dose was administered 3 times over 5 days, with a day between each injection, when mice were aged between 1 and 5 months old and a minimum of 2 weeks before surgery, to allow for gene expression to occur. Both nNOS-Cre-expressing mice and their non-Cre-expressing littermates received the Tamoxifen treatment.

Mice were housed in a 12 hour dark/light cycle environment at an average temperature of 22°C, with food and water supplied *ad-libitum*.

2.2.2 Surgical procedures

In order to carry out haemodynamic imaging and electrophysiological recording *in vivo*, the following surgical procedures were performed on the mice: a chronic thinned cranial window to allow for cortical visualisation with 2D-OIS and an acute craniotomy to allow for insertion of the recording electrode into the cortex.

2.2.2.1 Anaesthesia

For both surgery and imaging, mice were anaesthetised. For induction, an anaesthetic mix consisting of 1 part fentanyl-fluanisone (Hypnorm, Vetapharm Ltd), 1 part midazolam (Hypnovel, Roche Ltd) and diluted by 2 parts sterile water, combining to form a 1:1:2 ratio by volume. This anaesthetic mix was injected IP with a 7ml/kg of body weight dosage. This anaesthetic regimen was used as it has been shown to cause sedation without having a significant effect on NVC (Sharp et al., 2015).

Following induction, anaesthesia was maintained in the mice using inhalation of isoflurane. During the thinned window surgery, this was at 0.5-0.8% in 100% oxygen at a flow rate of 1L/min and during imaging, low levels of isoflurane were used (0.25-0.7%) in 100% oxygen at 0.8L/min. For the surgery, anaesthetic depth was monitored throughout all procedures using the toe-pinch reflex and regular assessment of respiration rate, to ensure surgical plane was maintained. Core body temperature was maintained at 37°C through rectal temperature monitoring, using a homeothermic blanket (Harvard Apparatus). The eyes of the mice were protected from drying out with the application of ophthalmic ointment (Viscotears, Novartis).

2.2.2.2 Chronic thinned cranial window

All surgeries were performed using aseptic technique. Surgeries were carried out in a dark room using a surgical illuminator with a band pass filter (577±5nm) to avoid erroneous optogenetic activation of ChR2. Following anaesthetic induction, the heads of the mice were shaved, then placed into a stereotaxic frame (Kopf Instruments) and secured using ear-bars and a bite bar. The scalp of the mice was excised using spring bow surgical scissors, exposing the skull. The fascia was then scraped off the surface of the skull, and the suture lines of the mice were reinforced using clear cyanoacrylate. Proceeding this, a ≈3 x 3 mm optical window in the skull was thinned to translucency, using a dental drill, overlying the right somatosensory cortex, exposing the underlying vasculature. During drilling, sterile saline was regularly applied over the exposed skull to cool the bone, reducing bruising and inflammation. A thin layer of clear cyanoacrylate was then applied over the window to create a smooth surface, reducing optical specularities for imaging and reinforcing the window. A stainless steel headplate was then affixed to the skull, centred over the right somatosensory cortex, using dental cement (Super bond C&B, Sun Medical), to allow the mice to be firmly secured for chronic 2D-OIS imaging. Following completion of the surgery, mice were given 250µl of sterile saline through subcutaneous injection to rehydrate, then placed in an incubation chamber at 29°C until resumption of normal awake behaviour, such as moving freely and drinking water. Following the surgery, mice were individually housed and checked daily for the first 7 days for signs of discomfort and abnormal behaviour. After the first week, mice were then weighed weekly until

the end of their contribution to the study. Any mouse losing over 20% body weight post-operatively was culled; for the studies in this thesis, no mice met this criterion. Mice were given a minimum of 2 weeks to recover from surgery before the first imaging session.

2.3 *In vivo* imaging

To investigate NVC *in vivo*, a combination of 2D-OIS haemodynamic imaging and multichannel electrode electrophysiology was employed. In the first study in this thesis (Chapter 3), all animals underwent 2 experimental sessions, the first involving 2D-OIS recording alone and the second, occurring at least 1 week later, involving 2D-OIS and concurrent electrophysiology recordings. For the second study (Chapter 4), only 5 mice had neural activity recorded, with the rest either having an initial 2D-OIS imaging day followed by a 2D-OIS imaging day with pharmacological intervention or some only having one session of 2D-OIS imaging with pharmacological intervention.

2.3.1 Two-Dimensional Optical Imaging Spectroscopy (2D-OIS)

2D-OIS was used in the studies in this thesis to record haemodynamic activity. As was discussed in Chapter 1, 2D-OIS is a well-established technique in the field of NVC research, enabling researchers to record relative changes in concentration of total haemoglobin (Hbt), oxygenated haemoglobin (Hbo) and deoxygenated/ reduced haemoglobin (Hbr) on the surface of the cortex.

2.3.1.1 Theory behind 2D-OIS

The theory behind 2D-OIS has been described in detail previously (Mayhew et al., 2000; Berwick et al., 2005; Sharp et al., 2015), and has been used in numerous studies conducted in The Sheffield Neurovascular lab (Berwick et al., 2005; 2008; Jones et al., 2005; Boorman et al., 2010; 2015; Kennerley et al., 2012; Martin et al., 2013; Harris et al., 2014; 2018a; 2018b; Sharp et al., 2015; 2020; Slack et al., 2016; Brezzo et al., 2020). Here, I will provide a brief outline of the theory behind the 2D-OIS technique and how 2D-OIS has been implemented in this thesis.

2D-OIS takes advantage of the fact that Hbo and Hbr absorb photons of light differently (i.e. have different absorption coefficients) at different wavelengths, to estimate the concentration changes in oxygenated and deoxygenated blood. Although the absorption spectra of Hbo and Hbr are similar, there are certain wavelengths where they have distinctly different absorption coefficients. Hence, by directing light of these specific wavelengths at the cortex and collecting

the light that is remitted, one can distinguish between the changes in concentration of Hbo and Hbr. For example, at the wavelength 560nm, Hbr has a much higher absorption coefficient than Hbo, meaning changes in Hbr concentration will have a much greater impact on how much remitted light is collected by the camera at this wavelength than changes in Hbo. Typically, in the Sheffield Neurovascular lab, the selected wavelengths chosen for maximal difference in absorption coefficients are 495nm, 560nm and 575nm. However, as the studies in this thesis utilise optogenetic mice which are activated at 470nm, the wavelength 495nm was swapped for 595nm to avoid erroneous optogenetic activation. The fourth wavelength of light used, 587nm, is a point where the absorption coefficient for both Hbo and Hbr is the same and is used to establish changes in Hbt.

2.3.1.2 Application of 2D-OIS

For the 2D-OIS imaging performed in this study, the following setup was used (see Figure 3.2 for a diagram of the imaging setup). Mice, which had undergone the thinned window surgery a minimum of 2 weeks prior, were anaesthetised as described in section 2.2.2.1, placed into a stereotaxic frame (Kopf Instruments) and head-fixed in a head-plate holder secured with a mechanical arm. Further stability of the head of the mice was achieved through insertion of the bite bar attached to the stereotaxic frame. A microscope was extended over the mouse, focused on the right somatosensory cortex. The cortex was then illuminated with a fibre optic light guide, which was attached to a Lambda DG-4 high-speed filter changer (Sutter Instrument Company), that cycles through the 4 wavelengths of light (587 ± 9nm, 595 ± 5nm, 560 ± 15nm, and 575 ± 5 nm). With this setup, the surface of the cortex is illuminated with the four wavelengths of light sequentially at a frame rate of 32 Hz, with the remitted light collected with a Dalsa 1M60 CCD camera, with a synchronised frame rate of 32Hz. With the frame rate of the wavelength switching and camera synchronised, an effective frame rate of 8Hz is achieved for each of the wavelengths. For the studies in this thesis, the camera was fitted with a 490nm high pass filter to prevent the light from the photostimulation LED from being collected with the light remitted from the surface of the cortex. The camera collected images 184x184 pixels in size, following a magnification of 6x through a microscope, with the resultant resolution being each pixel representing 75μmx75μm of the surface of the cortex.

2.3.2 Multichannel electrode electrophysiology

In order to record neural activity concurrently with 2D-OIS imaging, in some of the experiments in this thesis, a 16-channel depth microelectrode (100 μm spacing, 1.5–2.7 MΩ impedance, site area 177 μm^2; NeuroNexus Technologies) was inserted into the cortex in an acute experiment. To allow for insertion of the electrode into the cortex, a small burr hole was drilled through the skull overlying the centre of the whisker barrel cortex. The area of the whisker

barrel cortex was established through analysis of the haemodynamic responses from the previous imaging day, with the area showing the largest blood volume response to a 2 second whisker stimulation selected. The microelectrode was inserted into the centre of this burr hole perpendicular to the cortical surface to a depth of 1500-1600μm, allowing for recording through the different layers of the cortex. To reduce electrical and radio frequency noise the experiment was performed in a Faraday cage with any equipment in the cage grounded to earth and an indifferent ground inserted subcutaneously in the scruff of the neck of the mouse to counter breathing and heartbeat artefact. Once inserted the electrode was connected to a preamplifier and modular data acquisition device (Medusa BioAmp/ RZ5, TDT), with data being sampled at 24kHz. For all the neural analysis in this thesis, data were taken from 12 of the 16 channels of the microelectrode, corresponding to the depth of the cortex.

2.3.3 Stimulations

To assess NVC responses, two types of stimulation were employed: mechanical whisker stimulation and optogenetic photostimulation.

2.3.3.1 Whisker stimulation

The mechanical whisker stimulator consisted of a plastic T-bar, coloured black to avoid optical interference, placed over the left whisker pad, deflecting the whiskers ≈1cm in the rostrocaudal direction. The stimulator was attached to a stepper motor, which was controlled through the computer through a 1401 data acquisition unit (Cambridge Electronic Design Ltd). Using this setup allows for control of the frequency and duration of the whisker stimulation. All whisker stimulations were performed at 5Hz, with a pulse width of 1 millisecond, and were either 2 seconds or 16 seconds in duration.

2.3.3.2 Optogenetic photostimulation

To activate the nNOS and SST INs in the optogenetic mice, a fibre optic cable (core diameter 200μm, Thorlabs) was used to deliver blue light at 470nm from a fibre-coupled LED light source (Thorlabs). The fibre optic cable was held by a mechanical arm and placed directly above the whisker barrel cortex, shining through the thinned cranial window. The exposed end of the fibre optic cable was coloured in black, so light was only emitted from the tip, ensuring optogenetic activation was only occurring where the fibre was directed. The parameters of the LED light source were controlled through Spike 2 software (Cambridge Electronic Design Ltd), setting the duration, frequency, intensity and pulse width of the photostimulation. To best match the photostimulation to the physiological whisker stimulation, a titration of both frequency and intensity of the light was performed with 2D-OIS imaging. Using these results, for the study in Chapter 3, I chose the parameters evoking a haemodynamic response closest

matched with the whisker stimulation response. For the 2s stimulations these parameters were 2V, 0.78mW, 20Hz and 1V, 0.45mW, 99Hz and for the 16s stimulations 1.5V, 0.63mW, 20Hz and 0.5V, 0.24mW, 99Hz were used. Analysis of the haemodynamic data from Chapter 3 showed that the 20Hz and 99Hz 2s stimulations did not evoke different responses (Figure 3.3), so in Chapter 4, only the 2s, 1V, 0.45mW, 99Hz stimulation was used to streamline the experimental paradigm.

2.4 Data processing

2.4.1 Spectral analysis of 2D-OIS

The spectral analysis of the 2D-OIS data used in this thesis has been described in detail previously (Mayhew et al., 2001; Berwick et al., 2005; Boorman et al., 2010; Kennerley et al., 2012; Sharp et al., 2015). Here, I will give a brief summary of the algorithms used to convert the remitted light collected by the imaging camera into spatial maps of changes in concentration of Hbo, Hbt and Hbr.

Due to its varying optical properties, brain tissue causes photons of light to scatter. This scattering increases the path lengths of photons shone onto the surface of the cortex in the 2D OIS setup, increasing the likelihood that they will be absorbed and meaning that when the remitted photons are collected by the camera, they have an unknown differential path length. This unknown effect on the remitted light could affect the 2D OIS calculated changes in haemodynamics, so a Monte Carlo Simulation is used to estimate the differential effect the brain tissue will have on the path lengths of the remitted photons.

Using the differential path lengths at the different wavelengths, calculated with the Monte Carlo Simulation, and the specific absorption coefficients for Hbo and Hbr at the different wavelengths (see section 2.3.1.1), a modified Beer-Lambert equation is used to relate the change in measured attenuation at each wavelength with the changes in concentration of Hbo and Hbr. To convert these calculated changes in concentration of Hbo and Hbr into relative μM change, an initial assumption of baseline haemoglobin concentration and tissue oxygen saturation is required. For the first study in this thesis (Chapter 3), the whisker region was used for 2D OIS analysis, and so a baseline concentration of 100μM haemoglobin is used with a tissue oxygen saturation of 70%. For the second study (Chapter 4), the artery region was used, and so a tissue oxygen saturation of 80% was assumed, with baseline haemoglobin concentration still assumed to be 100μM. These values came from previous work in the lab,

investigating the differing haemoglobin concentration and oxygen saturation in different vascular regions (Berwick et al., 2005; Kennerley et al., 2009).

By applying this analysis to the light attenuation detected in each of the 184x184 pixels collected by the camera, a spatial map of the haemodynamic changes across the cortex is produced.

2.4.2 Electrophysiological data processing

The electrophysiological data collected in this thesis were sampled at 24 kHz, this is a much higher frequency than neurons can fire at, and so for analysis was downsampled to 6kHz, reducing the computational load. To extract multi-unit activity (MUA), a 500Hz high pass filter was applied. A threshold of 1.5 times the standard deviation of the mean was set, with a spike being detected each time this threshold was exceeded. This data was then split into 100ms temporal bins, with the number of spikes per 100ms of data counted. In both studies in this thesis, the neural data were reported as fractional change of MUA by normalising the 100ms binned data to a 2s baseline at the beginning of each trial.

2.5 References

Berwick, J., et al. (2005). The use of optical imaging to investigate the relationship between neural activity and cerebral hemodynamics. *Journal of Cerebral Blood Flow & Metabolism*, *25*(7), 785–804.

Berwick, J., et al. (2008). The relationship between the BOLD signal and the local field potential in the rat somatosensory cortex. *NeuroImage*, *40*(4), 1489–1499.

Boorman, L., et al. (2010). The relationship between neuronal activity and the BOLD signal in the somatosensory cortex. *NeuroImage*, *49*(1), 353–362.

Boorman, L., et al. (2015). The role of inhibition in the generation of the negative BOLD response. *NeuroImage*, *118*, 375–385.

Brezzo, C., et al. (2020). The relationship between the BOLD signal and the local field potential in the mouse somatosensory cortex. *NeuroImage*, *218*, 116977.

Harris, S. S., et al. (2014). The relationship between the BOLD signal and the local field potential in the mouse somatosensory cortex. *NeuroImage*, *97*, 11–21.

Harris, S. S., et al. (2018a). The relationship between the BOLD signal and the local field potential in the mouse somatosensory cortex. *NeuroImage*, *178*, 12–22.

Harris, S. S., et al. (2018b). The relationship between the BOLD signal and the local field potential in the mouse somatosensory cortex. *NeuroImage*, *178*, 23–33.

Jones, M., et al. (2005). The relationship between the BOLD signal and the local field potential in the rat somatosensory cortex. *NeuroImage*, *24*(3), 776–785.

Kennerley, A. J., et al. (2012). The relationship between the BOLD signal and the local field potential in the rat somatosensory cortex. *NeuroImage*, *62*(2), 989–998.

Madisen, L., et al. (2012). A toolbox of Cre-dependent optogenetic transgenic mice for light-induced activation and silencing. *Nature Neuroscience*, *15*(5), 793–802.

Martin, C. J., et al. (2013). The relationship between the BOLD signal and the local field potential in the rat somatosensory cortex. *NeuroImage*, *79*, 11–21.

Mayhew, J. E., et al. (2000). The relationship between the BOLD signal and the local field potential in the rat somatosensory cortex. *NeuroImage*, *12*(6), 630–642.

Mayhew, J. E., et al. (2001). The relationship between the BOLD signal and the local field potential in the rat somatosensory cortex. *NeuroImage*, *13*(6), 975–987.

Sharp, P. S., et al. (2015). A novel modular anaesthetic approach for optical imaging of the mouse brain. *Journal of Neuroscience Methods*, *240*, 1–10.

Sharp, P. S., et al. (2020). The relationship between the BOLD signal and the local field potential in the mouse somatosensory cortex. *NeuroImage*, *218*, 116978.

Slack, R., et al. (2016). The relationship between the BOLD signal and the local field potential in the mouse somatosensory cortex. *NeuroImage*, *128*, 1–11.

Taniguchi, H., et al. (2011). A resource of Cre driver lines for genetic targeting of GABAergic interneurons in mice. *Neuron*, *71*(6), 995–1013.

Chapter 3: Key aspects of neurovascular control mediated by specific populations of inhibitory cortical interneurons

This chapter was published in Cerebral Cortex in November 2019

Lee, L., Boorman, L., Glendenning, E., Christmas, C., Sharp, P., Redgrave, P., Shabir, O., Bracci, E., Berwick, J., & Howarth, C. (2020). Key Aspects of Neurovascular Control Mediated by Specific Populations of Inhibitory Cortical Interneurons. Cerebral Cortex, 30(4), 2452–2464.

3.1 Paper Title and Authors

Key aspects of neurovascular control mediated by specific populations of inhibitory cortical interneurons

Lee L[1], Boorman L[1], Glendenning E[1], Christmas C[1], Sharp P[1], Redgrave P[1], Shabir O[1], Bracci E[1], Berwick J*[1], Howarth C*[1]

*These authors contributed equally to this work

[1]Department of Psychology, University of Sheffield, Sheffield, UK

I, Llywelyn Lee, am the sole first author on this manuscript. I performed the majority of the experiments, experimental planning, data analysis, statistical tests and wrote up the manuscript. This was with the help of the co-authors on this paper, whose contributions are listed below.

Emily Glendenning, Osman Shabir, Paul Sharp assisted with various aspects of the experiments. Claire Christmas helped with the immunohistochemistry. Luke Boorman helped with generating the artefact removal code. Enrico Bracci provided the SST and nNOS mouse lines. Pete Redgrave helped edit the manuscript. Clare Howarth and Jason Berwick supervised the research, helped with experimental design, assisted in the experiments, and proofread and helped edit the manuscript.

3.2 Abstract

Inhibitory interneurons can evoke vasodilation and vasoconstriction, making them potential cellular drivers of neurovascular coupling. However, the specific regulatory roles played by particular interneuron subpopulations remain unclear. Our purpose was therefore to adopt a cell-specific optogenetic approach to investigate how somatostatin (SST) and neuronal nitric oxide synthase (nNOS)-expressing interneurons might influence the neurovascular relationship. In mice, specific activation of SST- or nNOS-interneurons was sufficient to evoke haemodynamic changes. In the case of nNOS-interneurons, robust haemodynamic changes occurred with minimal changes in neural activity, suggesting that the ability of BOLD fMRI to reliably reflect changes in neuronal activity may be dependent on type of neuron recruited. Conversely, activation of SST-interneurons produced robust changes in evoked neural activity with shallow cortical excitation and pronounced deep layer cortical inhibition. Prolonged activation of SST-interneurons often resulted in an increase in blood volume in the centrally activated area with an accompanying blood volume decrease in surrounding brain regions, analogous to the negative BOLD signal. These results demonstrate the role of specific populations of cortical interneurons in the active control of neurovascular function.

Keywords BOLD fMRI, neurovascular coupling, nitric oxide synthase, optogenetics, somatostatin.

3.3 Introduction

Neurovascular coupling (NVC) is the mechanism through which local cerebral blood flow (CBF) changes are tightly coupled to increases in neural activity (Roy CS and CS Sherrington 1890). Since the reserves of oxygen and glucose within neurons are strictly limited, such coupling is essential for normal brain function (Buxton RB 2010; Leithner C and G Royl 2014). Variations in blood oxygenation and volume evoked by neural activity underlie functional imaging signals, such as blood oxygen level dependent functional magnetic resonance imaging (BOLD-fMRI, (Ogawa S et al. 1990)), which are commonly used as a surrogate measure of local changes in neuronal activity. While most research has focused on the ability of excitatory neurons (Lecrux C et al. 2011; Lacroix A et al. 2015) and astrocytes (Zonta M et al. 2003; Mulligan SJ and BA MacVicar 2004; Lind BL et al. 2013) to elicit changes in CBF, there has been less focus on the role of inhibitory neurons. GABAergic interneurons innervate local microvessels (Vaucher E et al. 2000; Cauli B et al. 2004; Hamel E 2006) and have been shown to induce both vasodilation and constriction (Cauli B *et al.* 2004), making them potential cellular drivers of NVC.

Although recent studies have investigated the contribution of inhibitory interneurons to cerebral blood flow regulation by using an optogenetic approach targeting VGAT-expressing neurons (Anenberg E et al. 2015; Uhlirova H et al. 2016; Vazquez AL et al. 2018), the role of specific subpopulations of GABAergic interneurons remains unknown. Somatostatin (SST)-expressing neurons, which account for around 30% of GABAergic interneurons in the somatosensory cortex (Rudy B et al. 2011), contact brain microvessels, in particular those in the superficial layers of the cortex (Kocharyan A et al. 2008). The release of GABA by SST interneurons has been suggested to contribute to basal forebrain stimulation-evoked cortical CBF responses (Kocharyan A *et al.* 2008). In addition, approximately 28% of GABAergic neurons (Cauli B *et al.* 2004), including a small subset of SST interneurons predominantly located in cortical layers II/III and V/VI (Karagiannis A et al. 2009; Yavorska I and M Wehr 2016), express neuronal nitric oxide synthase (nNOS). This further subpopulation of interneurons releases nitric oxide (NO), which has for a long time been known to be a potent vasodilator (Furchgott RF and JV Zawadzki 1980; Ignarro LJ et al. 1987; Palmer RM et al. 1987). nNOS interneurons are therefore of particular interest in terms of CBF regulation. To investigate the role of these two subpopulations of GABAergic interneuron we used a cell-type specific optogenetic approach that specifically targeted SST- or nNOS-expressing interneurons. By separately activating these two subsets of inhibitory interneurons (those expressing SST or nNOS) we sought to determine how they might regulate cortical haemodynamics. We were able to show that activating both subsets of interneurons evoked a localised haemodynamic response. Importantly, in the case of optogenetic-activation of

nNOS interneurons, the observed haemodynamic changes occurred with only a minimal change in measured multiunit neural activity. Alternatively, after activating SST interneurons negative haemodynamic responses were observed in the cortical areas surrounding the local area of optogenetic stimulation. This observation is similar to reported negative BOLD fMRI responses, which have been linked to inhibitory neuron activity (Shmuel A et al. 2002; Stefanovic B et al. 2004; Shmuel A et al. 2006; Boorman L et al. 2010; Boorman L et al. 2015). These observations suggest that specific subpopulations of cortical GABAergic interneurons have specific roles in NVC. Also, that the ability of BOLD signals to act as a surrogate measure of local neural activation may in part be dependent upon which subpopulation of neurons are being activated.

3.4 Materials and Methods

3.4.1 Animals

All animal procedures were performed in accordance with the guidelines and regulations of the UK Government, Animals (Scientific Procedures) Act 1986 and approved by the University of Sheffield Ethical review and licensing committee. Mice had ad libitum access to food and water and were housed on a 12 hour dark/light cycle. We used 39 mice of both sexes including 18 nNOS-CreER x ChR2-EYFP mice (M/F, 19-33g); 12 Sstm2.1Crezjh/j x ChR2-EYFP mice (M/F, 22-44g), 5 C57Bl/6J mice (F, 23-25g) and 4 non-ChR2-expressing littermates of nNOS-ChR2 mice (M, 33-39g). Sstm2.1Crezjh/j x ChR2-EYFP (SST-ChR2) mice were obtained by crossing homozygous SOM-IRES-Cre mice (Stock 013044, Jackson Laboratory, USA, (Network. NNBCD 2009; Taniguchi H et al. 2011)) with homozygous ChR2(H134R)-EYFP mice (Stock 024109, Jackson Laboratory, (Madisen L et al. 2012)), as described previously (Elghaba R et al. 2016).

The nNOS-CreER x ChR2-EYFP (nNOS-ChR2) mice were obtained by crossing heterozygous nNOS-CreER (Stock 014541, Jackson Laboratory, (Taniguchi H *et al.* 2011)) with homozygous Ai32 mice (Stock 024109, Jackson Laboratory, (Madisen L *et al.* 2012)). Littermates lacking the nNOS-CreER insertion do not express ChR2 and were used as control mice in this study. ChR2 expression was induced by intraperitoneal (IP) injection of Tamoxifen (Sigma-Aldrich, Gillingham, UK) at 100 mg/kg, administered 3 times over 5 days. Treatment with tamoxifen was carried out when mice were aged between 1-2 months old, this took place a minimum of 2 weeks prior to surgery to allow for gene expression to take place.

3.4.2 Preparation of Chronic Cranial Window

A thinned cranial window was prepared over the right whisker barrel cortex, as previously described (Sharp PS et al. 2015). Anaesthesia was induced through IP injection of fentanyl-fluanisone (Hypnorm, Vetapharm Ltd, Leeds, UK), midazolam (Hypnovel, Roche Ltd, Welwyn Garden City, UK) and sterile water (in a ratio of 1:1:2 by volume; 7ml/kg) and maintained using isoflurane (0.5-0.8%) in 100% oxygen at a flow rate of 1L/min. All surgeries were carried out in a dark room using a surgical illuminator with a band pass filter (577 ±5nm) to avoid erroneous optogenetic activation in the ChR2-expressing mice. Mice were placed on a stereotaxic frame (Kopf Instruments, Tujunga, USA), on a homeothermic blanket (Harvard Apparatus, Cambridge, UK) maintaining rectal temperature at 37ºC. The bone overlying the right somatosensory cortex was thinned to translucency using a dental drill, forming an ≈3mm^2 optical window. A thin layer of clear cyanoacrylate was applied and a stainless steel head plate secured to the skull using dental cement (Super bond C&B, Sun Medical). Surgery was performed at least 2 weeks before the first experimental imaging session.

For experiments, anaesthesia was induced as described above and maintained using isoflurane (0.25-0.7%) in 100% oxygen at a flow rate of 0.8L/min. Mice were placed on a stereotaxic frame and head fixed via their head plate. Animals were placed on a homeothermic blanket maintaining rectal temperature at 37ºC.

3.4.3 2-Dimensional optical imaging spectroscopy (2D-OIS)

Animals underwent two experimental sessions. Session one, at least two weeks post-surgery, involved 2D-OIS recordings and application of both short and long duration whisker and light stimulations. Session two, occurring at least one week after session 1, involved concurrent electrophysiology and 2D-OIS recordings while applying both short and long duration stimulations (see below for full details).

As described previously (Berwick J et al. 2005), 2D-OIS was used to record changes in cortical haemodynamics, allowing the estimation of changes in cortical oxyhaemoglobin (HbO_2), deoxyhaemoglobin (Hbr) and total haemoglobin concentration (Hbt). The cortex was illuminated with 4 wavelengths of light (587±9 nm, 595±5nm, 560±15 nm, 575±5 nm) using a Lambda DG-4 high-speed filter changer (Sutter Instrument Company, USA). The re-emitted light was collected at a frame rate of 32Hz using a Dalso 1M60 CCD camera which was synchronized to the filter switching, thus producing an effective frame rate of 8 Hz. The camera was fitted with a 490 nm high pass filter to prevent light from the photostimulation LED being collected with the re-emitted light. The spatial maps recorded from the re-emitted light then underwent spectral analysis based upon the path length scaling algorithm (PLSA)

described previously (Mayhew J et al. 1999; Berwick J *et al.* 2005). In brief, the algorithm uses a modified Beer-Lambert Law with a path length correction factor to convert detected attenuation in the re-emitted light into predicted absorption. These absorption values were then used to generate estimates of the changes in HbO_2, Hbr and Hbt from baseline values. The concentration of haemoglobin in tissue was assumed to be 100 μM and oxygen saturation was assumed to be 70%. This spectral analysis produced 2D images of the micromolar changes in volume of HbO_2, Hbr and Hbt over time.

3.4.4 Stimulations

Whisker stimulation was performed using a plastic T-bar attached to a stepper motor, which deflected the whiskers ≈1cm in the rostro-caudal direction (Sharp PS *et al.* 2015). Whiskers were deflected at 5Hz for either 2 seconds or 16 seconds. To improve the signal-to-noise for each experiment whisker stimulation was presented 30 times in trials lasting 15-25 seconds each (2s stimulation) or presented 15 times in trials lasting 70 seconds each (16s stimulation).

Photostimulation was performed using a fibre-coupled LED light source (470nm, ThorLabs, Newton, USA) and was delivered to the point of activation using a fibre optic (core diameter 200μm, ThorLabs). The cortex was illuminated for 2s (pulse width 10ms, 20Hz, 2V, 0.78mW or 99Hz, 1V, 0.45mW) or 16s (pulse width 10ms, 20Hz, 1.5V, 0.63mW or 99Hz, 0.5V, 0.24mW). These parameters were titrated to produce haemodynamic responses which were similar to physiologically-evoked responses. To improve the signal-to-noise for each experiment, photostimulation was presented 20-40 times in trials lasting 15-25 seconds each (2s stimulation) or presented 15 times in trials lasting 70 seconds each (16s stimulation).

3.4.5 Electrophysiology

In order to concurrently measure haemodynamic and neural responses, in a final imaging session (occurring at least one week subsequent to an imaging session in which only 2D-OIS data was acquired) a 16 channel depth microelectrode (100μm spacing, 1.5-2.7MΩ impedance, site area 177 μm^2; NeuroNexus Technologies, Ann Arbor, USA) was inserted into the whisker barrel cortex through a small cranial burr hole. The electrode was positioned in the centre of the whisker region (area showing the largest blood volume response to a 2s mechanical whisker stimulation, defined by 2D-OIS in the previous imaging session) and inserted to a depth of 1500-1600μm. The electrode was connected to both a preamplifier and data acquisition device (Medusa BioAmp/RZ5, TDT, Alachua, USA). Data was sampled at 24kHz. For analysis, data was downsampled to 6kHz and multiunit activity (MUA) analysed. Data from the 12 channels covering the depth of the cortex are displayed in figures 3.4,3.6 and 3.7.

3.4.6 Analysis

Analysis was performed using MATLAB (MathWorks). Using the 2D-OIS-generated spatial map of HbO_2 response to stimulation, a region of interest (ROI) was selected for use in subsequent time-series analysis. In order to select an ROI (red ROI in Figures 3.3, 3.5), the HbO_2 image is processed to remove edge pixels and a Gaussian 3x3 filter applied. For the response period, each pixel is averaged across time to generate a mean value. The threshold for a pixel to be included in the ROI was set at 1.5 x standard deviation. Thus, the ROI represents the area with the largest haemodynamic response to the stimuli. For each experimental paradigm, the response across all pixels in the ROI was averaged in order to generate a time series for each haemodynamic profile (Hbt, HbO_2 and Hbr). As described above haemodynamic data were acquired with a 490nm high pass filter, resulting in minimal light artefact from the stimulating LED. For 20Hz stimulation this residual artefact was removed using a high pass filter followed by a modified boxcar function, for 99Hz stimulation only the modified boxcar function was applied. For each experiment, mean time series for Hbt, HbO_2 and Hbr were produced by averaging across trials. Matching experiments (e.g. 2s photostimulation) from the same mouse on different imaging days were averaged together, so that each mouse only contributed one time series per experiment.

For the negative surround analysis, an automated ‘negative response’ ROI was selected, with a threshold of 1.5 x standard deviation, as described above. In 3 SST-ChR2 mice in which no negative surround response was observed to either 99Hz or 20Hz 16s optogenetic stimulation, ‘negative response’ ROIs were selected manually in an equivalent brain region.

3.4.7 Statistical analysis and experimental design

In order to compare haemodynamic responses we focused on Hbt, which is our most reliable measure. Statistical comparisons were performed using GraphPad Prism (La Jolla, USA). A two-way ANOVA with Tukey’s multiple comparisons test was performed in order to undertake intergroup comparisons of MUA for different electrode depths in the presence and absence of a negative surround haemodynamic response. A one-way ANOVA with Tukey’s multiple comparisons test was used to compare Hbt peaks in response to various paradigms (whisker stimulation, photostimulation of NOS-ChR2 mice, photostimulation of SST-ChR2 mice), and to compare photostimulation-evoked MUA in different mouse lines (NOS-ChR2 mice, SST-ChR2 mice, control mice). T-tests (paired or unpaired, as appropriate) were used to compare between two groups (MUA in superficial vs deep electrode channels, LFP deflection, and initial vs secondary peak haemodynamic response). P values <0.05 were considered to be statistically significant. Data are presented as mean ± standard error in the mean (s.e.m). Experiments and analysis were performed unblinded to mouse type.

3.4.8 Immunohistochemistry

At the end of the experiments, mice were given an overdose of pentobarbital and perfused with saline followed by 4% paraformaldehyde (PFA) in phosphate-buffered saline (PBS), via cardiac perfusion. Brains were extracted, postfixed in 4% PFA for 24 hours at 4^{o}C and cryoprotected in 30% sucrose in PBS at 4^{o}C for 48 hours. The brains were sectioned using a cryostat (Thermo Fisher Scientific, Loughborough, UK) to produce 30 µm coronal sections which were placed into PBS with 0.3% Triton X-100 (PBST) for 20 minutes to permeabilize the tissue. Free-floating sections were blocked with 10% normal donkey serum (Jackson ImmunoResearch, Ely, UK, when staining for nNOS and EYFP) or 10% normal rabbit serum (Vector Laboratories, Peterborough, UK, when staining for SST) in PBST for 1 hour, and then incubated overnight at 4^{o}C in blocking solution with primary antibodies against GFP (anti-GFP, rabbit polyclonal, [ab290], Abcam, Cambridge, UK, 1:200, recognises EYFP, which is a genetic mutant of GFP); nNOS (anti-nNOS, goat polyclonal, [ab1376], Abcam, 1:250) or SST (anti-Somatostatin, rat monoclonal (YC7), [MAB354], Millipore, Watford, UK, 1:500). Sections were washed with PBS and incubated in the appropriate fluorescent secondary antibodies: Alexa 568 donkey anti-rabbit (Thermo Fisher Scientific, 1:500 dilution in PBS), Alexa 488 donkey anti-goat (Thermo Fisher Scientific, 1:500 dilution in PBS) for 2 hours at room temperature, or in the case of the SST stain: incubated in biotinylated rabbit anti-rat (Vector Laboratories, 1:100 dilution in PBS with 1.5% normal rabbit serum) for 30mins at room temperature. The SST staining sections were then washed with PBS and incubated with Alexa 647 Streptavidin (Thermo Fisher Scientific, 1:400 dilution with PBS) for 90 minutes. All sections were mounted onto gelatin-coated slides following immunohistochemical staining and imaged with a fluorescence stereo microscope (M205 FA, Leica Microsystems, Milton Keynes, UK).

3.5 Results

3.5.1 Short duration optogenetic stimulation of specific interneurons evokes a localised haemodynamic response

Genetically modified mice expressing channelrhodopsin-2 (ChR2) in either SST- or nNOS-expressing interneurons (referred to as SST-ChR2 or nNOS-ChR2 mice, respectively) were used to investigate how light induced activity of these inhibitory interneurons may alter cortical haemodynamics. Expression of ChR2 in the appropriate cell types was confirmed using immunohistochemistry (Figure 3.1). Expression of ChR2 was evidenced by the presence of enhanced yellow fluorescent protein (EYFP), the reporter for ChR2 expression, and co-localisation was seen with either SST (Figure 3.1A) or nNOS (Figure 3.1B), as appropriate. The majority of SST-positive neurons are expected to express ChR2 (Taniguchi H *et al.* 2011). Although off-target recombination has previously been reported in the SOM-IRES-Cre mouse (Hu H et al. 2013), the morphological features of observed $EYFP^+$ cells (Figure 3.1A) suggested they were SST-expressing interneurons. In the case of the nNOS-ChR2 line, in 9 representative images (from 3 animals) we counted 274 $nNOS^+$ cells of which 248 (90.5%) were ChR2-$EYFP^+$ and 26 (9.5%) were ChR2-$EYFP^-$.

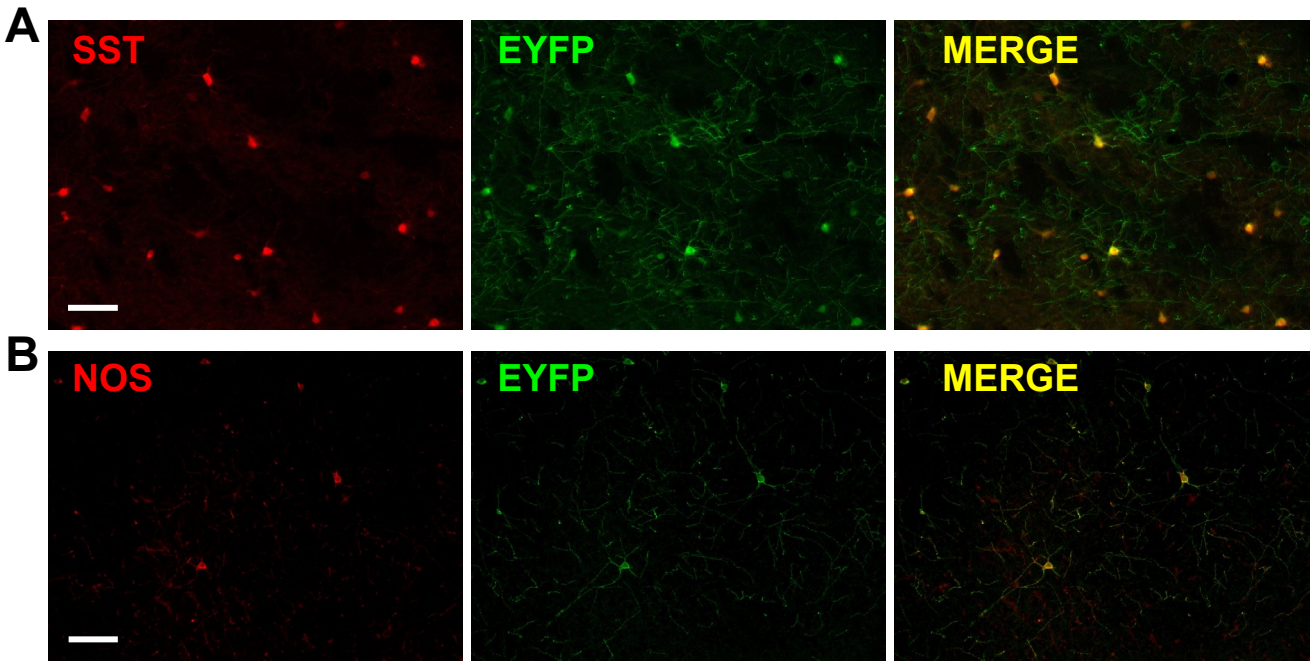

Figure 3.1: Cell-specific expression of ChR2 Immunohistochemistry showing staining for **(A)** SST (red) and ChR2 (green, EYFP is the reporter for ChR2) and merge (yellow) in cortex from SST-ChR2 mouse. **(B)** nNOS (red) and ChR2 (green, EYFP is the reporter for ChR2) and merge (yellow) in cortex from nNOS-ChR2 mouse. Scalebar represents 100µm.

Using an anaesthetised mouse (Figure 3.2), we assessed whether short duration optogenetic stimulation of specific subtypes of interneuron evoked a localised haemodynamic response. 2-dimensional optical imaging spectroscopy (2D-OIS) was used to record high-resolution 2D maps of the changes in blood volume (Hbt), oxygenated haemoglobin (HbO_2) and reduced haemoglobin (Hbr) evoked by stimulation. Each animal initially received a mechanical whisker stimulation (2s, 5Hz), evoking changes in Hbt, HbO_2 and Hbr which were localised to the whisker barrel cortex (Figure 3.3A). These haemodynamic changes allowed us to map the whisker barrel cortex and, in turn, guide the placement of the optical fibre used for photostimulation (Figure 3.2). The time series of the haemodynamic response to whisker stimulation shows an increase in Hbt and HbO_2 during the stimulation with a corresponding washout of Hbr (Figure 3.3A).

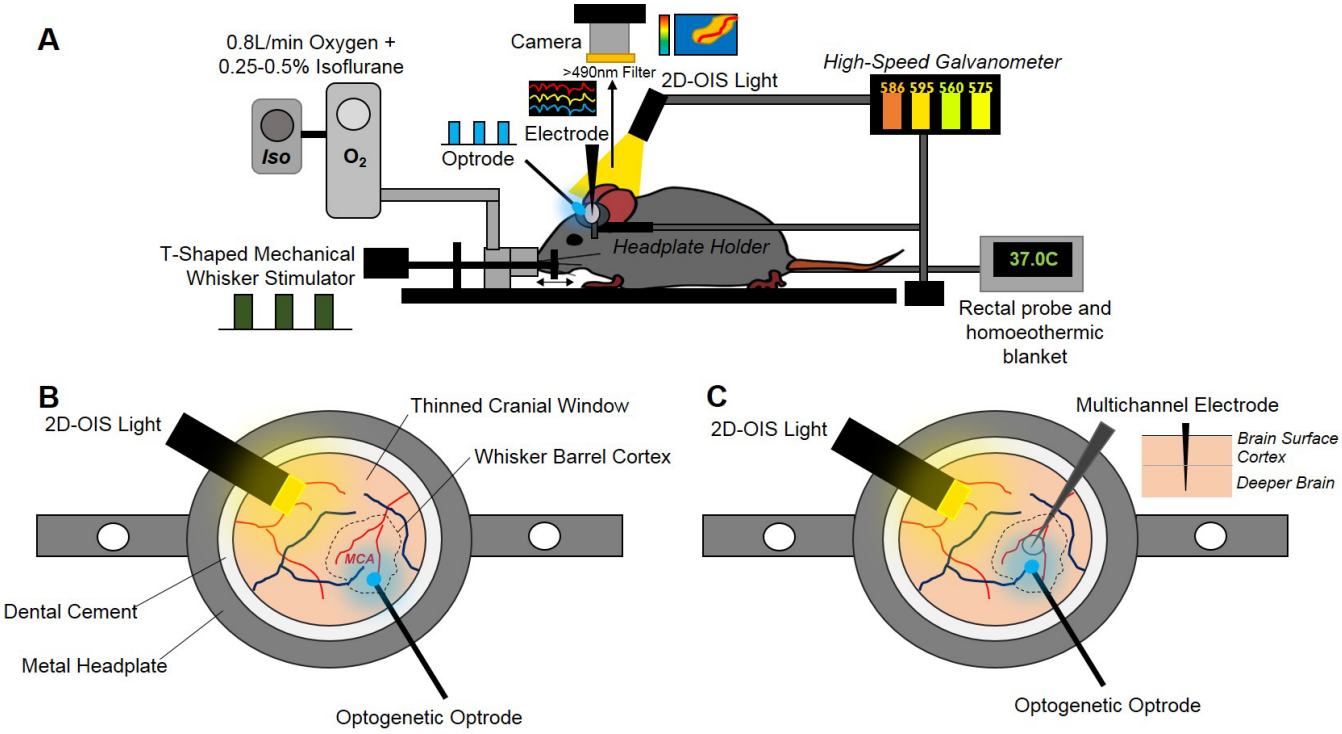

Figure 3.2: Chronic imaging preparation (A) Imaging setup showing inhalational anaesthetic maintenance, mechanical whisker stimulation, temperature regulation, haemodynamic imaging (2D-OIS), optogenetic stimulation & multichannel electrode electrophysiology **(B)** 1st imaging session 2-weeks post-surgery with optogenetic optrode placed over MCA/ whisker barrel cortex region **(C)** 2nd imaging session 3-weeks post-surgery with electrode inserted into whisker barrel cortex + optrode for optogenetic stimulation.

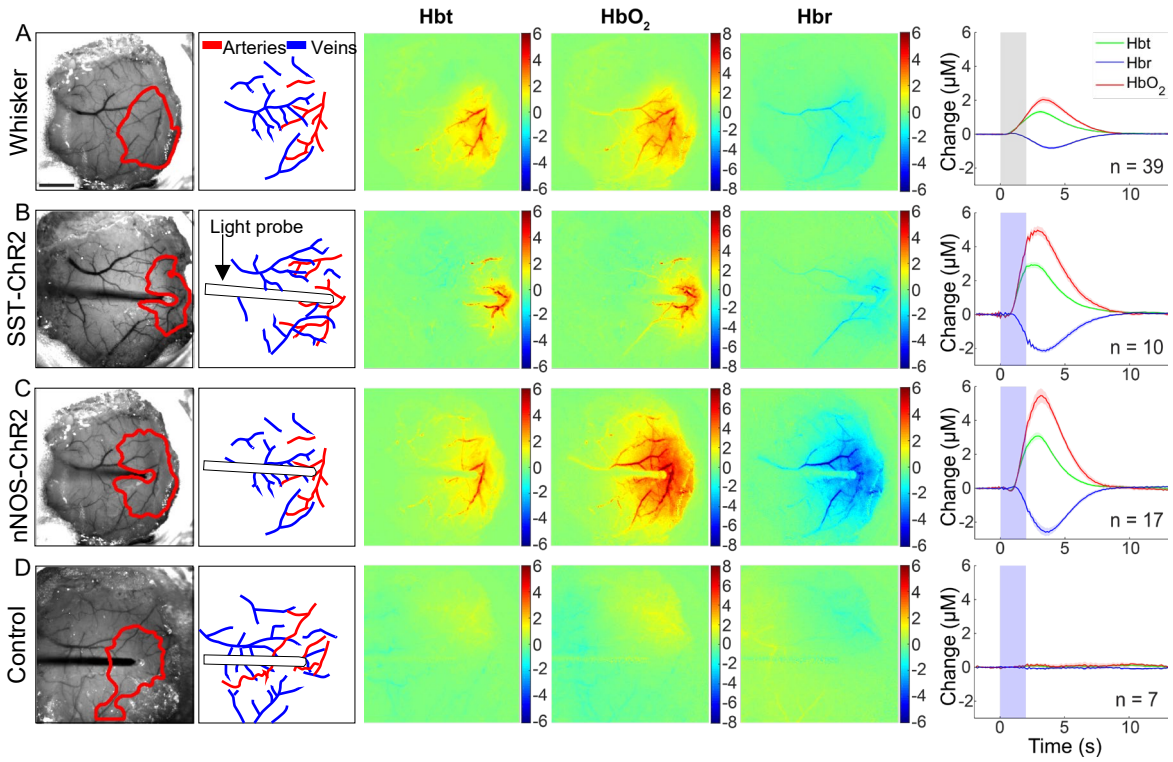

Figure 3.3: Haemodynamic responses to 2s stimulation (A) mechanical whisker stimulation (5Hz) **(B)** photostimulation (99Hz, 0.45mW or 20Hz, 0.78mW) of SST-ChR2 mouse **(C)** photostimulation of nNOS-ChR2 mice **(D)** photostimulation of control mice. 1st column: Representative surface vasculature overlying somatosensory cortex (at 575nm illumination), region of interest (ROI) for analysis shown in red. Scalebar represents 1mm. 2nd column: Vessel map showing surface arteries and veins. 3rd, 4th and 5th column: Representative spatial activation map of trial-averaged changes in [Hbt], [HbO_2] and [Hbr], respectively, with respect to baseline during stimulation. Colour bar represents change (μM). 6th column: Mean haemodynamic time series within whisker barrel cortex ROI (mean ± s.e.m, n represents number of mice). Grey box indicates whisker stimulation, blue box indicates photostimulation.

A fibre-coupled blue (470nm) LED, placed directly above the whisker barrel cortex, was used to apply photostimulation in order to activate ChR2-expressing neurons. The fibre optic was positioned in the centre of the whisker barrel cortex (Figure 3.2) and short duration photostimulation (2s: 99Hz, 0.45mW and 20Hz, 0.78mW) was applied. Similarly to whisker stimulation, for both SST-ChR2 and nNOS-ChR2 mice, a short 2s stimulation produced a robust haemodynamic response focused around the tip of the fibre optic light guide. Photostimulation elicited a functional hyperemia response, showing a localised increase in Hbt and HbO_2 with corresponding washout of Hbr (Figure 3.3B, C: data from 99Hz and 20Hz stimulations were combined as there was no significant difference in peak response (a one-way ANOVA showed an overall effect of stimulation type ($F_{11,113} = 20.6$, $p < 0.0001$) however, Tukey's multiple comparisons test showed that there was no significant difference in response to stimulations which only differed in frequency of stimulation (e.g. 2s nNOS stimulation at 20Hz vs 99Hz)). Although these haemodynamic changes were similar in shape and duration to those seen in response to whisker stimulation (Figure 3.3A), with amplitudes which were within the range of physiological responses (Gu X et al. 2018), some notable differences in rise time and area under the curve were observed (see Supplementary Tables 3.1-3.3 for details). As was observed with whisker stimulation, increases in Hbt and HbO_2 were strongest in the middle cerebral artery (MCA) branches overlaying the whisker barrel cortex with a decrease in Hbr which was clearly apparent in the draining veins (Figure 3.3). When comparing peak values of the evoked Hbt response, a one-way ANOVA showed an overall effect of stimulation type ($F_{3,69} = 51.88$, $p<0.0001$) however, Tukey's multiple comparisons test showed that there was no significant difference in Hbt peak between SST-ChR2 and nNOS-ChR2 mice ($p = 0.9531$).

Previous studies have reported photostimulation-evoked fMRI (Christie IN et al. 2013) and cerebral blood flow (Rungta RL et al. 2017) responses in optogenetically naïve (non-ChR2-expressing) animals. While these studies used a laser to drive the optogenetic response, which may cause issues with heating, our light stimulation used a cold LED light source. To confirm our response was not an artefact we applied our photostimulation paradigm to control animals (either C57bl/6J or non-ChR2-expressing littermates of nNOS-ChR2 animals) and confirmed that such stimulation failed to elicit haemodynamic responses (Figure 3.3D).

These data demonstrate that short duration activation of specific interneuron subpopulations is sufficient to induce a localised haemodynamic response.

3.5.2 Electrophysiological response to short duration stimulation is dependent on the specific interneuron population activated

Having demonstrated that specific activation of either SST or nNOS interneurons resulted in localised haemodynamic responses, in a second experimental session we assessed the associated evoked electrophysiological activity. 16 channel Neuronexus probes were inserted into the centre of the whisker barrel cortex in order to measure electrophysiological responses to both whisker stimulation and photostimulation (Figure 3.2). Electrophysiological and haemodynamic measurements were made concurrently. Across all animals, 2s mechanical whisker stimulation evoked a typical electrophysiological response, with peak local multi-unit activity (MUA) centred around layer 4 of the cortex. The evoked increases in multi-unit activity extended throughout the cortex (Figure 3.4A).

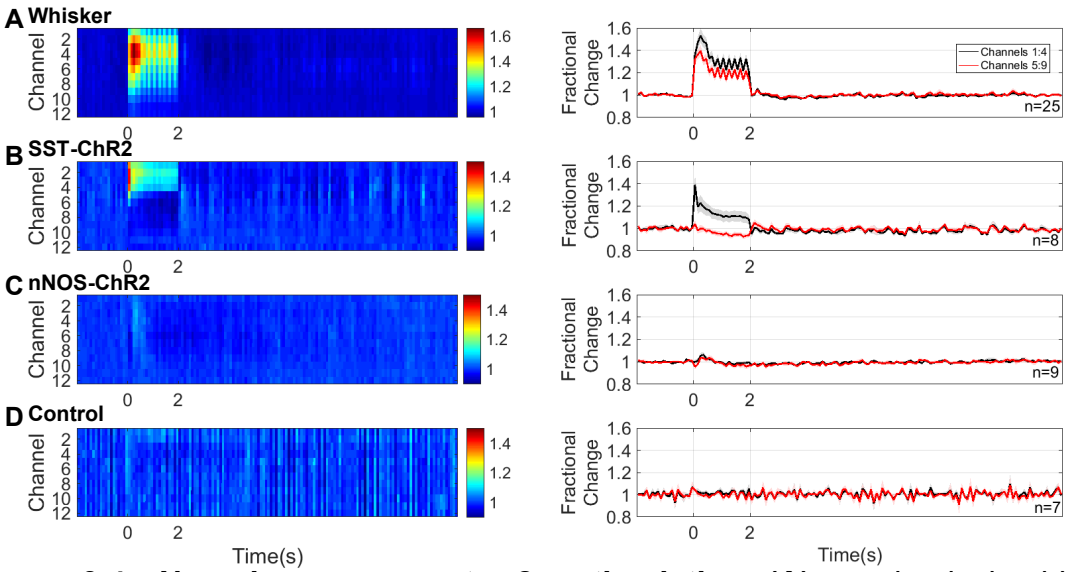

Figure 3.4: Neural responses to 2s stimulation (A) mechanical whisker stimulation (5Hz) **(B)** photostimulation (99Hz, 0.45mW or 20Hz, 0.78mW) of SST-ChR2 mice **(C)** photostimulation of nNOS-ChR2 mice **(D)** photostimulation of control mice. 1st column: Mean MUA response across cortical layers. Colour bar represents fractional change. 2nd column: mean time series of response through different cortical layers. Data shown are mean ± s.e.m, n represents number of mice.

Two second photostimulation of SST interneurons evoked an increase in local MUA which was limited to the superficial depth of the cortex (mean fractional change: channels 1:4=1.14±0.05, compared to channels 5:9=0.96±0.02, p = 0.0026, n=8, paired t test, Figure 3.4B). EEG power band analysis (Supplementary Figure 3.1) showed that photostimulation of SST interneurons resulted in an increased power both at the frequency of stimulation (20Hz) and harmonics of it (40, 80Hz). Such increased power in the stimulation frequency harmonic ranges has previously been reported by Ahlgrim et al. (2019). These data confirm that photostimulation of ChR2-expressing SST interneurons results in measurable changes in neural activity in the superficial depth of the cortex.

Surprisingly, the equivalent photostimulation of ChR2-expressing nNOS interneurons elicited a minimal change in local neural activity during the light stimulation period (Figure 3.4C). Given the robust haemodynamic response evoked by activation of nNOS interneurons (Figure 3.3C), such a minimal change in neural activity was unexpected. This lack of robust population responses was confirmed by EEG power band analysis (Supplementary Figure 3.1).

We confirmed that there were no measurable changes in neural activity evoked by photostimulation in control animals (Figure 3.4D).

When comparing photostimulation-evoked MUA in channels 1-4 across the groups of animals, a one-way ANOVA showed an overall significant effect ($F_{2,21}$ = 6.223, p =0.0075). Tukey's multiple comparisons test found that the neural activity evoked in SST-ChR2 mice was significantly different to that evoked in nNOS-ChR2 (p = 0.0092) and control animals (p=0.0325). Taken together, our haemodynamic and electrophysiology data suggest that, in response to short duration activation, both SST and nNOS interneurons are able to evoke robust changes in blood volume and saturation. However, in the case of specific nNOS interneuron activation, the robust haemodynamic response occurred with only minimal change in local MUA.

3.5.3 Long duration stimulation evokes a localised haemodynamic response whose time course differs depending on the specific interneurons activated

Having assessed the responses evoked by short duration interneuron stimulation, in the same group of animals we also performed long duration (16s) stimulation experiments across both modalities (whisker and photostimulation). Mechanical whisker stimulation (16s, 5Hz) was applied and the evoked haemodynamic changes observed using 2D-OIS. Long duration whisker stimulation evoked changes in Hbt, HbO_2 and Hbr which were localised to the whisker barrel cortex (Figure 3.5A). The time series of the haemodynamic response to whisker stimulation shows an increase in Hbt and HbO_2 during the stimulation period with a

corresponding washout of Hbr (Figure 3.5A). The shape of these responses are comparable to those previously reported in awake animals (Sharp PS *et al.* 2015).

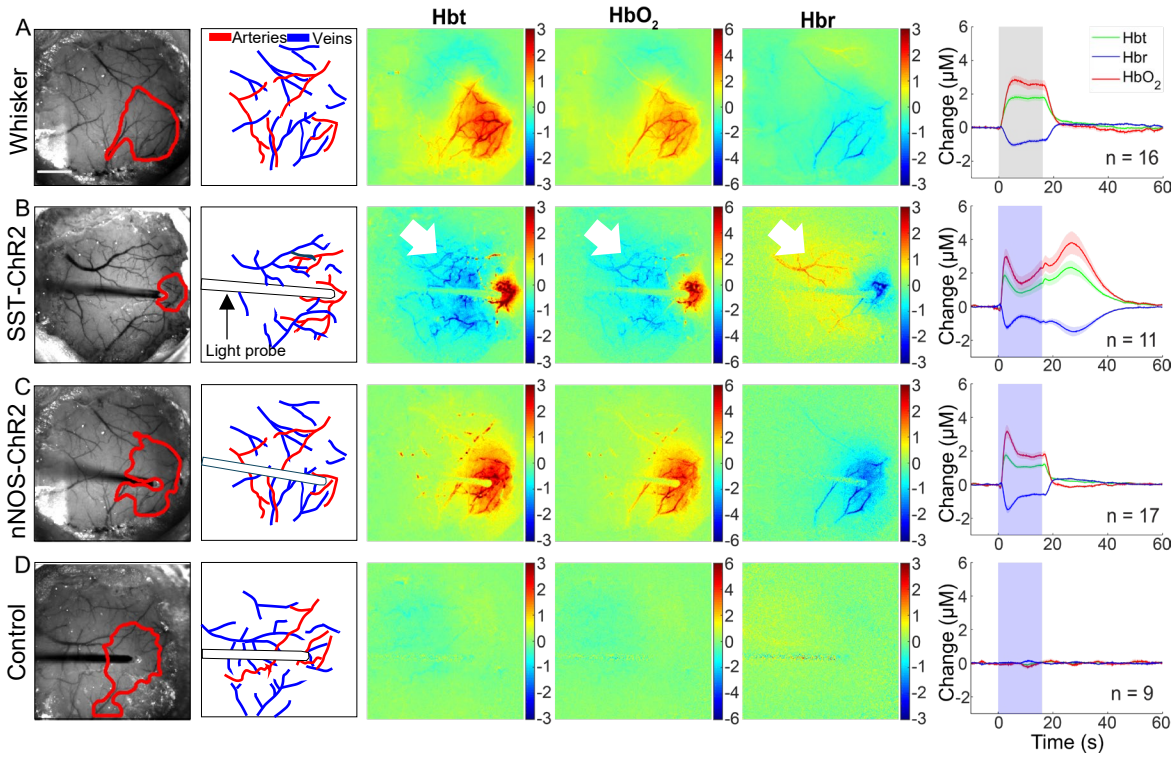

Figure 3.5: Haemodynamic responses to 16s stimulation (A) mechanical whisker stimulation (5Hz) **(B)** photostimulation (99Hz, 0.24mW or 20Hz, 0.63mW) of SST-ChR2 mouse **(C)** photostimulation of nNOS-ChR2 mice **(D)** photostimulation of control mice. 1st column: Representative surface vasculature overlying somatosensory cortex (at 575nm illumination), region of interest (ROI) for analysis shown in red. Scalebar represents 1mm. 2nd column: Vessel map showing surface arteries and veins. 3rd, 4th and 5th Column: Representative spatial activation map of trial-averaged changes in [Hbt], [HbO_2] and [Hbr], respectively, with respect to baseline during stimulation. Colour bar represents change (μM). 6th column: Mean haemodynamic time series within whisker barrel cortex ROI (mean ± s.e.m, n represents number of mice). Grey box indicates whisker stimulation, blue box indicates photostimulation. White arrowheads indicate negative surround response.

LED photostimulation was performed as described above but with the stimulation period extended to 16 seconds (99Hz, 0.24mW and 20Hz, 0.63mW). As noted above, data were combined as no significant difference in response was observed. Specific activation of either SST (Figure 3.5B) or nNOS (Figure 3.5C) interneurons resulted in a localised haemodynamic response at the point of stimulation which consisted of an initial increase in Hbt and HbO_2 with a corresponding washout of Hbr; these Hbt increases had a faster rise time and time to peak than those evoked by whisker stimulation (see Supplementary tables 3.1-3.2 for details). 16s photostimulation failed to elicit haemodynamic responses in naïve animals (Figure 3.5D). When comparing peak evoked haemodynamic responses, a one-way ANOVA showed a significant effect of stimulation type ($F_{3,49}$=12.6, p<0.0001) on Hbt response. However, Tukey's multiple comparisons test found that this was only significant in the case of photostimulation of naïve animals (Hbt peak: compared to whisker stimulation, p<0.0001; compared to SST activation, p<0.0001; compared to nNOS activation, p<0.0001).

In the case of photostimulation of SST-ChR2 mice, although the initial haemodynamic changes in the central region were similar to those in response to whisker stimulation, there were some important differences. Some SST-ChR2 animals showed a robust negative surround haemodynamic response (see white arrowheads on representative images in Figure 3.5B), where the haemodynamic changes were the opposite of the centrally activated region. SST-ChR2 mice also showed a robust increase in blood volume and saturation after the cessation of the 16s optical stimulation, these observations will be described further below. In contrast, no evidence of either a negative surround or secondary haemodynamic response was observed following specific activation of nNOS interneurons.

3.5.4 Electrophysiological response to long duration stimulation is dependent on specific interneuron population activated

Having demonstrated that longer duration optogenetic activation of either SST- or nNOS-expressing interneurons reliably results in haemodynamic responses, in a second experimental session we assessed the associated evoked electrophysiological activity. These experiments were performed in the same group of animals as the short duration stimulation investigations. In all animals, 16s mechanical whisker stimulation evoked a typical electrophysiological response which extended throughout the cortex (Figure 3.6A).

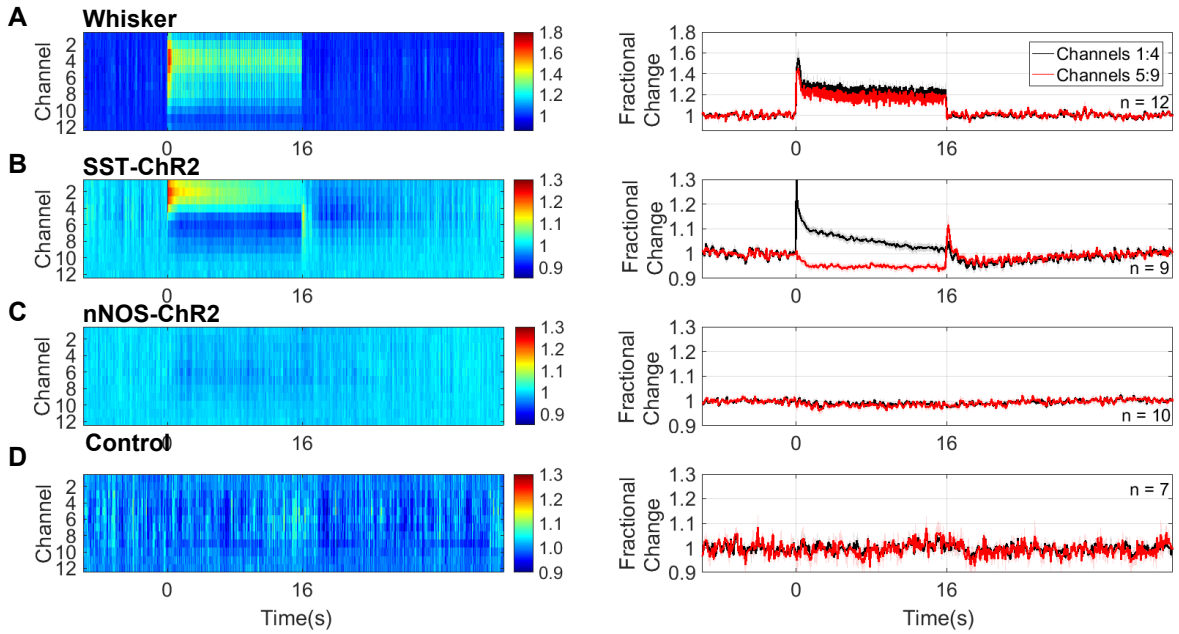

Figure 3.6: Neural responses to 16s stimulation (A) mechanical whisker stimulation (5Hz) **(B)** photostimulation (99Hz, 0.24mW or 20Hz, 0.63mW) of SST-ChR2 mice **(C)** photostimulation of nNOS-ChR2 mice **(D)** photostimulation of control mice. 1st column: Mean MUA response across cortical layers. Colour bar represents fractional change. 2nd column: mean time series of response through different cortical layers. Data shown are mean ± s.e.m, n represents number of mice.

16s photostimulation of SST-expressing interneurons evoked an increase in local MUA in the superficial depth of the cortex and a reduction in MUA deeper in the cortex (mean fractional change in MUA: channels 1:4, 1.06±0.01, n=9, compared to channels 5:9, 0.95±0.01, n=10, p <0.0001, unpaired t test, Figure 3.6B). Following cessation of the photostimulation there was a brief increase in MUA in the deeper layers, followed by a prolonged decrease below baseline in MUA which extended across cortical depth (0.97±0.01 channels 1:4, 0.98±0.01 channels 5:9, p = 0.6, unpaired t test). An increase in EEG power was observed at the frequency of stimulation (20Hz) and harmonics of it (40, 80Hz; Supplementary Figure 3.2). These data confirm that specific activation of SST interneurons results in measurable changes in local neural activity in the cortex, the polarity of which is dependent on cortical depth.

An equivalent 16s photostimulation of nNOS-expressing interneurons elicited a minimal change in local neural activity during the light stimulation period (Figure 3.6C), Although this result is surprising, given the robust haemodynamic response evoked by the photostimulation (Figure 3.5C), it is consistent with the minimal MUA changes in response to 2s photostimulation of nNOS-expressing interneurons (Figure 3.4C). EEG power band analysis confirmed a lack of robust population responses (Supplementary Figure 3.2).

We confirmed that, as expected, no changes in neural activity were detected in response to 16s photostimulation of control animals (Figure 3.6D).

3.5.5 Long duration stimulation of SST-expressing interneurons can evoke a negative surround haemodynamic response

When assessing the effect of long duration activation of SST interneurons, in addition to the positive haemodynamic response observed in the central activated region (surrounding the optic fibre), a negative surround haemodynamic response was observed in 9/16 experiments. The negative surround haemodynamic response, which occurs in the cortical region surrounding the central area, consisted of a decrease in Hbt and HbO_2 and increase in Hbr (white arrowheads, Figure 3.5B). Interestingly, the temporal dynamics of the blood volume reduction in the central region (Figure 3.7A, red trace) were almost identical to those seen in the surround (Figure 3.7A, blue trace). In order to further investigate the origins of the negative surround haemodynamic response, and to assess whether there was a neural marker associated with its presence, experiments in which simultaneous multi-channel electrophysiology and haemodynamic responses were recorded in the central region, were split into those in which a negative surround haemodynamic response was (Figure 3.7A, n = 9 experiments, 6 mice) and was not (Figure 3.7B, n = 7 experiments, 6 mice) observed in response to photostimulation. In those experiments in which a negative surround response

was observed (decreased Hbt in response to photoactivation of SST neurons, Figure 3.7A) a second increase in Hbt was also observed. This secondary haemodynamic response, which lasted for around 20 seconds after the photostimulation period ended, was absent in experimental sessions in which there was no negative surround haemodynamic response (Figure 3.7B). In the central region, both the initial Hbt increase which occurred during light stimulation and the secondary Hbt increase were of similar magnitude (initial peak: 2.12±0.48μM, secondary peak: 2.81±0.57μM, $p = 0.39$, paired t test, Figure 3.7A; centre region).

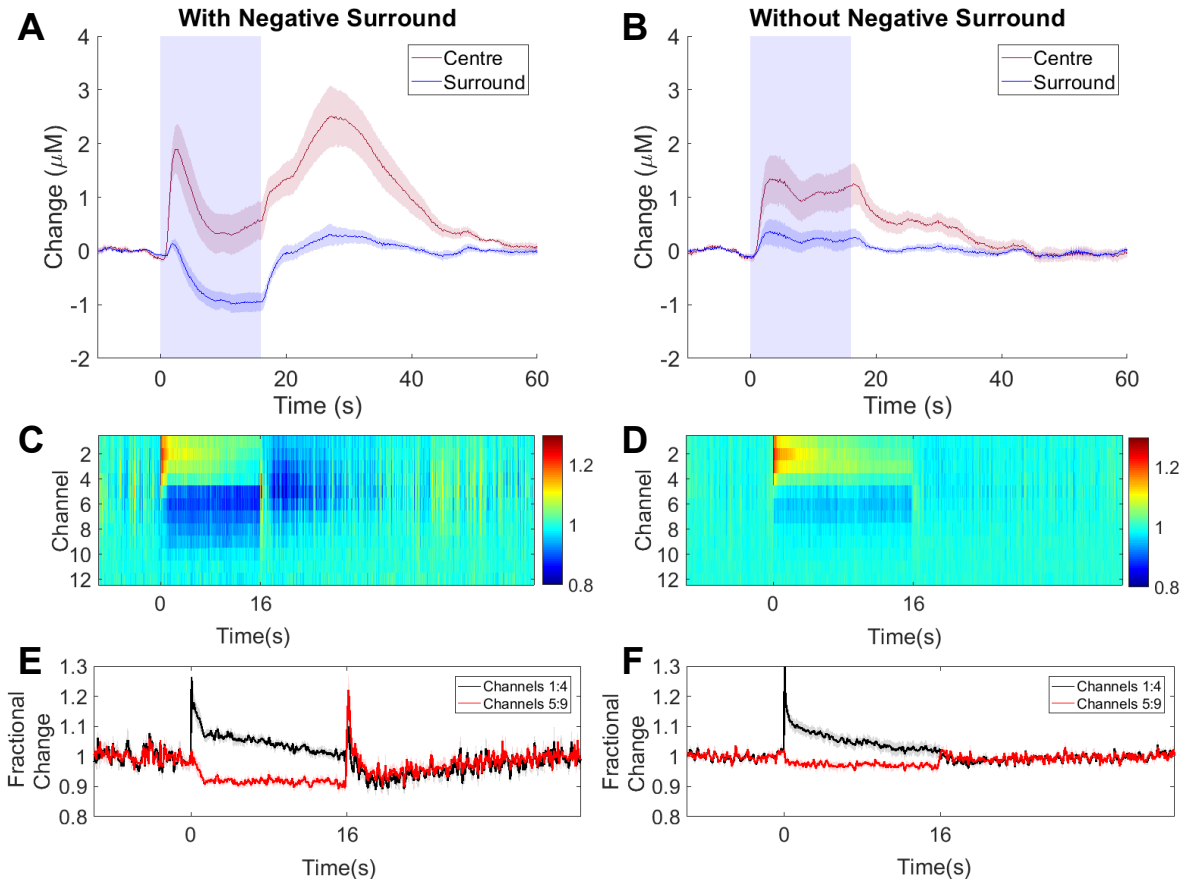

Figure 3.7: 16s photostimulation elicits a negative surround in some SST-ChR2 mice. (A,B) Mean time series showing mean changes in [Hbt] with respect to baseline in SST-ChR2 mice which did (**A**, n=9/16 experiments) and did not (**B**, n=7/16 experiments) display a negative surround haemodynamic response. Blue box indicates photostimulation. Response in centre region shown in red, surround region in blue. **(C,D)** Mean MUA response in central region across cortical layers for experiments which did (**C**, n=9 experiments from 6 mice) and did not (**D,** n=7 experiments from 6 mice) display a negative surround haemodynamic response. Colour bar represents fractional change. **(E,F)** Mean time series of response through different cortical layers for experiments which did **(E)** and did not **(F)** display a negative surround haemodynamic response. Data shown are mean ± s.e.m.

16s photoactivation of SST interneurons evoked an increase in MUA in the superficial depth of the cortex and a decrease in MUA deeper in the cortex. The neuronal response in the superficial layers of the cortex was similar in all experiments, however, the reduction in MUA occurring in the deeper cortical layers was significantly stronger in experiments displaying a negative surround haemodynamic response (Figure 3.7C-F). A two-way ANOVA showed a significant effect of both electrode channel depth ($F_{1,26}$=59.47, p<0.0001) and presence of negative surround haemodynamic response ($F_{1,26}$=5.204, p = 0.031), but not for their interaction ($F_{1,26}$=3.61, p=0.0686). Tukey's multiple comparisons test found that the change in MUA in deeper cortical layers (channels 5:9) was significantly different in the presence and absence of a negative surround haemodynamic response (p = 0.0253). Furthermore, in experiments which displayed a negative surround response, at the end of stimulation there was a brief transient increase in MUA in the deeper cortical layers, followed by a long lasting period (20s) of suppressed MUA below baseline which extended throughout the depth of the cortex (Figure 3.7C, E). Neither of these phenomena were observed in experiments which were lacking a negative surround haemodynamic response (Fig 3.7D, F). Further analysis of the electrophysiological data revealed the presence of a downward deflection in local field potential (LFP) during this 'rebound' increase in MUA activity. The size of this downward deflection was significantly greater in experiments which displayed a negative surround response, compared to those which did not (0.213±0.03 volts and 0.069±0.01 volts, respectively, p=0.003, t test).

3.6 Discussion

The present *in vivo* study investigated the contribution of two overlapping populations of GABAergic interneurons to neurovascular coupling using complementary optogenetic, imaging (2D-OIS), and electrophysiological procedures. We demonstrated that photoactivation of either SST- or nNOS-expressing interneurons was sufficient to evoke a robust localised haemodynamic response. This shows that these two subsets of interneurons individually are able to drive changes in cerebral haemodynamics. In the case of specific activation of nNOS interneurons, reliable changes in haemodynamics were evoked in the presence of minimal changes in local neural activity. Meanwhile prolonged duration stimulation of SST-expressing interneurons sometimes resulted in an additional, post-stimulus, haemodynamic response and a negative surround response which is analogous to the negative BOLD fMRI signal seen in previous studies by both our group and others (Shmuel A *et al.* 2006; Devor A et al. 2007; Boorman L *et al.* 2010; Boorman L *et al.*

2015). The polarity of the detected change in local neural activity evoked by SST-expressing interneurons is dependent on cortical depth, with increased MUA occurring at superficial depths and reduced MUA occurring deeper in the cortex.

Taking first the nNOS-expressing interneurons, we found that specific optical stimulation was sufficient to elicit large localised increases in blood volume and saturation. This finding confirms the general idea that GABAergic neuron activity can produce increases in blood flow (Anenberg E *et al.* 2015; Vazquez AL *et al.* 2018) and vessel diameter (Uhlirova H *et al.* 2016), but extends current understanding by showing that these effects can be obtained by specifically stimulating the subclass of nNOS-expressing interneurons. We are confident that the effects we report are a consequence of the action of the LED on the channelrhodopsin in the nNOS-expressing neurons in our transgenic animals because identical optical stimulation in wild-type controls was without effect. These findings provide additional support for the proposal that nNOS interneurons play a critical role in the fundamental process of neurovascular coupling (Duchemin S et al. 2012). The effects in the current study are likely to be mediated through the release of NO from these neurons, which is known to be a potent vasodilator (Furchgott RF and JV Zawadzki 1980; Ignarro LJ *et al.* 1987; Palmer RM *et al.* 1987).

However, perhaps the most significant finding with nNOS interneuron stimulation was that the robust haemodynamic response occurred with only a minimal change in local MUA. Compared with the effects of mild sensory stimulation where a large MUA response was associated with a moderate haemodynamic response (Figures 3.3A, 3.4A, 3.5A, 3.6A), selective stimulation of nNOS interneurons caused a larger haemodynamic response but with only a small change in MUA (Figures 3.3B, 3.4B, 3.5B, 3.6B). These findings would be consistent with a small population of optically activated nNOS interneurons (~2% of neurons in the light-activated area (Valtschanoff JG et al. 1993)) being responsible for the small change in MUA, yet having a dramatic effect on local haemodynamic activity. If correct, it would mean they would be in a position to play a critical role in the coupling of neural and haemodynamic activity.

While it is unlikely that nNOS interneurons play an exclusive role in neurovascular coupling, these results have demonstrated for the first time that a particular subpopulation of cortical interneurons can evoke robust haemodynamic responses without being associated with the large increases in overall neural activity that would normally be expected. This observation suggests that separate populations of brain neurons, specifically nNOS interneurons, may have a disproportionate effect on cerebral haemodynamics. This suggests that any procedure or intervention that specifically targets these populations of cortical interneurons is

likely to uncouple the neurovascular relationship upon which interpretations of BOLD signalling as an indirect proxy for neural activity depends.

We turn now to the case of SST-expressing interneurons. Our results show that a short 2s stimulation of SST interneurons also produced a large increase in blood volume and saturation in the activated area. With a longer duration stimulation period (16s), a longer latency negative haemodynamic response developed in adjacent unstimulated tissue (n=9/16 experiments; Figure 3.7), where the central positive haemodynamic response was surrounded by an inhibitory zone in adjacent tissue (Figures 3.5B, 3.7A). This inhibitory response was characterised by a marked reduction in blood volume and saturation. The temporal dynamics and magnitude of this response are similar to the negative BOLD surround region reported in previous studies by our group and others (Shmuel A *et al.* 2006; Boorman L *et al.* 2015). Although Uhlirova et al. (2016) have previously reported *post-stimulus*, NPY-mediated, vasoconstriction in response to optogenetic stimulation of VGAT-expressing interneurons, the present study is the first demonstration of reduced blood volume (indicative of vessel constriction) occurring *concurrently* with stimulation of a single subpopulation of cortical interneurons.

To understand better the neural basis of the centre-surround pattern of haemodynamic responses elicited by stimulating SST interneurons we performed simultaneous 2D-OIS and multi-channel electrophysiology in the central stimulated region. Given that under ostensibly constant experimental conditions the surround haemodynamic inhibition was observed in some cases but not others, we sought to take advantage of this response variability by comparing the electrophysiological responses in the stimulated region when surround inhibition was present and when it was absent (Figure 3.7). In both instances MUA responses in the superficial cortical layers were similar. However, only in cases where the negative surround response was present, was there a strong suppression of MUA in the deep cortical layers. Then in the stimulation offset period, after a transient increase in MUA activity, we observed a prolonged period (~20s) of suppressed MUA below baseline across all layers.

A novel aspect of the present experiments with SST interneuron stimulation was the presence of a haemodynamic offset response when the 16s stimulation was terminated. This effect was observed in some cases but not others. The reason for this is unclear, although slight variations in the depth of anaesthesia (which can alter SST firing (Adesnik H et al. 2012)) could be responsible. This variability in response may be maintained in awake animals as changes in behaviour or brain state (Adesnik H *et al.* 2012; Urban-Ciecko J and AL Barth 2016; Yavorska I and M Wehr 2016) can also significantly reduce the firing rate of SST neurons. Thus, only in those cases where central photostimulation induced a surround

inhibition response was the prolonged offset response in the central, previously stimulated, region observed. This later secondary peak in Hbt may be related to the long-lasting inhibition which is observed in these animals following photoactivation.

These responses during and after the 16s SST-stimulation period are difficult to interpret in terms of normal activation-induced neurovascular coupling.

Firstly, there seems to be a strong association between the presence of MUA inhibition in deep cortical layers and the inhibitory haemodynamic response in surrounding tissue. How might central activation of SST interneurons reduce blood volume in surrounding regions? Karnani et al. (2016) showed that lateral inhibition between adjacent cortical regions is mediated by lateral projecting SST interneurons. We have previously shown that a decrease in deep layer multi-unit activity is correlated with the negative surround BOLD signal in rat sensory cortex (Boorman L *et al.* 2010; Boorman L *et al.* 2015), our results presented here are qualitatively similar, suggesting SST interneurons projecting into neighbouring regions may be responsible. However, as SST neurons can inhibit pyramidal neurons and other inhibitory neurons (as reviewed by Yavorska I and M Wehr 2016) and these experiments were performed without the use of pharmacological blockers, we cannot rule out the possibility that the observed negative surround haemodynamic response is a result of suppression of excitatory transmission (Urban-Ciecko J and AL Barth 2016).

Secondly, there was a similarly strong association between reductions in deep-layer MUA and the occurrence of a large offset haemodynamic response in the previously stimulated region. It is particularly important to note that the positive post-stimulus haemodynamic response occurred without any corresponding long-lasting increase in MUA. Indeed, the central area MUA was suppressed during this positive haemodynamic response. In light of our findings with the nNOS interneurons (see above), one possibility could be that following SST interneuron stimulation offset, the small population of nNOS cells in the central stimulated region become active, potentially due to removal of inhibition from the activated SST interneurons, thereby causing the large haemodynamic response during a period of overall MUA suppression (Figure 3.7C, E). Alternatively, Mariotti et al. (2018) reported that activation of cortical SST interneurons caused delayed long-lasting $[Ca^{2+}]_i$ elevations in astrocytes. Increased astrocyte $[Ca^{2+}]_i$ is known to produce significant vasodilation (Zonta M *et al.* 2003; Gordon GR et al. 2008; Lind BL *et al.* 2013), therefore SST interneuron-evoked astrocyte $[Ca^{2+}]_i$ increases could cause the observed positive post-stimulus haemodynamic response. However, whether the time course of SST activation of astrocytes accords with the other neural and haemodynamic changes observed here remains to be determined.

On the other hand, the positive post-stimulus haemodynamic response may be associated with the brief post-stimulus transient increase in MUA activity. This activity occurs at a deeper depth in the cortex than the SST activation-evoked superficial increase in MUA, suggesting that a different population of neurons may be responsible for this MUA 'rebound'. The observation of a concurrent downward deflection in the LFP suggests that pyramidal cells may be involved in the observed 'rebound' activity (Bean BP 2007; Uhlirova H *et al.* 2016).

Given that up to 40% of SST neurons co-express nNOS (Yavorska I and M Wehr 2016), it is likely that a subset of neurons is activated in response to both nNOS-ChR2 and SST-ChR2 activation. Based on previous reports (Perrenoud Q et al. 2012), the overlapping population of SST+/nNOS+ neurons are likely to be located in layer VI of the cortex and to be predominantly type I nNOS interneurons (which are strongly labelled for nNOS and have high expression levels of SST, conversely only around 18% of type II nNOS neurons co-express SST). This suggests that NO release could, at least in part, be responsible for the SST-evoked haemodynamic responses. Interestingly, although nNOS interneurons comprise a smaller number of neurons than SST interneurons, we observed haemodynamic responses of similar amplitude during activation of either SST or nNOS-expressing neurons. This could be explained by the fact that NO is a potent vasodilator (Furchgott RF and JV Zawadzki 1980; Ignarro LJ *et al.* 1987; Palmer RM *et al.* 1987). On the other hand, as the latent increase in Hbt is only observed in the case of 16s SST activation, it is likely that this response is somehow SST-dependent. Future pharmacological studies could determine the contribution of each of these neuronal sub-populations to neurovascular regulation and confirm whether NO is indeed contributing to the observed haemodynamic responses.

While the use of anaesthesia in this study may be considered a limitation (Gao YR et al. 2017), we have previously demonstrated that in our chronic preparation (as used in the present study) mechanical somatosensory-evoked haemodynamic responses are comparable to those observed in the awake animal (Sharp PS *et al.* 2015). Furthermore, haemodynamic responses evoked by the activation of VGAT-expressing neurons exhibit similar amplitudes and time courses in anaesthetised and awake animals (Uhlirova H *et al.* 2016). Therefore, we expect that activating SST or nNOS interneurons (subsets of the VGAT population) in an awake animal would evoke similar haemodynamic responses to those reported here.

Overall, the results of this study extend our knowledge of how specific subpopulations of cortical GABAergic interneurons mediate key aspects of neurovascular control. This has implications for our understanding of several diseases in which neurovascular coupling and inhibitory interneurons are dysfunctional or lost; including epilepsy (Dudek FE and LR Shao

2003; Kumar SS and PS Buckmaster 2006; Harris S et al. 2013) and Alzheimer's disease (Zlokovic BV 2010; Verret L et al. 2012). Indeed, the demonstration that the targeting of a single cell population reliably evokes robust haemodynamic changes in the absence of associated large increases in neural activity suggests a potential novel treatment strategy for diseases in which chronic hypoperfusion plays a role, such as Alzheimer's disease. Meanwhile, the novel demonstration of deep layer inhibition during specific activation of SST interneurons could potentially be used to shut down aberrant neuronal activity, thus offering therapeutic strategies for diseases such as epilepsy. Future work should focus on the relationship between interneuron deficits, dysfunctional neurovascular coupling, and disease progression.

3.7 Acknowledgements

We would like to thank Michael Port for building and maintaining the whisker stimulation device and 2D-OIS apparatus.

3.8 Funding

This work was supported by a Wellcome Trust and Royal Society Sir Henry Dale Fellowship (grant number 105586/Z/14/Z to C.H.) and the Medical Research Council UK (grant number MR/M013553/1 to J.B and L.B).

3.9 References

Adesnik H, Bruns W, Taniguchi H, Huang ZJ, Scanziani M. 2012. A neural circuit for spatial summation in visual cortex. Nature. 490:226-231.

Ahlgrim NS, Manns JR. 2019. Optogenetic Stimulation of the Basolateral Amygdala Increased Theta-Modulated Gamma Oscillations in the Hippocampus. Front Behav Neurosci. 13:87.

Anenberg E, Chan AW, Xie Y, LeDue JM, Murphy TH. 2015. Optogenetic stimulation of GABA neurons can decrease local neuronal activity while increasing cortical blood flow. J Cereb Blood Flow Metab. 35:1579-1586.

Bean BP. 2007. The action potential in mammalian central neurons. Nature Reviews Neuroscience. 8:451.

Berwick J, Johnston D, Jones M, Martindale J, Redgrave P, McLoughlin N, Schiessl I, Mayhew JE. 2005. Neurovascular coupling investigated with two-dimensional optical imaging spectroscopy in rat whisker barrel cortex. Eur J Neurosci. 22:1655-1666.

Boorman L, Harris S, Bruyns-Haylett M, Kennerley A, Zheng Y, Martin C, Jones M, Redgrave P, Berwick J. 2015. Long-latency reductions in gamma power predict hemodynamic changes that underlie the negative BOLD signal. J Neurosci. 35:4641-4656.

Boorman L, Kennerley AJ, Johnston D, Jones M, Zheng Y, Redgrave P, Berwick J. 2010. Negative blood oxygen level dependence in the rat: a model for investigating the role of suppression in neurovascular coupling. J Neurosci. 30:4285-4294.

Buxton RB. 2010. Interpreting oxygenation-based neuroimaging signals: the importance and the challenge of understanding brain oxygen metabolism. Front Neuroenergetics. 2:8.

Cauli B, Tong XK, Rancillac A, Serluca N, Lambolez B, Rossier J, Hamel E. 2004. Cortical GABA interneurons in neurovascular coupling: relays for subcortical vasoactive pathways. J Neurosci. 24:8940-8949.

Christie IN, Wells JA, Southern P, Marina N, Kasparov S, Gourine AV, Lythgoe MF. 2013. fMRI response to blue light delivery in the naive brain: implications for combined optogenetic fMRI studies. Neuroimage. 66:634-641.

Devor A, Tian P, Nishimura N, Teng IC, Hillman EM, Narayanan SN, Ulbert I, Boas DA, Kleinfeld D, Dale AM. 2007. Suppressed neuronal activity and concurrent arteriolar vasoconstriction may explain negative blood oxygenation level-dependent signal. J Neurosci. 27:4452-4459.

Duchemin S, Boily M, Sadekova N, Girouard H. 2012. The complex contribution of NOS interneurons in the physiology of cerebrovascular regulation. Front Neural Circuits. 6:51.

Dudek FE, Shao LR. 2003. Loss of GABAergic Interneurons in Seizure-induced Epileptogenesis. Epilepsy Curr. 3:159-161.

Elghaba R, Vautrelle N, Bracci E. 2016. Mutual Control of Cholinergic and Low-Threshold Spike Interneurons in the Striatum. Front Cell Neurosci. 10:111.

Furchgott RF, Zawadzki JV. 1980. The obligatory role of endothelial cells in the relaxation of arterial smooth muscle by acetylcholine. Nature. 288:373-376.

Gao YR, Ma Y, Zhang Q, Winder AT, Liang Z, Antinori L, Drew PJ, Zhang N. 2017. Time to wake up: Studying neurovascular coupling and brain-wide circuit function in the un-anesthetized animal. Neuroimage. 153:382-398.

Gordon GR, Choi HB, Rungta RL, Ellis-Davies GC, MacVicar BA. 2008. Brain metabolism dictates the polarity of astrocyte control over arterioles. Nature. 456:745-749.

Gu X, Chen W, Volkow ND, Koretsky AP, Du C, Pan Y. 2018. Synchronized Astrocytic Ca. Cell Rep. 23:3878-3890.

Hamel E. 2006. Perivascular nerves and the regulation of cerebrovascular tone. J Appl Physiol (1985). 100:1059-1064.

Harris S, Bruyns-Haylett M, Kennerley A, Boorman L, Overton PG, Ma H, Zhao M, Schwartz TH, Berwick J. 2013. The effects of focal epileptic activity on regional sensory-evoked neurovascular coupling and postictal modulation of bilateral sensory processing. J Cereb Blood Flow Metab. 33:1595-1604.

Hu H, Cavendish JZ, Agmon A. 2013. Not all that glitters is gold: off-target recombination in the somatostatin-IRES-Cre mouse line labels a subset of fast-spiking interneurons. Front Neural Circuits. 7:195.

Ignarro LJ, Buga GM, Wood KS, Byrns RE, Chaudhuri G. 1987. Endothelium-derived relaxing factor produced and released from artery and vein is nitric oxide. Proc Natl Acad Sci U S A. 84:9265-9269.

Karagiannis A, Gallopin T, Dávid C, Battaglia D, Geoffroy H, Rossier J, Hillman EM, Staiger JF, Cauli B. 2009. Classification of NPY-expressing neocortical interneurons. J Neurosci. 29:3642-3659.

Karnani MM, Jackson J, Ayzenshtat I, Hamzehei Sichani A, Manoocheri K, Kim S, Yuste R. 2016. Opening Holes in the Blanket of Inhibition: Localized Lateral Disinhibition by VIP Interneurons. J Neurosci. 36:3471-3480.

Kocharyan A, Fernandes P, Tong XK, Vaucher E, Hamel E. 2008. Specific subtypes of cortical GABA interneurons contribute to the neurovascular coupling response to basal forebrain stimulation. J Cereb Blood Flow Metab. 28:221-231.

Kumar SS, Buckmaster PS. 2006. Hyperexcitability, interneurons, and loss of GABAergic synapses in entorhinal cortex in a model of temporal lobe epilepsy. J Neurosci. 26:4613-4623.

Lacroix A, Toussay X, Anenberg E, Lecrux C, Ferreirós N, Karagiannis A, Plaisier F, Chausson P, Jarlier F, Burgess SA, Hillman EM, Tegeder I, Murphy TH, Hamel E, Cauli B. 2015. COX-2-Derived Prostaglandin E2 Produced by Pyramidal Neurons Contributes to Neurovascular Coupling in the Rodent Cerebral Cortex. J Neurosci. 35:11791-11810.

Lecrux C, Toussay X, Kocharyan A, Fernandes P, Neupane S, Lévesque M, Plaisier F, Shmuel A, Cauli B, Hamel E. 2011. Pyramidal neurons are "neurogenic hubs" in the neurovascular coupling response to whisker stimulation. J Neurosci. 31:9836-9847.

Leithner C, Royl G. 2014. The oxygen paradox of neurovascular coupling. J Cereb Blood Flow Metab. 34:19-29.

Lind BL, Brazhe AR, Jessen SB, Tan FC, Lauritzen MJ. 2013. Rapid stimulus-evoked astrocyte Ca2+ elevations and hemodynamic responses in mouse somatosensory cortex in vivo. Proc Natl Acad Sci U S A. 110:E4678-4687.

Madisen L, Mao T, Koch H, Zhuo JM, Berenyi A, Fujisawa S, Hsu YW, Garcia AJ, 3rd, Gu X, Zanella S, Kidney J, Gu H, Mao Y, Hooks BM, Boyden ES, Buzsaki G, Ramirez JM, Jones AR, Svoboda K, Han X, Turner EE, Zeng H. 2012. A toolbox of Cre-dependent optogenetic transgenic mice for light-induced activation and silencing. Nat Neurosci. 15:793-802.

Mariotti L, Losi G, Lia A, Melone M, Chiavegato A, Gómez-Gonzalo M, Sessolo M, Bovetti S, Forli A, Zonta M, Requie LM, Marcon I, Pugliese A, Viollet C, Bettler B, Fellin T, Conti F, Carmignoto G. 2018. Interneuron-specific signaling evokes distinctive somatostatin-mediated responses in adult cortical astrocytes. Nat Commun. 9:82.

Mayhew J, Zheng Y, Hou Y, Vuksanovic B, Berwick J, Askew S, Coffey P. 1999. Spectroscopic analysis of changes in remitted illumination: the response to increased neural activity in brain. Neuroimage. 10:304-326.

Mulligan SJ, MacVicar BA. 2004. Calcium transients in astrocyte endfeet cause cerebrovascular constrictions. Nature. 431:195-199.

Network. NNBCD. 2009. Cre recombinase-expressing mice generated for the NIH Neuroscience Blueprint Cre Driver Network In. MGI Direct Data Submission.

Ogawa S, Lee TM, Kay AR, Tank DW. 1990. Brain magnetic resonance imaging with contrast dependent on blood oxygenation. Proc Natl Acad Sci U S A. 87:9868-9872.

Palmer RM, Ferrige AG, Moncada S. 1987. Nitric oxide release accounts for the biological activity of endothelium-derived relaxing factor. Nature. 327:524-526.

Perrenoud Q, Geoffroy H, Gauthier B, Rancillac A, Alfonsi F, Kessaris N, Rossier J, Vitalis T, Gallopin T. 2012. Characterization of type I and type II nNOS-expressing interneurons in the barrel cortex of mouse. Front Neural Circuits.

Roy CS, Sherrington CS. 1890. On the Regulation of the Blood-supply of the Brain. J Physiol. 11:85-158.117.

Rudy B, Fishell G, Lee S, Hjerling-Leffler J. 2011. Three groups of interneurons account for nearly 100% of neocortical GABAergic neurons. Dev Neurobiol. 71:45-61.

Rungta RL, Osmanski BF, Boido D, Tanter M, Charpak S. 2017. Light controls cerebral blood flow in naive animals. Nat Commun. 8:14191.

Sharp PS, Shaw K, Boorman L, Harris S, Kennerley AJ, Azzouz M, Berwick J. 2015. Comparison of stimulus-evoked cerebral hemodynamics in the awake mouse and under a novel anesthetic regime. Sci Rep. 5:12621.

Shmuel A, Augath M, Oeltermann A, Logothetis NK. 2006. Negative functional MRI response correlates with decreases in neuronal activity in monkey visual area V1. Nat Neurosci. 9:569-577.

Shmuel A, Yacoub E, Pfeuffer J, Van de Moortele PF, Adriany G, Hu X, Ugurbil K. 2002. Sustained negative BOLD, blood flow and oxygen consumption response and its coupling to the positive response in the human brain. Neuron. 36:1195-1210.

Stefanovic B, Warnking JM, Pike GB. 2004. Hemodynamic and metabolic responses to neuronal inhibition. Neuroimage. 22:771-778.

Taniguchi H, He M, Wu P, Kim S, Paik R, Sugino K, Kvitsiani D, Fu Y, Lu J, Lin Y, Miyoshi G, Shima Y, Fishell G, Nelson SB, Huang ZJ. 2011. A resource of Cre driver lines for genetic targeting of GABAergic neurons in cerebral cortex. Neuron. 71:995-1013.

Uhlirova H, Kılıç K, Tian P, Thunemann M, Desjardins M, Saisan PA, Sakadžić S, Ness TV, Mateo C, Cheng Q, Weldy KL, Razoux F, Vandenberghe M, Cremonesi JA, Ferri CG, Nizar K, Sridhar VB, Steed TC, Abashin M, Fainman Y, Masliah E, Djurovic S, Andreassen OA, Silva GA, Boas DA, Kleinfeld D, Buxton RB, Einevoll GT, Dale AM, Devor A. 2016. Cell type specificity of neurovascular coupling in cerebral cortex. Elife. 5.

Urban-Ciecko J, Barth AL. 2016. Somatostatin-expressing neurons in cortical networks. Nat Rev Neurosci. 17:401-409.

Valtschanoff JG, Weinberg RJ, Kharazia VN, Schmidt HH, Nakane M, Rustioni A. 1993. Neurons in rat cerebral cortex that synthesize nitric oxide: NADPH diaphorase histochemistry, NOS immunocytochemistry, and colocalization with GABA. Neurosci Lett. 157:157-161.

Vaucher E, Tong XK, Cholet N, Lantin S, Hamel E. 2000. GABA neurons provide a rich input to microvessels but not nitric oxide neurons in the rat cerebral cortex: a means for direct regulation of local cerebral blood flow. J Comp Neurol. 421:161-171.

Vazquez AL, Fukuda M, Kim SG. 2018. Inhibitory Neuron Activity Contributions to Hemodynamic Responses and Metabolic Load Examined Using an Inhibitory Optogenetic Mouse Model. Cereb Cortex. 28:4105-4119.

Verret L, Mann EO, Hang GB, Barth AM, Cobos I, Ho K, Devidze N, Masliah E, Kreitzer AC, Mody I, Mucke L, Palop JJ. 2012. Inhibitory interneuron deficit links altered network activity and cognitive dysfunction in Alzheimer model. Cell. 149:708-721.

Yavorska I, Wehr M. 2016. Somatostatin-Expressing Inhibitory Interneurons in Cortical Circuits. Front Neural Circuits. 10:76.

Zlokovic BV. 2010. Neurodegeneration and the neurovascular unit. Nat Med. 16:1370-1371.

Zonta M, Angulo MC, Gobbo S, Rosengarten B, Hossmann KA, Pozzan T, Carmignoto G. 2003. Neuron-to-astrocyte signaling is central to the dynamic control of brain microcirculation. Nat Neurosci. 6:43-50.

3.9 Supplementary Materials

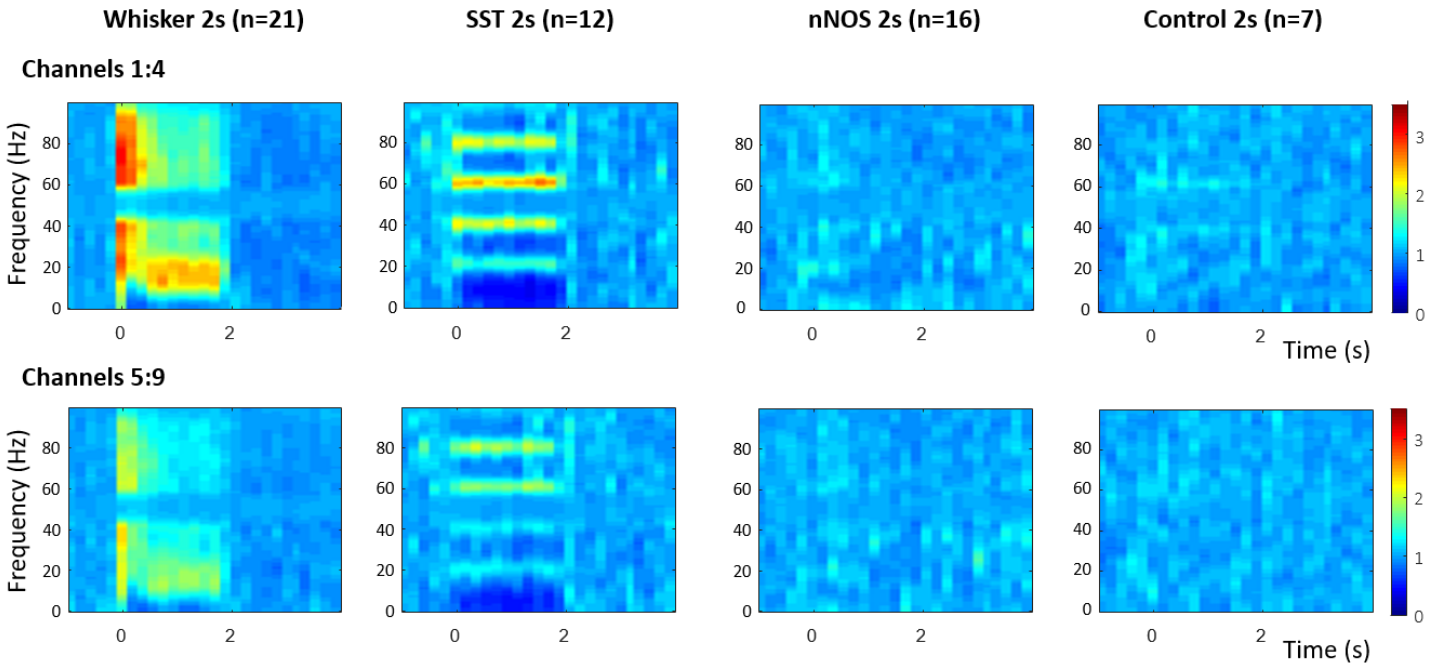

Supplementary Figure 1: Frequency power response to 2s stimulation. Mechanical whisker stimulation (5Hz, row 1), and photostimulation (99Hz, 0.45mW or 20Hz, 0.78mW) of SST-ChR2 mice (row 2), nNOS-ChR2 mice (row 3), control mice (row 4). Mean data shown, n represents number of mice.

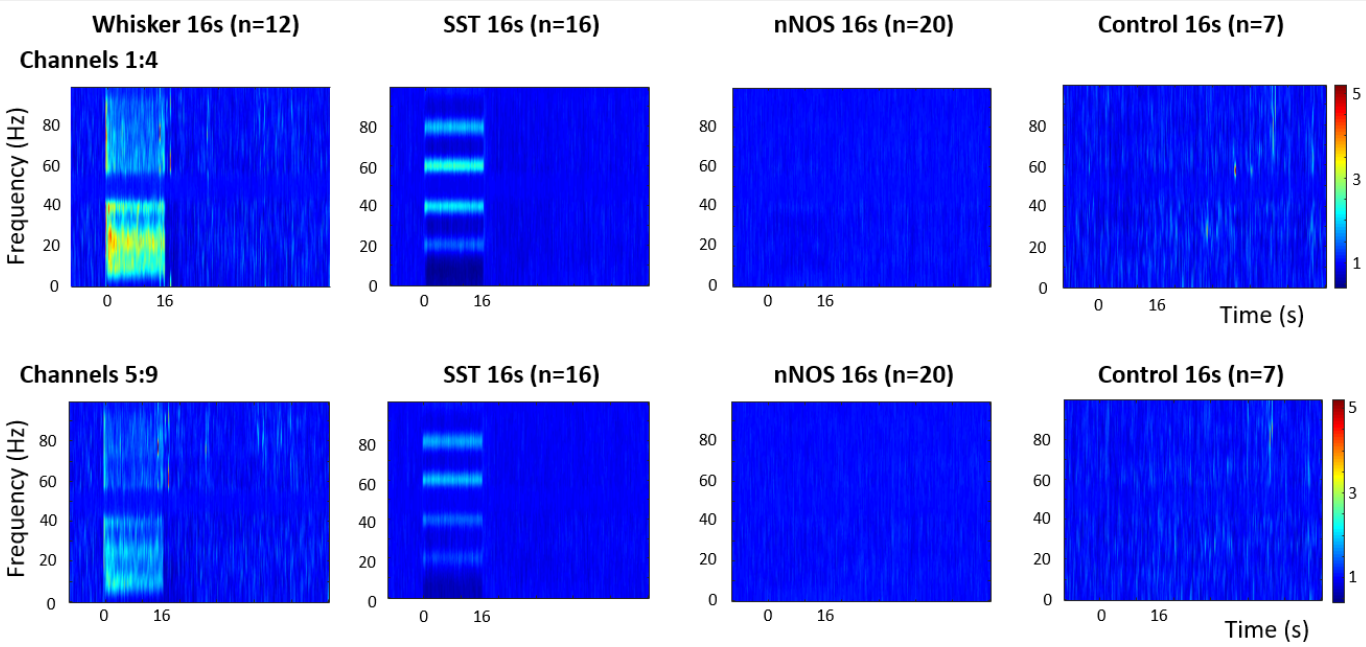

Supplementary Figure 2: Frequency power response to 16s stimulation. Mechanical whisker stimulation (5Hz, row 1), and photostimulation (99Hz, 0.244mW or 20Hz, 0.63mW) of SST-ChR2 mice (row 2), nNOS-ChR2 mice (row 3), control mice (row 4). Mean data shown, n represents number of mice.

Supplementary Table 3.1: Rise time of Hbt

Stimulation paradigm	Rise time (s) [mean ± s.e.m]	n (mice)
2s whisker	1.68 ± 0.04	39
2s NOS	1.12 ± 0.07	17
2s SST	0.89 ± 0.09	10
16s whisker	3.06 ± 0.21	16
16s NOS	1.13 ± 0.11	17
16s SST	0.77 ± 0.11	11

Photostimulation-evoked a significantly shorter Hbt rise time (taken as rise time between 10-85% of first peak response) than that evoked by whisker stimulation. When comparing rise time of evoked Hbt responses, for 2s stimulation a one-way ANOVA showed an overall effect of stimulation type ($F_{2,63}$ =62.73, p<0.0001). Tukey's multiple comparisons test revealed that there was a significant difference between whisker stimulation-evoked responses and both NOS-activation (p<0.0001) and SST-activation (p<0.0001) responses and between NOS and SST-evoked responses (p = 0.044).

For 16s stimulation, a one-way ANOVA showed a significant effect of stimulation type ($F_{2,41}$ =59.61, p<0.0001) on 16s stimulation-evoked Hbt response. Tukey's multiple comparisons test found a significant difference between whisker stimulation and NOS (p<0.0001) or SST-activation (p<0.0001).

Supplementary Table 3.2: Time to peak, Hbt

Stimulation paradigm	Time to peak (s, mean ± s.e.m)	n (mice)
2s whisker	2.61 ± 0.05	39
2s NOS	2.00 ± 0.08	17
2s SST	1.71 ± 0.11	10
16s whisker	4.26 ± 0.17	16
16s NOS	2.12 ± 0.16	17
16s SST	1.71 ± 0.24	11

Photostimulation-evoked a significantly shorter time to peak Hbt than that evoked by whisker stimulation. When comparing time to peak of the Hbt time series, for 2s stimulation a one-way ANOVA showed an overall effect of stimulation type ($F_{2,63}$ =47.56, p<0.0001). Tukey's multiple comparisons test revealed that there was a significant difference between whisker stimulation-evoked responses and both NOS-activation (p<0.0001) and SST-activation (p<0.0001) responses.

For 16s stimulation, a one-way ANOVA showed a significant effect of stimulation type ($F_{2,41}$ =57.2, p<0.0001) on 16s stimulation-evoked Hbt response. Tukey's multiple comparisons test revealed that there was a significant difference between whisker stimulation-evoked responses and both NOS-activation (p<0.0001) and SST-activation (p<0.0001) responses.

Supplementary Table 3.3: Area under curve, Hbt

Stimulation paradigm	Area under curve (mean ± s.e.m)	n (mice)
2s whisker	5.65 ± 0.42	39
2s NOS	10.7 ± 0.58	17
2s SST	11.38 ± 0.73	10
16s whisker	41.73 ± 4.56	16
16s NOS	28.27 ± 2.41	17
16s SST	64.79 ± 8.05	11

When comparing area under curve of the Hbt time series, for 2s stimulation a one-way ANOVA showed an overall effect of stimulation type ($F_{2,63}$ =35.86, p<0.0001). Tukey's multiple comparisons test revealed that there was a significant difference between whisker stimulation-evoked responses and both NOS-activation (p<0.0001) and SST-activation (p<0.0001) responses.

For 16s stimulation, a one-way ANOVA showed a significant effect of stimulation type ($F_{2,41}$ =13.35, p<0.0001) on 16s stimulation-evoked Hbt response. However, in this case, Tukey's multiple comparisons test found a significant difference between whisker stimulation and SST activation (p = 0.007) and between NOS and SST-activation (p<0.0001).

Chapter 4: Nitric oxide is not responsible for initial sensory-induced neurovascular coupling response in the barrel cortex of lightly anaesthetised mice

This chapter was published in Neurophotonics in June 2025

Lee, L., Boorman, L., Glendenning, E., Shen, C., Berwick, J., & Howarth, C. (2025). Nitric oxide is not responsible for initial sensory-induced neurovascular coupling response in the barrel cortex of lightly anesthetized mice. Neurophotonics, 12(S2), S22802.

4.1 Paper Title and Authors

Nitric oxide is not responsible for initial sensory-induced neurovascular coupling response in the barrel cortex of lightly anaesthetized mice

Llywelyn Lee[1,2,3], Luke W. Boorman[1], Emily Glendenning[1,2,3], Changlin Shen[1], Jason Berwick[1,2,3], Clare Howarth[1,2,3]

[1]Department of Psychology, University of Sheffield, Sheffield, S1 4DP, UK

[2]Neuroscience Institute, University of Sheffield, Sheffield, UK

[3]Healthy Lifespan Institute (HELSI), University of Sheffield, Sheffield, UK

I, Llywelyn Lee, am the sole first author on this manuscript. I performed the majority of the data collection, alongside the experimental planning, data analysis, statistical tests and wrote up the manuscript. This was with the help of the co-authors on this paper, whose contributions are listed below.

Emily Glendenning assisted with some of the thinned window surgeries. Luke Boorman helped with generating the altered-baseline analysis code. Changlin Shen assisted with data analysis in a subset of the data. Clare Howarth and Jason Berwick supervised the research, helped with experimental design, assisted in the experiments and provided critical review and commentary on all versions of the manuscript.

4.2 Abstract

Significance: Neurovascular coupling matches changes in neural activity to localised changes in cerebral blood flow. While much is known about the role of excitatory neurons in neurovascular coupling, that of inhibitory interneurons is unresolved. While nNOS-expressing interneurons are capable of eliciting vasodilation, the role of nitric oxide in neurovascular coupling is debated.

Aim: This study investigated the role of nitric oxide in haemodynamic responses evoked by nNOS-expressing interneurons and whisker stimulation in mouse sensory cortex.

Approach: In lightly anaesthetised mice expressing channelrhodopsin-2 in nNOS-interneurons, 2D optical imaging spectroscopy was applied to measure stimulation-evoked cortical haemodynamic responses. To investigate the underlying vasodilatory pathways involved, the effects of pharmacological inhibitors of NOS and 20-HETE were assessed.

Results: Haemodynamic responses evoked by nNOS-expressing interneurons were altered in the presence of the NOS inhibitor LNAME, revealing an initial 20-HETE-dependent vasoconstriction. In contrast, the initial sensory-evoked haemodynamic response was largely unchanged.

Conclusions: Our results challenge the involvement of nNOS-expressing interneurons and nitric oxide in the initiation of functional hyperemia, suggesting that nitric oxide may be involved in the recovery, rather than initiation, of sensory-induced haemodynamic responses.

Keywords

Nitric oxide, nNOS interneuron, neurovascular coupling, vasomotion, inhibitory interneuron, optogenetics

4.3 Introduction

The ability to regulate cerebral blood flow (CBF) in a localised and dynamic manner in response to neuronal activity is essential for the maintenance of healthy brain function. While the regulation of CBF by glutamatergic neurons has been well investigated[1], regulation by GABAergic inhibitory interneurons (INs) has received less attention. Using optogenetic approaches to specifically activate distinct neural populations, recent research has revealed not only that cortical INs are capable of regulating CBF[2-4], but that subpopulations of cortical INs, which release different vasoactive molecules[5], can drive distinct haemodynamic responses[6-9]. The vasodilatory pathways involved in specific IN-evoked haemodynamic responses remain understudied. Understanding how, and when, INs regulate CBF would inform our interpretation of functional imaging signals such as blood oxygen level dependent functional magnetic resonance imaging (BOLD fMRI), in which blood-based signals act as a proxy for neural activity[10]. Furthermore, understanding IN regulation of CBF has relevance for conditions in which altered CBF and IN dysfunction have previously been reported, such as Alzheimer's disease[11-13], epilepsy[14,15] and ageing[16,17].

Having previously demonstrated that neuronal nitric oxide synthase-expressing interneurons (nNOS INs) are able to evoke robust changes in cerebral blood volume and oxygenation[7], in this study we aimed to investigate the vasodilatory pathways underlying nNOS IN-evoked haemodynamic changes. A prime candidate was nitric oxide (NO), which is produced by three isoforms of the enzyme nitric oxide synthase (NOS): neuronal NOS (nNOS), expressed in neurons; endothelial NOS (eNOS), expressed in vascular endothelial cells; and inducible NOS (iNOS), expressed during inflammatory responses[18]. NO release by nNOS INs (which target blood vessels[19,20]) may also underpin CBF responses evoked by VGAT-expressing INs[4]. Furthermore, NO is involved in maintaining basal vascular tone[21] and has been suggested as a key mediator in sensory-evoked neurovascular coupling (as reviewed in [22]). NO can evoke vasodilation via several vasoactive pathways. In addition to relaxing smooth muscle cells via a cGMP-associated pathway[23], NO can also inhibit the production of 20-hydroxyeicosatetraenoic acid (20-HETE[24]), a vasoconstrictor[25-27], thus enhancing vasodilation[28-30]. However, the role of NO in neurovascular coupling remains unresolved, with genetic or pharmacological inhibition of NOS reported to decrease[29,31-34], increase[31,35] and have no effect on[4,29,31,36-39] haemodynamic responses to sensory stimulation.

Therefore, this study investigated the involvement of NO in nNOS IN-evoked and sensory stimulation-evoked haemodynamic changes. To this end, in whisker barrel cortex of lightly anaesthetised mice, we recorded haemodynamic responses to short duration (2s) optogenetic activation of nNOS INs and whisker stimulation, in the presence and absence of the

pharmacological non-selective NOS inhibitor N-nitro-L-arginine-methyl-ester (LNAME), which suppresses NO production. We report that although NO is involved in the initial haemodynamic response to nNOS IN activation, counteracting the constrictive effects of 20-HETE release, NO is not involved in the initiation of sensory-evoked haemodynamic responses but does alter return to baseline dynamics. The observed effect on post-stimulus recovery may be due to an interaction with LNAME-evoked vascular oscillations.

4.4 Materials and Methods

4.4.1 Animals

All procedures involving animals were performed in accordance with the UK Government, Animals (Scientific Procedures) Act 1986, were approved by the University of Sheffield ethical review and licensing committee, and were reported in line with the ARRIVE guidelines[40]. Mice had ad libitum access to food and water and were housed on a 12 hour dark/light cycle. 23 mice were used (14 males and 9 females), aged 4-9 months old (6.58 ± 1.36 months) and weighing 20-36g (29.08 ± 5.73g) on date of surgery. Mice were nNOS-CreERT x ChR2-EYFP (nNOS-ChR2), obtained by crossing heterozygous nNOS-CreERT mice (Stock 014541, Jackson Laboratory[41]) with homozygous ChR2(H134R)-EYFP mice (Stock 024109, Jackson Laboratory[42]), as used previously[7]. Mice positive for the nNOS-CreERT insertion (confirmed by genotyping of ear clips from pups) were used in these experiments. ChR2 expression was induced by intraperitoneal (i.p.) injection of tamoxifen (Sigma-Aldrich) at 100mg/kg, administered 3 times with a day between each injection. Treatment with tamoxifen was carried out when mice were aged between 1-5 months, and took place a minimum of 2 weeks prior to surgery to allow for gene expression to occur. Randomisation sequences were not used to assign animals to different pharmacological agents.

4.4.2 Surgical Preparation of Chronic Cranial Window

At least 2 weeks prior to experimental sessions, surgery to prepare a thinned cranial window over the right somatosensory cortex was performed as previously described by Sharp et al. (2015)[43]. In brief, i.p. injection of fentanyl-fluanisone (Hypnorm, Vetapharm Ltd), midazolam (Hypnovel, Roche Ltd) and sterile water (in a ratio of 1:1:2 by volume; 7ml/kg) was used to induce anaesthesia and anaesthesia was maintained using isoflurane (0.5-0.8%) in 100% oxygen at a flow rate of 1L/min. Surgical anaesthetic plane was monitored by regularly checking toe-pinch reflex response. To avoid optogenetic activation of ChR2, surgeries were performed in a dark room using a surgical light with a band pass filter (577±5 nm). Mice were

placed in a stereotaxic frame (Kopf Instruments) with a homoeothermic blanket (Harvard Apparatus) maintaining rectal temperature at 37˚C. Using a dental drill, an area of bone (~3mm x 3mm) overlying the right whisker barrel cortex was thinned to translucency and a thin layer of clear cyanoacrylate was applied to smooth and reinforce the area. Dental cement (Super bond C&B, Sun Medical) was used around the window to secure a stainless steel head-plate to the skull. Following surgery, mice were singly housed and were monitored using the mouse grimace scale[44] and weighed weekly. Any animals losing over 20% body weight post-operatively were culled; for this study no mice met this criteria.

4.4.3 2-Dimensional Optical Imaging Spectroscopy

Anaesthesia was induced via i.p. injection of fentanyl-fluanisone (Hypnorm, Vetapharm Ltd), midazolam (Hypnovel, Roche Ltd) and sterile water (in a ratio of 1:1:2 by volume; 7ml/kg) and anaesthesia was maintained using isofluorane (0.25%-0.7%) with 100% oxygen at a flow rate of 0.8L/min. Mice were head fixed within a stereotaxic frame, using the head-plate that was attached during surgery. A homeothermic blanket maintained rectal temperature of the mouse at 37˚C. 2-Dimensional Optical Imaging Spectroscopy (2D-OIS) allows changes in cortical haemodynamics (oxygenated haemoglobin: Hbo, deoxygenated haemoglobin: Hbr, and total haemoglobin: Hbt) to be measured. 2D-OIS was performed using our previously published methodology[45]. In brief, using a Lambda DG-4 high-speed filter changer (Sutter Instrument Company, USA), the cortex under the thinned window was illuminated with four wavelengths of light (587±9nm, 595±5nm, 560±15nm, 575±5nm). The remitted light was collected with a Dalso 1M60 CCD camera with a frame rate of 32 Hz. This was synchronised to the wavelength switching, resulting in an effective frame rate of 8Hz. To avoid collecting light from the 470nm photostimulation LED, the camera was fitted with a 490nm high pass filter. Spectral analysis was carried out pixel-by-pixel on the remitted light, based on the path length scaling algorithm (PLSA) as described previously[45,46], which allowed the generation of estimates for the changes from baseline of Hbo, Hbr and Hbt. The analysis assumed a baseline tissue concentration of haemoglobin of 100μM and oxygen saturation of 70%. This spectral analysis resulted in the production of 2-dimensional spatial images representing micromolar changes in the concentration of Hbo, Hbr and Hbt, over the time course of an experiment.

4.4.4 Electrophysiology

In some experiments neural activity was recorded concurrently with haemodynamic activity, to effectively assess both these aspects of neurovascular coupling. A cranial burr-hole was made in the right whisker barrel cortex (identified by response to whisker stimulation in a previous 2D-OIS experiment) to allow insertion of a 16-channel microelectrode (100μm spacing, 1.5-2.7MΩ impedance, site area 177μm^2; Neuronexus Technologies) to a depth of

~1600μm. To record neural activity, the electrode was connected to a preamplifier and data acquisition device (Medusa BioAmp/RZ5, TDT), and data were collected at 24kHz. During post-hoc analysis, data were downsampled to 6kHz and a 500Hz high pass filter was applied. A 'spike' was detected when data exceeded a threshold of 1.5 times the standard deviation above the mean. The number of spikes occurring in 100ms bins were counted and reported as MUA. Data from the 12 electrode channels corresponding to cortical depth were used, with data from channels 3-6 being used for time series analysis. To produce fractional change in MUA, responses were normalised to a 2s baseline. Trials were averaged to produce a mean response for each stimulation paradigm for each animal. For statistical analysis, the peak MUA and mean MUA during the stimulation period were calculated for each animal. Group means were produced by averaging across animals. One mouse was excluded from statistical analysis due to the presence of excessive noise.

4.4.5 Stimulations

Photostimulation: A fibre-coupled 470nm LED light source (ThorLabs) connected to a fibre optic cable (core diameter 200μm, Thorlabs, USA) delivered blue light for photostimulation of ChR2. 2s light delivery consisted of 10ms pulses at 99Hz (1V, 0.45 mW). We have previously confirmed that these photostimulation parameters do not elicit haemodynamic responses in non-ChR2-expressing mice[7].

Whisker stimulation: A plastic T-bar attached to a stepper motor moved whiskers of the left whisker pad ~1cm in the rostro-caudal direction[43]. Whiskers were stimulated for 2s, at 5Hz.

Simultaneous presentation of photostimulation and whisker stimulation was applied in order to assess whether the evoked haemodynamic responses summed in a linear manner.

In order to mitigate the effects of time since anaesthesia or pharmacological treatment, optogenetic, whisker and simultaneous stimulations were interleaved within each experiment. To improve the signal to noise ratio, each experiment contained 20-30 repeats of each stimulation type, with an inter-stimulus interval (ISI) of 25s.

4.4.6 Pharmacology

To reduce NO production, mice were treated with the non-selective NOS inhibitor N(G)-Nitro-L-arginine methyl ester (LNAME, Sigma). LNAME (10mg/ml made up with sterile saline) was administered via i.p. bolus injection (75mg/kg; which has been shown to reduce NOS activity within the cortex by 93% within 1 hour of injection[47]). 20-HETE production was inhibited by treatment with a selective inhibitor of CYP4A and 4F, N-(4-butyl-2-methylphenyl)-N'-hydroxy-methanimidamide (HET0016)[48]. HET0016 (Santa Cruz Biotechnology) was administered i.v. (tail vein, 10 mg/kg; a 5mg/ml solution was made up with 10% lecithin saline[49,50]).

3 cohorts of mice were used in these studies: 12 mice received LNAME alone, 5 mice received HET0016 alone, and 6 mice received LNAME and HET0016 together.

4.4.7 Procedure

Following anaesthetic induction, an electrode was inserted into the right whisker barrel cortex (if needed). 2D-OIS measurements of haemodynamic changes evoked by stimulation (photostimulation and/or whisker stimulation) were monitored continuously. Injection of pharmacological agent(s) occurred approximately 1 hour after 2D-OIS experiments started which, in the case of electrode insertion, allowed sufficient time for haemodynamics to recover from the resulting cortical spreading depolarisation (CSD)[51]. Timings of agent injection were kept consistent, regardless of whether an electrode was inserted. For this study, data from specific timepoints pre- and post-treatment were analysed. Pre-treatment responses to stimulation were taken from the experiment immediately prior to the injection of pharmacological agent(s). Responses to stimulation post-treatment were taken from the experiment occurring at the following time after injection of pharmacological agent(s): LNAME: 70-135 minutes (mean= 108±7 minutes) after injection which, in agreement with previous studies[47,52], was sufficient time for LNAME to have maximal effect (Fig 4.2); HET0016: 70-145 minutes (mean= 125±12 minutes); LNAME and HET0016: 70-135 minutes (121±9 minutes) after injection; No inhibitor (timing control experiments): 80-120 minutes (100±6 minutes) after the 'injection' timepoint.

4.4.8 Data analysis

All experiments and analysis were performed unblinded. Data analysis was performed using MATLAB (MathWorks). Using the spatial map of Hbt changes evoked by 2s whisker stimulation, generated by 2D-OIS, a region of interest (ROI) was automatically selected[7]. In brief, each pixel was averaged across time during the response period, to generate a mean pixel value. Any pixel whose value was greater than 1.5x standard deviation was included in the ROI. The resulting ROI (white ROI, Fig 4.1b) represents the area with the greatest haemodynamic response to the whisker stimulation, and therefore represents the whisker barrel cortex. Within this ROI, the arterial region most responsive to the pharmacological intervention was manually selected (purple ROI, Fig 4.1b). For each stimulation paradigm, the response across all pixels within the arterial ROI was averaged, producing the three haemodynamic time series (Hbo, Hbr and Hbt).

Baseline assumptions: For spectral analysis within the arterial ROI, before pharmacological intervention, a baseline oxygen saturation of 80% (in line with previously published values for anaesthetised mice with supplemental oxygen[53,54]) and tissue concentration of haemoglobin of 100μM, were assumed[55,56]. Pharmacological agents, including LNAME[57,58], have previously

been shown to alter myogenic tone. As data were continuously collected during our experiments it was possible, for each mouse, to measure the change in Hbt and Hbo evoked by treatment with pharmacological agents. Although these changes were minor, baseline assumptions for spectral analysis at post-pharmacological treatment periods were individually amended accordingly (See Supplementary Table S4.1 for group mean values).

Comparison of stimulation-evoked responses: To compare stimulation-evoked responses in trials involving photostimulation, residual artefact from the 470nm LED was removed using a modified boxcar function. For all stimulations, micromolar changes in haemodynamics were converted to fractional change (as compared to a 5s period before stimulation), ensuring that the results were less sensitive to our baseline assumptions[59]. For each stimulation paradigm, mean time series were produced for each animal by averaging across trials. To produce the group mean time series, these responses were then averaged across animals within each group.

Low frequency vascular oscillations: The last 1000s of the Hbt timeseries of 'pre-' and 'post-' experiments were used to assess low frequency vascular oscillations. A cubic polynomial trend was removed from the data and the amplitude of the signal was normalised between 0 and 1, before computing the Fourier transform (FFT). The area under the curve (AUC) between 0.09-0.11Hz was calculated in order to compare oscillations centred around 0.1Hz (vasomotion). To produce the group mean, FFTs (and associated AUC) were averaged across animals within each group.

For visualisation purposes (Fig 4.7a,c), following removal of the cubic polynomial trend a first order Savitzky-Golay filter was applied to the individual Hbt time series to smooth high frequency components (such as heart rate).

4.4.9 Statistics and Reproducibility

Three metrics (Fig 4.1g) were extracted from the stimulation-evoked haemodynamic time series: *initial minima*: the minimum value of Hbt and Hbo and maximum value of Hbr during the initial response period (defined as 0.25-5s after stimulation onset); *peak:* the maximum value of Hbt and Hbo and minimum value of Hbr during the response period (defined as 0.25-10s after stimulation onset); and *peak-to-peak amplitude:* the change between peak and trough (minima) in Hbt, Hbo or Hbr ([*peak*] – [*minima*]). Statistical analysis was carried out using SPSS (versions 26 and 28). Paired dot plots and violin plots were prepared using GraphPad Prism (version 9.3.1 and 10.4.2, respectively). Shapiro-Wilk test was used to assess the normality of data (ANOVA was considered robust if data were approximately normally distributed) and Levene's test was used to test for equality of variances. Outliers were identified as extreme if they had a studentised residual >3. For experiments in which

LNAME was applied alone, to determine statistical significance, a 3-way mixed ANOVA (within-group factors: drug [pre/post], stimulation type [photostimulation/whisker]; between group factor: electrode [absent/present]) was used. For other pharmacological agents and MUA, a repeated measures 2-way ANOVA was used (factors: drug [pre/post], stimulation type [photostimulation/whisker]). To assess differences in arterial oscillations, spectral power (AUC) was compared using a mixed 2-way ANOVA (between-group factor: drug [LNAME/no drug]; within-group factor: time [pre/post agent application]). In the spectral power comparison, one data point was identified as an extreme outlier, however its inclusion did not alter the outcome of the statistical analysis and so all data were included. For all multi-way ANOVAs, simple effects tests were carried out to further interrogate any significant interaction effects. To assess the evolution of the effect of LNAME, 3 timepoints (pre-LNAME injection, 0 minutes after LNAME injection, and 60-70 minutes after LNAME injection) were compared using a 1-way ANOVA with Greenhouse-Geisser correction applied. A paired 2-tailed t-test was used to compare temporal characteristics (rise time [time from 10 to 85% of peak response], time to peak, and onset time) of the whisker stimulation-evoked haemodynamic response before and after LNAME and to assess whether there were sex-dependent differences. For cases in which Shapiro-Wilks test suggested that data were not normally distributed, a Mann-Whitney U test was used to compare groups. Results were considered statistically significant if $p < 0.05$, unless otherwise stated. All data are reported as mean ± standard error of the mean (SEM), n= number of mice, unless otherwise stated. Sample sizes were based on those in previously published studies using similar pharmacological approaches[47].

4.5 Results

4.5.1 NO is involved in the initial nNOS IN-evoked haemodynamic response, but not in the initiation of a sensory-evoked haemodynamic response

Genetically modified mice expressing channelrhodopsin-2 (ChR2) in nNOS INs were used to investigate the involvement of NO in nNOS IN- and sensory-evoked cortical haemodynamic responses. In this mouse line, we previously observed that ChR2 expression occurs in approximately 90% of nNOS INs[7] with a selectivity of 94.7% (248/262 cells, 3 mice, 3 sections from each mouse[7]). Thus blue light can be used to selectively activate nNOS INs. Here, in lightly anaesthetised mice we combined 2-dimensional optical imaging spectroscopy (2D-OIS), optogenetics and pharmacological blockade to assess whether the localised haemodynamic response evoked by short duration (2s) nNOS IN activation or sensory stimulation were dependent on NO produced by NOS. High resolution 2D maps of stimulation-evoked changes in blood volume (Hbt), oxygenated haemoglobin (Hbo) and deoxygenated haemoglobin (Hbr)

were recorded before and after treatment with LNAME (75mg/kg, i.p.[47]). Mice first received a short duration (2s) mechanical stimulation of the whiskers to define the whisker barrel cortex and guide placement of the optrode and, where appropriate, multi-channel electrode. The optrode, consisting of a fibre optic-coupled blue LED (470nm) placed directly above the centre of the whisker barrel cortex, delivered the photostimulation necessary to activate ChR2. Each animal received interleaved whisker stimulations (2s, 5Hz), photostimulations (2s, 99Hz) and, in a subset of animals, simultaneous photostimulation and whisker stimulation. The resulting haemodynamic changes were centred around the optrode (photostimulation: Fig 4.1a) and localised to the whisker barrel cortex (whisker stimulation: Fig 4.1d), as we have previously reported[7]. Prior to treatment with LNAME, both 2s photostimulation of cortical nNOS INs (Fig. 4.1 a,c, top rows) and sensory stimulation (Fig. 4.1 d,e, top rows) elicited localised increases in concentration of Hbt and Hbo and decreases in Hbr concentration. As previously described[7], the largest increases in Hbt and Hbo were observed in branches of the middle cerebral artery (MCA) overlying the whisker barrel cortex, and a decrease in Hbr was observed in the draining veins (Fig 4.1a,d, top row). In response to photostimulation of nNOS INs, the time series of the haemodynamic response taken from an arterial region of interest (ROI, purple ROI Fig. 4.1b) revealed a bidirectional response comprising of an initial decrease in Hbt and Hbo accompanied by a concomitant increase in Hbr ('initial minima'), followed by an increase in Hbt and Hbo and decrease in Hbr ('peak'), which peaked following the cessation of stimulation (Fig. 4.1f, top left). In contrast, the time series of the haemodynamic response to whisker stimulation consisted solely of an increase in Hbt and Hbo and corresponding washout of Hbr, which peaked following the cessation of stimulation ('peak', Fig 4.1f, bottom left), with no measurable 'initial minima'.

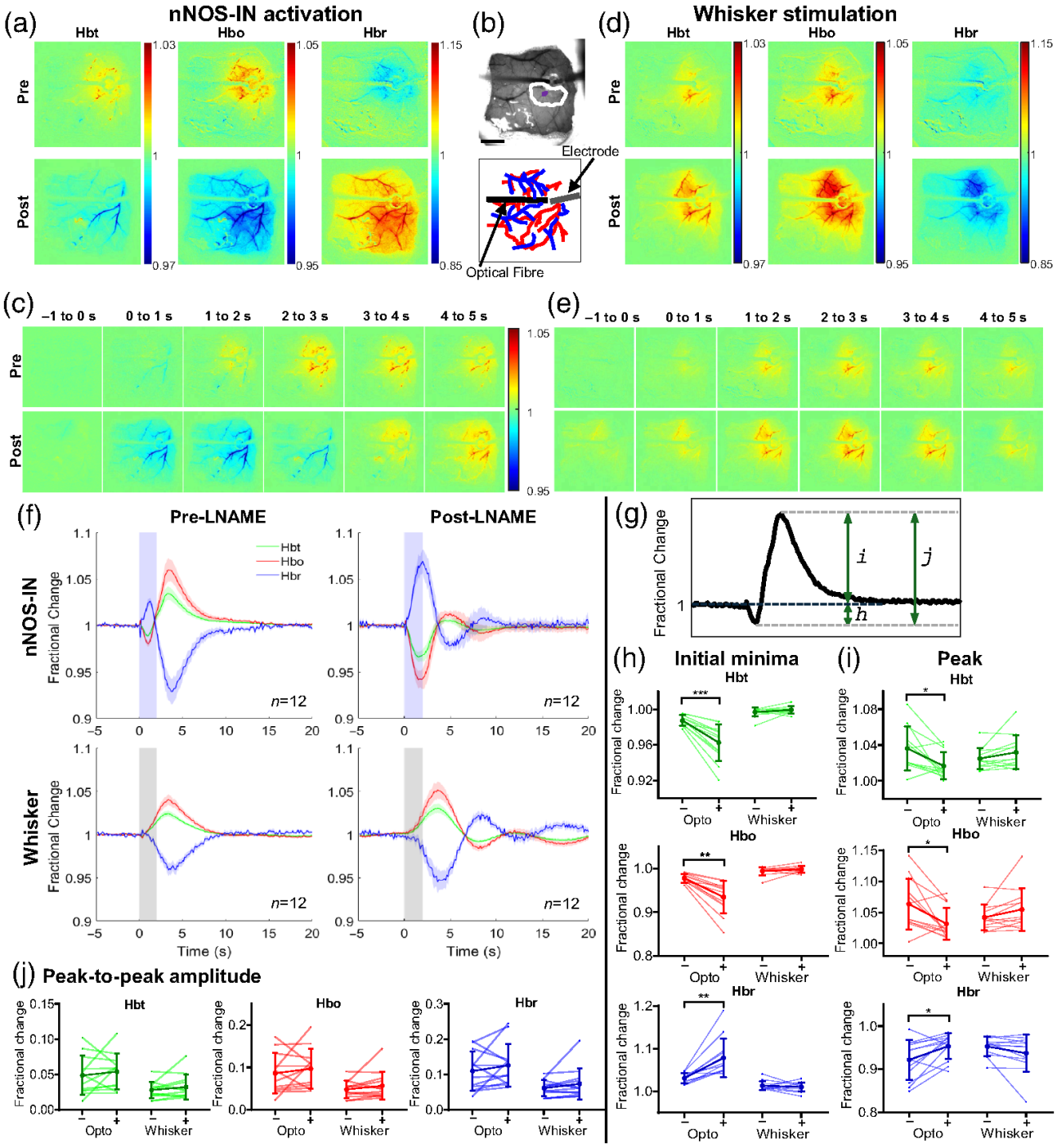
(a)
nNOS-IN activation
Hbt
Hbo
Hbr
Pre
Post
1.03
0.97
1.05
0.95
1.15
0.85
(b)
Electrode
Optical Fibre
(d)
Whisker stimulation
(c)
–1 to 0 s
0 to 1 s
1 to 2 s
2 to 3 s
3 to 4 s
4 to 5 s
(e)
(f)
Pre-LNAME
Post-LNAME
nNOS-IN
Whisker
Fractional Change
Hbt
Hbo
Hbr
n=12
Time (s)
(g)
i
j
h
(h)
Initial minima
(i)
Peak
Fractional change
Opto
Whisker
(j)
Peak-to-peak amplitude

Figure 4.1: NOS-dependence of haemodynamic responses evoked by 2s nNOS-IN activation or whisker stimulation. Data from representative mouse showing haemodynamic response to 2s optogenetic stimulation of nNOS-INs **(a-c)** or 2s whisker stimulation **(d-e)**. **(a,d)**: Trial-averaged stimulation-evoked changes in Hbt, Hbo and Hbr, as compared to baseline, pre-LNAME (upper) and post-LNAME (lower) injection. Colour bars represent fractional change. **(b):** Thinned cranial window (upper) with cortical surface vasculature visible (imaged at 575nm illumination), optic fibre and electrode can be seen. White ROI indicates whisker barrel cortex and purple ROI indicates arteriole region, from which timeseries data are extracted. Scalebar represents 1mm. Diagram (lower) indicating surface arteries (red) and veins (blue) visible through thinned skull window. **(c,e):** Evolution of trial-averaged changes in Hbt. Stimulation of nNOS-INs **(c)** or whiskers **(e)** occurs at 0-2s. Colour bar represents fractional change. Time points relative to stimulation onset (0s) are indicated above the images. **(f):** Group data (n=12 mice). Mean fractional change in Hbt, Hbo and Hbr in arteriolar ROI before (left) and after (right) LNAME. Blue shading indicates photostimulation period (upper), grey shading indicates whisker stimulation period (lower). Data: mean ± SEM **(g):** Hbt time series from example mouse illustrating three metrics used for analysis: initial minima **(h)**, peak **(i)**, peak-to-peak amplitude (change between peak and initial minima), **(j)**. **(h-j):** Fractional change in Hbt, Hbo and Hbr in response to optogenetic and whisker stimulation with (+) and without (-) LNAME. Darker lines represent group mean ± SD, lighter lines indicate trial-averaged mean for individual animals. n = 12 mice. *p<0.025, **p<0.005, ***p<0.0005. **(h):** Initial fractional change ('initial minima'). **(i):** Peak fractional change. **(j):** Maximum

70 minutes was found to be sufficient time for a significant effect of LNAME to be observed (Fig 4.2; $F(1.335,14.685)=21.442$, $p=0.00015$, $\eta^2=0.661$, n=12; Pre-LNAME vs 60-70 minutes, p = 0.0005; see Supplementary Table S4.2 for all pairwise comparisons). Therefore, post-LNAME haemodynamic measurements were obtained 70-135 minutes after systemic injection of LNAME. Following treatment with LNAME, the nNOS IN-evoked haemodynamic response was inverted, showing a decrease in Hbt and Hbo and an increase in Hbr (Fig 4.1a). Inspection of the timeseries of the haemodynamic response (Fig 4.1f) revealed a greater reduction in Hbt during the photostimulation period (as compared to pre-LNAME), followed by an increase in Hbt which peaked after stimulation offset (Fig 4.1c,f). In contrast, the initial haemodynamic

response evoked by whisker stimulation was unchanged by LNAME in terms of polarity and timing (Fig 4.1d, Supplementary Table S4.3). The localised haemodynamic response to whisker stimulation consisted of an increase in Hbt during the stimulation period, which peaked after stimulation offset, both before and after treatment with LNAME (Fig 4.1e, f).

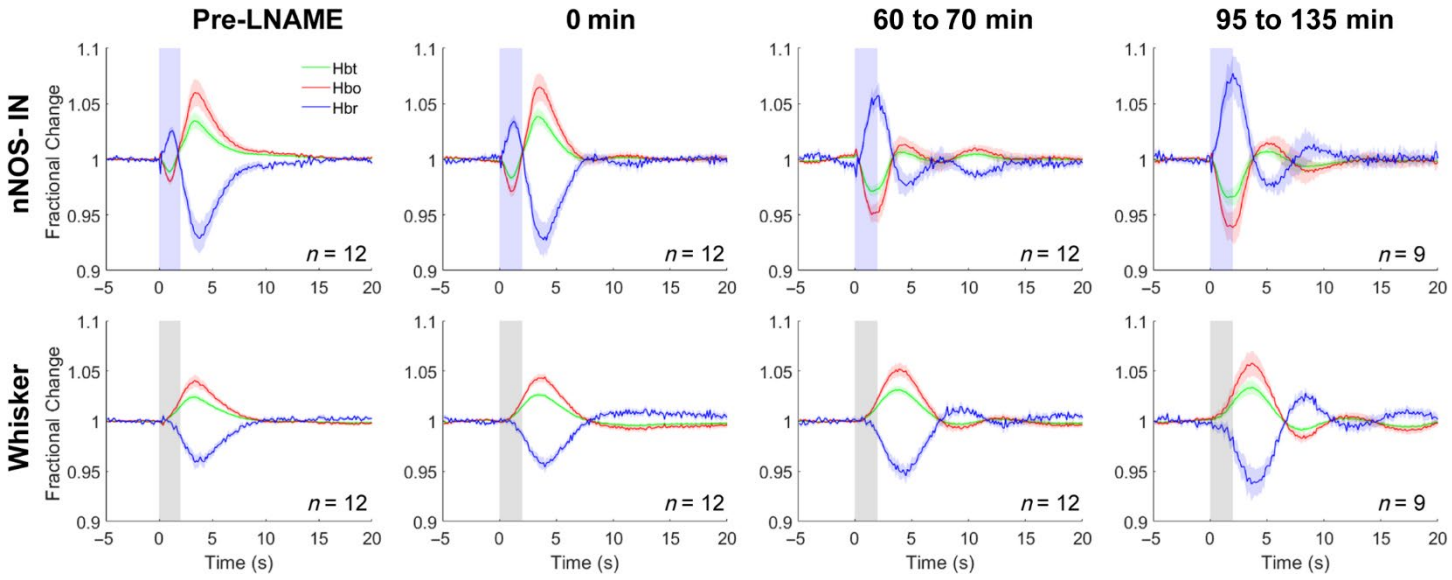

Figure 4.2: Development of effect of LNAME. Mean fractional change in Hbt, Hbo and Hbr in arteriolar ROI in response to 2s optogenetic stimulation of nNOS-INs (top row) or 2s whisker stimulation (lower row) at different time points relative to injection of LNAME. Column 1: experiment immediately prior to LNAME injection; Column 2: experiment immediately following LNAME injection; Column 3: experiment commencing 60-70 min post LNAME injection; Column 4: experiment commencing 95-135 min post LNAME injection. Blue shading indicates photostimulation period (top row), grey shading indicates whisker stimulation period (lower row). Data are mean ± SEM, n indicates number of mice. Note, the following data are also included in Figure 4.1: Pre-LNAME; Post-LNAME (95-135 min [n=9] and 60-70 min [n=3]).

A subset of animals underwent acute implantation of an electrode, to allow concurrent measurement of evoked haemodynamic (Fig 4.1) and neural (Fig 4.3) changes. As electrode placement elicits a CSD which can have long-lasting confounding effects on haemodynamic measures[59,60], insertion of an electrode was included as a factor in the statistical analysis of the haemodynamic data. Therefore, a 3-way mixed ANOVA was used to assess the effect of LNAME, stimulation type, and electrode insertion on the evoked haemodynamic response. Due to the bidirectional nature of the nNOS IN-evoked haemodynamic response, three metrics were analysed (Fig 4.1g), (1) maximal change during initial response ('initial minima', occurring between 0.25-5s after stimulation onset, Fig 4.1h), (2) maximal change during later response ('peak', occurring between 0.25-10s after stimulation onset, Fig 4.1i), and (3) peak-to-peak amplitude (calculated as [peak-initial minima], Fig 4.1j). For all haemodynamic profiles (Hbt,

Hbo and Hbr), for all metrics considered, no significant effect of electrode insertion was found (Supplementary Table S4.4-4.6), therefore haemodynamic data from all mice were combined (Fig 4.1). This lack of effect of CSD on haemodynamic responses is likely due to the fact that electrode insertion occurred approximately 50 minutes prior to collection of pre-LNAME data, sufficient time for haemodynamic recovery after CSD[51,60]. As a statistically significant interaction between stimulation type and LNAME was revealed for all haemodynamic profiles (initial minima: Supplementary Table S4.4, peak: Supplementary Table S4.5), suggesting that the effect of LNAME depends on the type of stimulation applied, simple effects tests to assess the effect of LNAME for each stimulation type were performed.

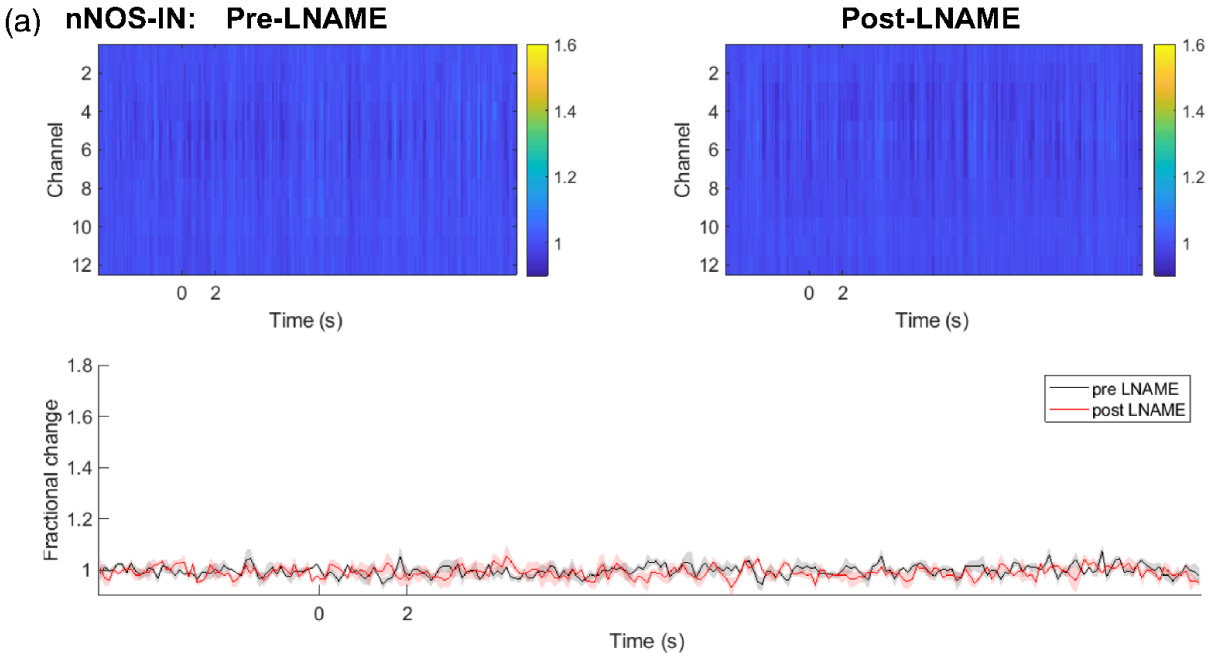
(a) nNOS-IN: Pre-LNAME
Post-LNAME
Channel
Time (s)
Fractional change
pre LNAME
post LNAME

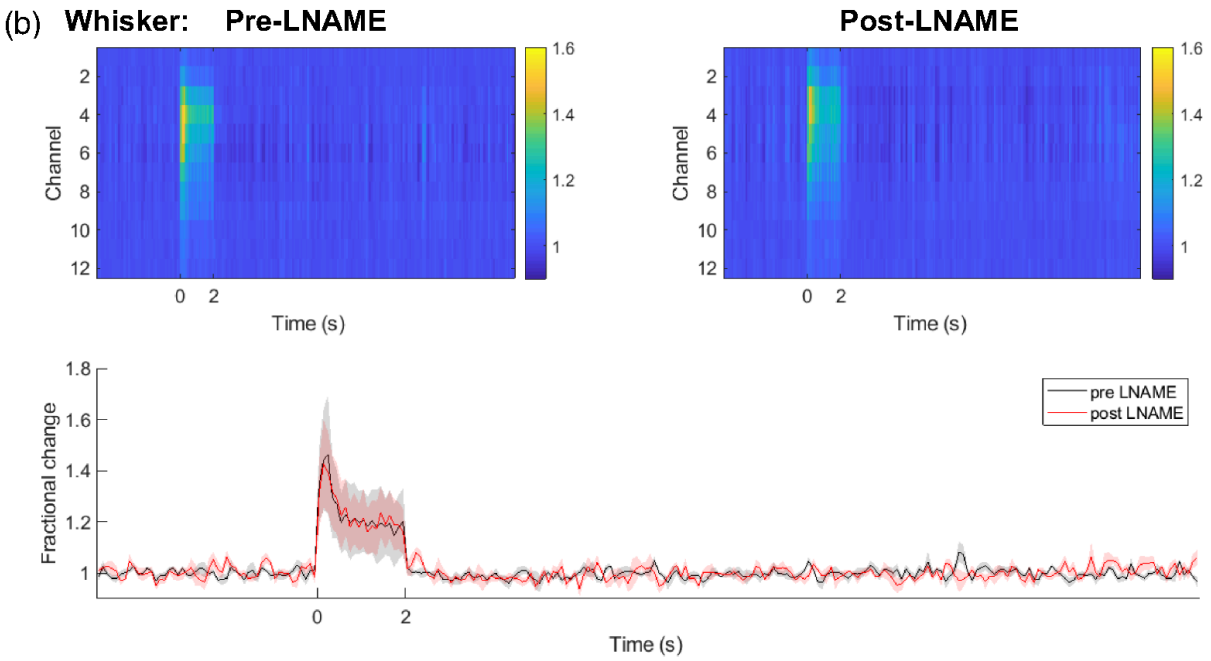
(b) Whisker: Pre-LNAME
Post-LNAME
Channel
Time (s)
Fractional change
pre LNAME
post LNAME

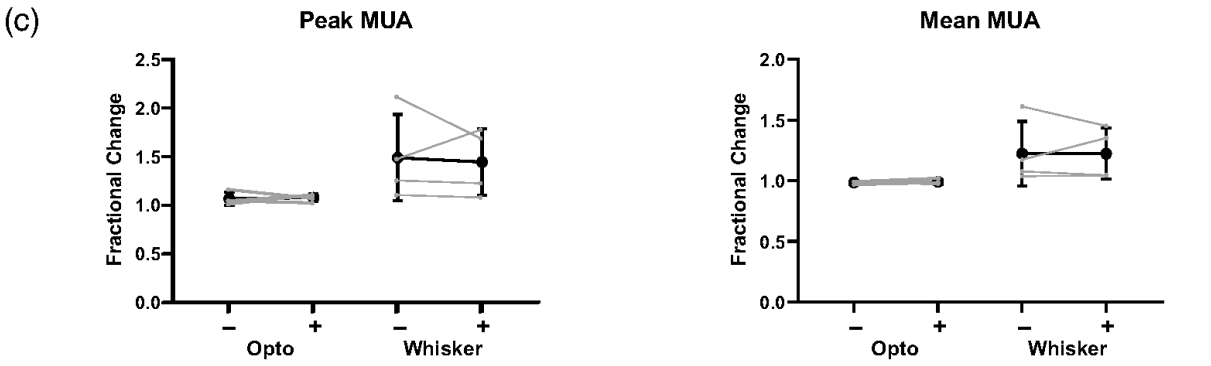
(c)
Peak MUA
Mean MUA
Fractional Change
Opto
Whisker

Figure 4.3: Stimulation-evoked multi-unit activity (MUA) is unchanged in presence of LNAME. Neural responses to **(a):** 2s optogenetic stimulation of nNOS-INs or **(b):** 2s whisker stimulation (stimulations start at 0s). **Top row:** mean change in MUA compared to baseline throughout cortical depth (as indicated by electrode channel number). Colour bar represents fractional change. **Left:** Pre-LNAME injection. **Right:** Post-LNAME injection. **Bottom row:** mean time series of response taken from channels 3-6 of electrode (mean ± SEM). Data were collected concurrently with subset of haemodynamic responses displayed in Figure 4.1. **(c):** Peak and Mean MUA during 2s optogenetic or whisker stimulation with (+) and without (-) LNAME. Darker lines represent group mean ± SD, lighter lines indicate trial-averaged means for individual animals. n=4 mice for all panels.

In the presence of LNAME, nNOS IN stimulation evoked a larger 'initial minima' (Fig 4.1h, n=12), resulting in a larger initial decrease in Hbt (pre= 0.988±0.002, post= 0.963±0.006, $p=4.69x10^{-4}$) and Hbo (pre= 0.977±0.003, post= 0.935±0.011, $p=8.28x10^{-4}$), and a greater initial increase in Hbr (pre= 1.031±0.004, post= 1.079±0.014, p= 0.002). Furthermore, post LNAME the 'peak' haemodynamic response to nNOS IN activation was reduced across all haemoglobin components (Hbt: pre= 1.036±0.007, post= 1.017±0.005, p= 0.013; Hbo: pre= 1.064±0.011, post= 1.032±0.008, p= 0.016; Hbr: pre= 0.921±0.012, post= 0.953±0.009, p= 0.023, Fig 4.1i, n=12), as compared to before LNAME injection.

This observed decrease in peak haemodynamic response may be due to an increased initial vasoconstriction (Fig 4.1h) occurring prior to an unchanged vasodilation. In support of this suggestion, the nNOS IN-evoked peak-to-peak amplitude (measured as minima to peak) in Hbt, Hbo and Hbr was indeed unchanged in the presence of LNAME (Fig 4.1j, Supplementary Table S4.6). These data suggest that while the initial haemodynamic response to nNOS IN activity is dependent on NO production by NOS, a second, NO-independent, pathway underlies the later increases in Hbt, Hbo, and associated washout of Hbr.

In contrast to the significant effect on the nNOS IN-evoked haemodynamic response, changes in Hbt, Hbo and Hbr evoked by whisker stimulation were unchanged in the presence of LNAME (Fig 4.1f-j, Supplementary Table S4.4-4.6). Furthermore, Hbt rise time (time between 10-85% of peak response), time to peak, and onset time were all unaffected by LNAME (Supplementary Table S4.3). These data suggest that NO is not involved in the initiation of sensory-evoked functional hyperemia in the somatosensory cortex.

The emergence of an oscillation in all haemodynamic components on return to baseline following stimulation in the presence of LNAME was notable in both photostimulation- and whisker stimulation-evoked responses (Fig 4.1f), suggesting that NO may play a role in damping the haemodynamic return to baseline following either nNOS IN or whisker stimulation.

To confirm that the observed LNAME-associated differences in nNOS IN-evoked haemodynamic changes were not due to factors such as duration of imaging under anaesthesia, in a subset of anaesthetised mice, time-matched experiments were also performed without application of LNAME. No time-associated significant differences were observed in haemodynamic responses to either photostimulation or whisker stimulation, confirming that the described changes are not due to factors associated with the duration of the experiment (Fig 4.4, Supplementary Table S4.7).

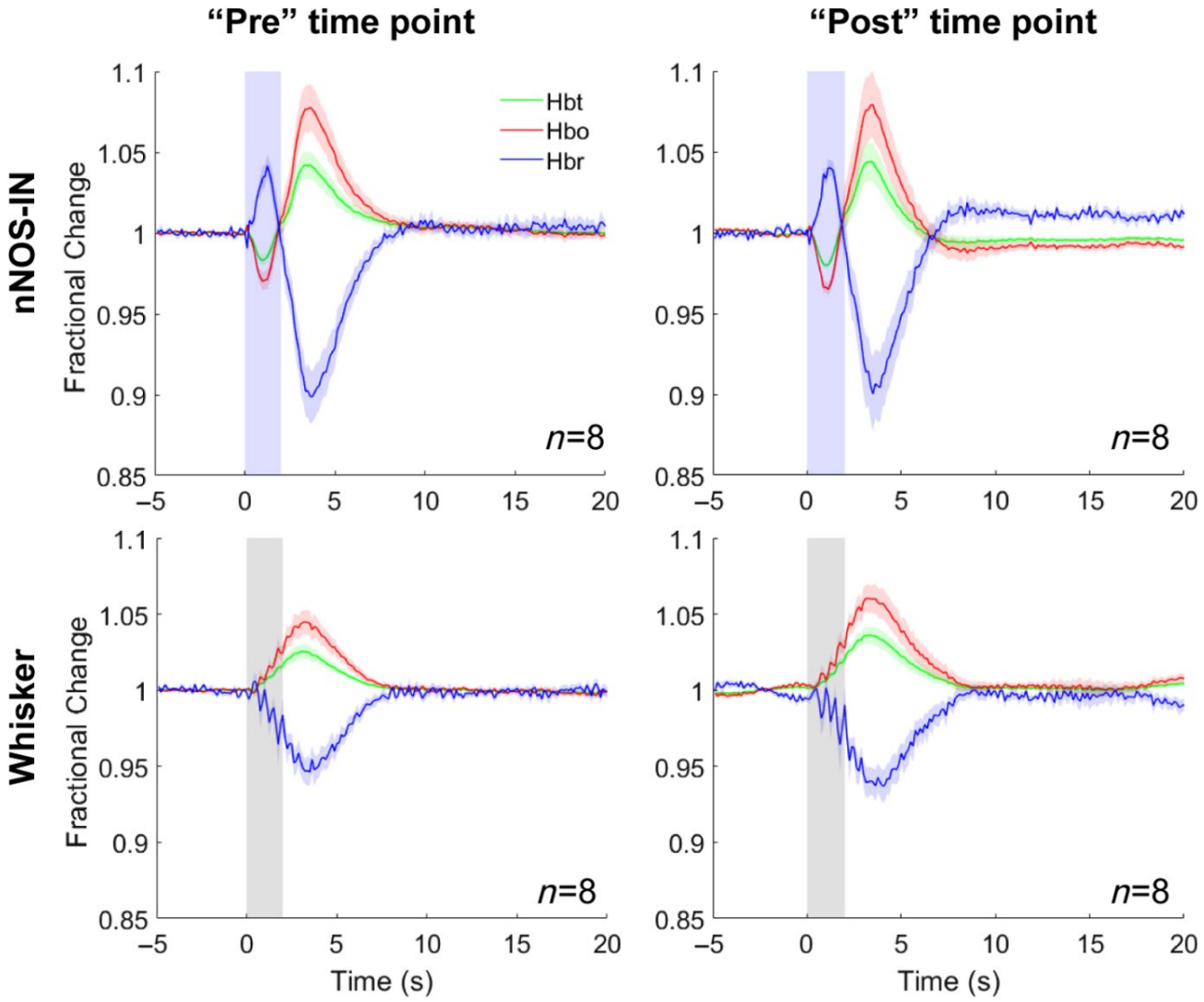

Figure 4.4: Time-matched experiments with no inhibitor applied. Mean fractional change in Hbt, Hbo and Hbr in arteriolar ROI in response to 2s optogenetic activation of nNOS-INs (top row) or 2s whisker stimulation (bottom row) in anaesthetised mice in which no pharmacological inhibitor was applied. The "pre" (left) and "post" (right) measurement points were time-matched to the pre and post time points in the experiments in which LNAME was administered (Fig 1). Blue shading indicates photostimulation period (top row), grey shading indicates whisker stimulation period (bottom row). Data are mean ± SEM, n represents number of mice.

Although sex hormones, including estrogen, have previously been suggested to interact with NO signalling and vascular tone[61], we found no effect of sex on the haemodynamic response to either photostimulation of nNOS INs or whisker stimulation, both in the absence and presence of LNAME (Supplementary Figure S4.1, Supplementary Table S4.8).

Taken together, these data suggest that while NO plays a key role in the initial haemodynamic response evoked by nNOS IN activation, the initiation of whisker stimulation-evoked haemodynamic changes are largely independent of NOS activity.

4.5.2 Evoked neural activity was unaltered by NOS inhibition

As the measured haemodynamic responses reflect stimulation-evoked neural activity, we assessed whether LNAME alters evoked neural activity. In a subset of mice, stimulation-evoked electrophysiological and haemodynamic changes were measured concurrently before and after LNAME injection to confirm that the observed LNAME effects reflect altered vascular responses, rather than a change in evoked neural activity. A sixteen channel Neuronexus electrode was inserted into the centre of the whisker barrel cortex in order to measure the electrophysiological response to stimulation. In agreement with our previous findings[7], 2s photostimulation of cortical nNOS INs evoked a robust haemodynamic response (Fig 4.1) in the absence of a measurable change in ongoing neural activity (multi-unit activity (MUA); Fig. 4.3a). The lack of measurable change in neural activity persisted in the presence of LNAME (Fig 4.3a,c). Similarly, whisker stimulation-evoked increases in MUA, which extended throughout the depth of the cortex and lasted for the duration of the stimulation (Fig 4.3b), were unaffected by LNAME (Fig 4.3b-c). These data confirm that LNAME had no effect (Peak MUA: $F(1,3)=0.032$, $p=0.869$; Mean MUA: $F(1,3)=0.003$, $p=0.958$, $n=4$; Supplementary Table S4.9) on the neural activity underlying the evoked localised haemodynamic responses (Fig 4.1).

4.5.3 NO reduces 20-HETE-evoked vasoconstriction during nNOS IN activation

As NO is known to inhibit 20-HETE formation[62] we hypothesised that the larger initial decrease in Hbt (indicative of vasoconstriction) observed in response to nNOS IN activation (Fig 4.1a,c,f,h) in the presence of the NOS inhibitor LNAME was due to 20-HETE production[63]. To further investigate the NOS-dependent vasoactive pathway underlying nNOS IN-evoked localised haemodynamic changes, in a separate cohort of mice nNOS IN and whisker stimulation-evoked haemodynamic changes were recorded before and after combined treatment with LNAME (75 mg/kg, i.p.) and HET0016 (a selective inhibitor of CYP4A and CYP4F[48] which produce 20-HETE, 10 mg/kg, i.v.[49]; Fig 4.5). Repeated measures 2-way ANOVAs (factors: drug, stimulation type) revealed interactions between stimulation and drug for both the Hbt initial minima ($F(1,5)=18.809$, $p=0.007$, $\eta^2= 0.790$, $n=6$; Supplementary Table

S4.10) and peak (F(1,5)=23.137, p=0.005, η^2= 0.822, n=6; Supplementary Table S4.11). Simple effects tests were therefore performed to assess the combined effect of LNAME and HET0016 on each stimulation type. For 2s photostimulation of nNOS INs, neither the initial minima in Hbt (Fig 4.5b, pre= 0.986±0.005, post= 0.973±0.01, p= 0.05, Supplementary Table S4.10), nor the peak Hbt (Fig 4.5c, pre= 1.07±0.011, post= 1.04±0.008, p= 0.052, Supplementary Table S4.11) were significantly different before and after treatment with LNAME and HET0016. Combined with the results of treating with LNAME alone (Fig 4.1), these data suggest that during short duration nNOS IN activation NO acts, at least in part, to reduce 20-HETE-elicited vasoconstriction.

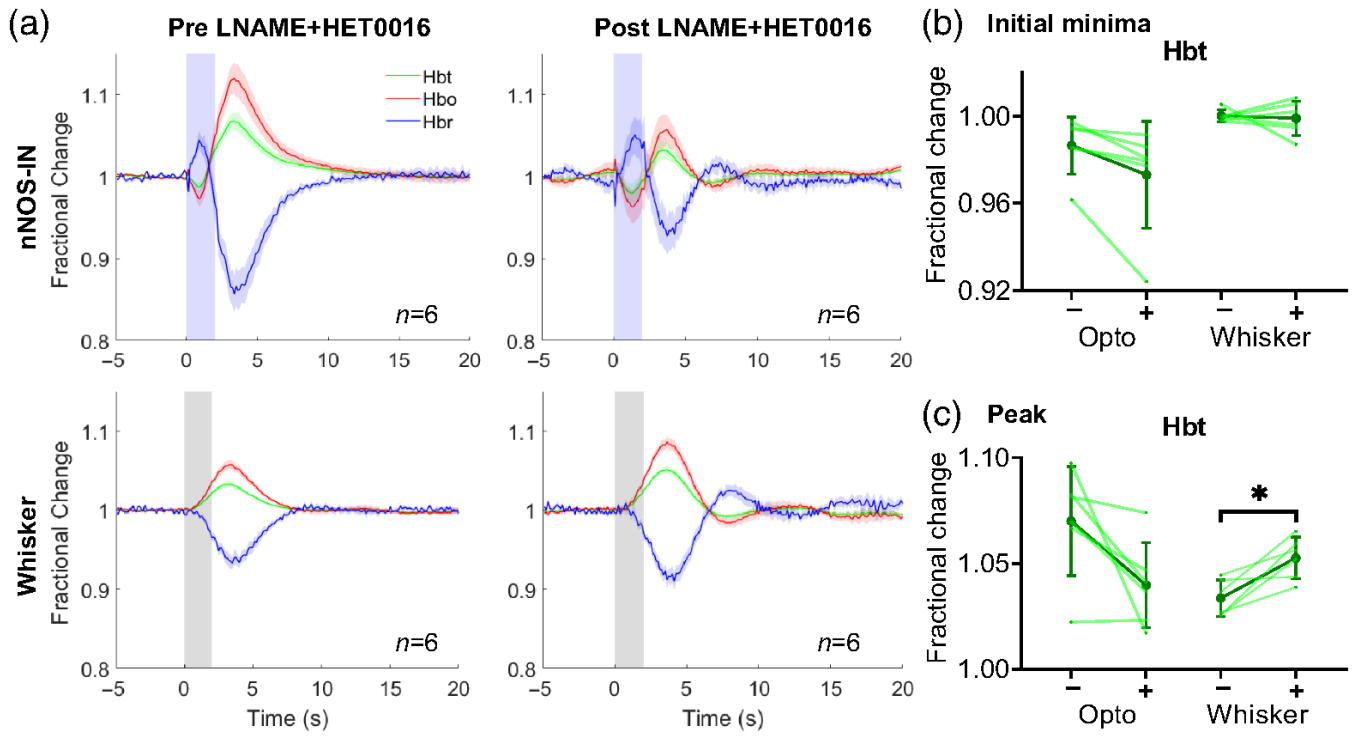

Figure 4.5: Haemodynamic responses evoked by nNOS-IN activation or whisker stimulation in presence of simultaneous inhibition of NOS and 20-HETE synthesis. Group data (n=6 mice). **(a):** Mean fractional change in Hbt, Hbo and Hbr in arteriolar ROI before (left) and after (right) LNAME and HET0016 injection. Blue shading indicates photostimulation period (upper panels), grey shading indicates whisker stimulation period (lower panels). Data are mean ± SEM. **(b-c):** Darker lines represent group mean ± SD, lighter lines indicate trial-averaged mean for individual animals. **(b):** Initial fractional change ('initial minima') in Hbt in response to optogenetic and whisker stimulation, with (+) and without (-) inhibitors (LNAME+HET0016). **(c):** Maximum fractional change in Hbt ('peak') evoked by optogenetic and whisker stimulation, with (+) and without (-) LNAME+HET0016. *p<0.025

In response to 2s whisker stimulation, the peak Hbt change was significantly greater when production of NO and 20-HETE were inhibited (Fig 4.5c, pre= 1.034±0.004, post= 1.053±0.004, p= 0.013, Supplementary Table S4.11), suggesting that production of 20-HETE during sensory stimulation causes a constriction which is overcome by a NO-independent vasodilatory mechanism.

As previously observed in the presence of LNAME alone (Fig 4.1f), an oscillation in all haemodynamic components was observed on return to baseline following stimulation in the presence of LNAME and HET0016 (Fig 4.5a), further supporting our suggestion that NO plays

a role in damping the haemodynamic return to baseline following nNOS IN activation or sensory stimulation.

If NO release by nNOS INs inhibits 20-HETE formation, it would be expected that applying HET0016 in the presence of this NO release would provide no additional reduction in 20-HETE formation and, therefore, have no effect on the nNOS IN-evoked initial reduction in Hbt. Indeed, simple effects tests (Supplementary Table S4.12) suggest that applying HET0016 alone (10 mg/kg, i.v.) did not significantly alter the initial Hbt minima evoked by photostimulation of nNOS INs (Supplementary Figure S4.2, pre= 0.986±0.008, post= 0.982±0.008, p = 0.043, n=5). Combining these data with the observed effects of LNAME (Fig 4.1) and concurrent LNAME and HET0016 (Fig 4.5) suggests that NO inhibits the production of 20-HETE in response to nNOS IN activation.

4.5.4 Haemodynamic responses to whisker stimulation and nNOS IN activation sum in a linear manner

Having demonstrated the differential involvement of NO and 20-HETE in the haemodynamic responses to nNOS IN activation and whisker stimulation, we hypothesised that whisker stimulation-evoked functional hyperemia and nNOS IN-evoked haemodynamic responses are driven by different vasoactive pathways. If this is the case, summing the change in Hbt evoked by photostimulation of cortical nNOS INs and that evoked by whisker stimulation should predict the change in Hbt evoked by simultaneous presentation of whisker and nNOS IN stimulation. To test this, a subset of animals received simultaneous photostimulation of nNOS INs and whisker stimulation, in addition to the separate photostimulation and whisker stimulation described above. In these mice, linear summation of the Hbt time series evoked by whisker stimulation and that evoked by photostimulation of cortical nNOS INs predicted the time series of the Hbt changes evoked by simultaneous stimulation of nNOS INs and whiskers, both in the absence and presence of LNAME (Fig 4.6). This linear summation further supports our suggestion that nNOS IN activation and whisker stimulation drive haemodynamic changes via different vasoactive pathways.

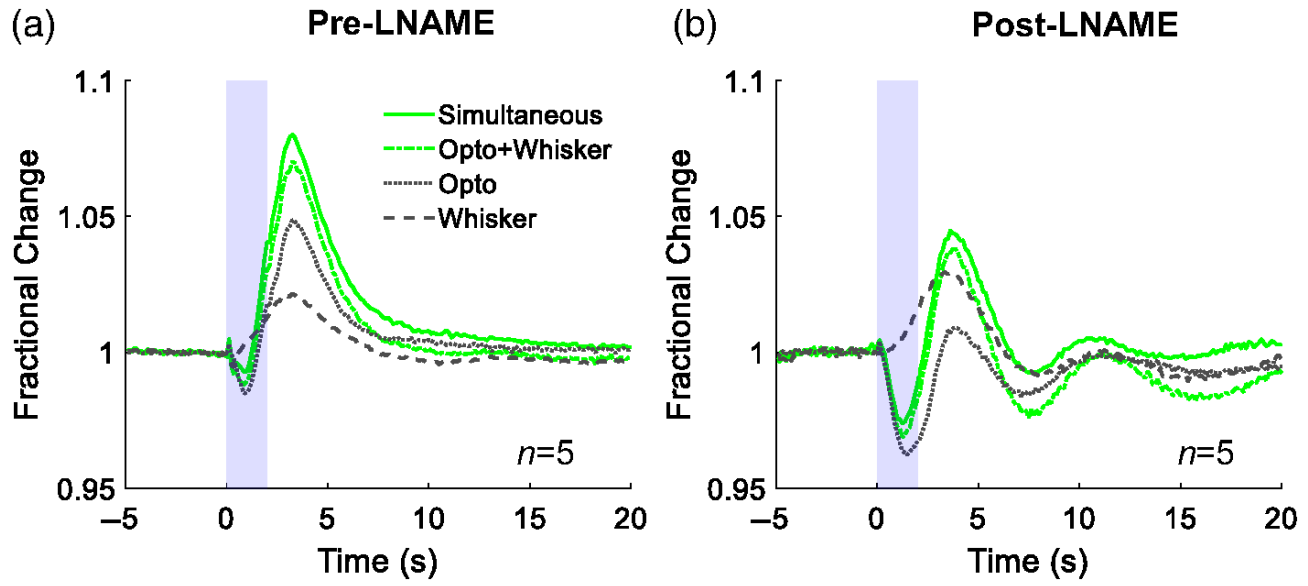

Figure 4.6: Change in Hbt evoked by simultaneous presentation of whisker and optogenetic stimulation is similar to that predicted by summing changes in Hbt evoked by independent optogenetic and whisker stimulation. Group data (n=5 mice): Mean fractional change in Hbt in arteriolar ROI before **(a)** and after **(b)** NOS inhibition with LNAME. Blue shading indicates stimulation period. Continuous green line indicates haemodynamic response to 2s simultaneous stimulation, dash and dot green line indicates the predicted response calculated by summing the responses to separate 2s optogenetic (grey dotted line) and 2s whisker (grey dashed line) stimulations. For visual clarity, error bars are not shown. (Separate optogenetic and whisker stimulation data are also included in Figure 1).

4.5.5 Systemic injection of LNAME enhances vasomotion in anaesthetised mice

Vasomotion, a low frequency oscillation in arteriole diameter occurring at ~0.1 Hz[64,65], emerges when NOS is inhibited[66]. Therefore, in addition to characterising the effect of NOS inhibition by LNAME on stimulation-evoked cortical haemodynamics, we also examined the effect of NOS inhibition on low frequency arterial oscillations. We detected an increase in the power of low frequency arterial oscillations, centred around 0.1Hz, after LNAME injection as compared to before injection (Fig 4.7, area under the curve (AUC): [0.09-0.11 Hz]; p=0.000062, n=12, Supplementary Table S4.13-4.14), which was not apparent in the absence of LNAME (Fig 4.7, 'pre' vs 'post' in no inhibitor condition, p=0.531, n=8, Supplementary Table S4.13-4.14). These data confirm that NOS inhibition results in enhanced low frequency vascular oscillations[31,67]. Additional peaks in the power spectrum which reflect the frequency of stimulation (ISI of 25s: 0.04Hz) and its harmonics can be seen in all cases (Fig 4.7). As stimulation paradigms were interleaved and LNAME alters the haemodynamic response to photostimulation of nNOS INs but not whisker stimulation (Fig 4.1), the peak associated with the stimulation pattern is shifted to a lower frequency in the presence of LNAME (Fig 4.7b).

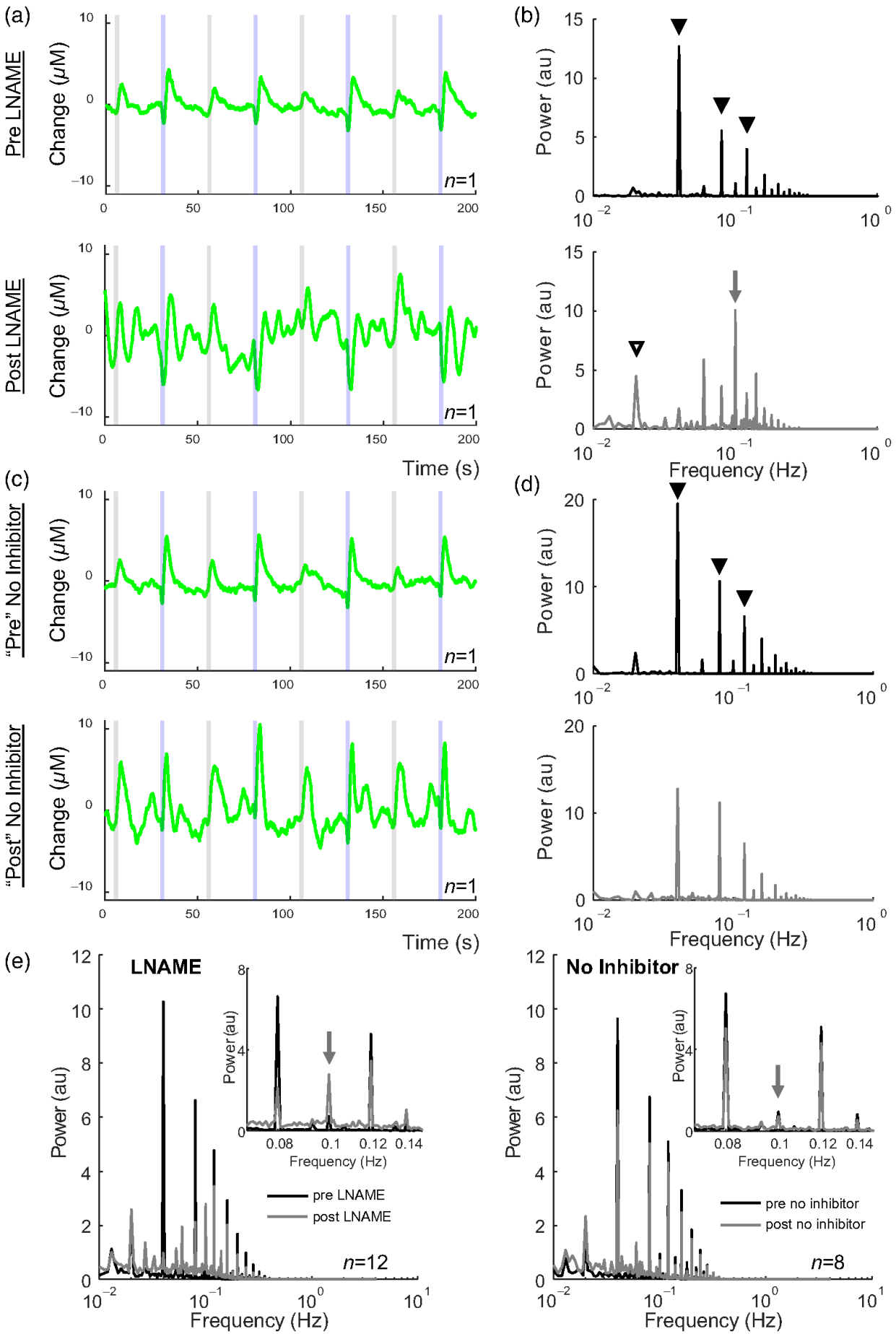
(a)
Pre LNAME
Change (μM)
n=1
Post LNAME
Change (μM)
n=1
Time (s)
(b)
Power (au)
Power (au)
Frequency (Hz)
(c)
"Pre" No Inhibitor
Change (μM)
n=1
"Post" No Inhibitor
Change (μM)
n=1
Time (s)
(d)
Power (au)
Power (au)
Frequency (Hz)
(e)
LNAME
Power (au)
Power (au)
pre LNAME
post LNAME
n=12
Frequency (Hz)
No Inhibitor
Power (au)
Power (au)
pre no inhibitor
post no inhibitor
n=8
Frequency (Hz)

Figure 4.7: LNAME enhances vasomotion. (a,c): Example 200s Hbt time series from experiments occurring before (upper) and after (lower) LNAME injection **(a)** or matched timepoints with no inhibitor **(c)**. Responses to individual stimulations can be seen. Grey shaded region indicates whisker stimulation, blue shaded region indicates optogenetic stimulation. **(b,d):** Example power spectrum of Hbt data (1000s duration analysed) from same experiments as **a,c**, before (upper, black) and after (lower, grey) LNAME injection **(b)** or matched timepoints with no inhibitor **(d)**. Peaks are observed at frequency of stimulation (ISI 25s: 0.04Hz) and its harmonics (black arrowheads). After LNAME injection, a peak at 0.1Hz (vasomotion, grey arrow) is observed and the apparent stimulation frequency is reduced (white arrowhead) **(e):** Mean power spectrum of oscillations in Hbt before (black) and after (grey) LNAME (left, n=12) or no inhibitor (right, n=8). **Inset**: highlight of 0.07-0.15Hz. Data from arteriolar ROI in experiments as shown in Figures 4.1 and 4.4. For visual clarity, error bars are not shown. n indicates number of mice.

4.5.6 Optogenetic stimulation of nNOS INs evokes non-conducted blood volume responses prior to LNAME application.

Following nNOS optogenetic stimulation, in addition to the stereotypical widespread haemodynamic response, we commonly observed an increase in blood volume at specific points along the surface arterial tree (see Fig 4.8a-c, black circles). After the addition of LNAME these specific regions of nNOS IN-evoked Hbt increase were not present (Fig 4.8d). These data suggest nNOS IN stimulation caused local non-conducted dilations in the arterial network, possibly through local release of NO. Such non-conducted blood volume increases were not observed following whisker stimulation, either in the absence (Fig 4.8e) or presence (Fig 4.8f) of LNAME.

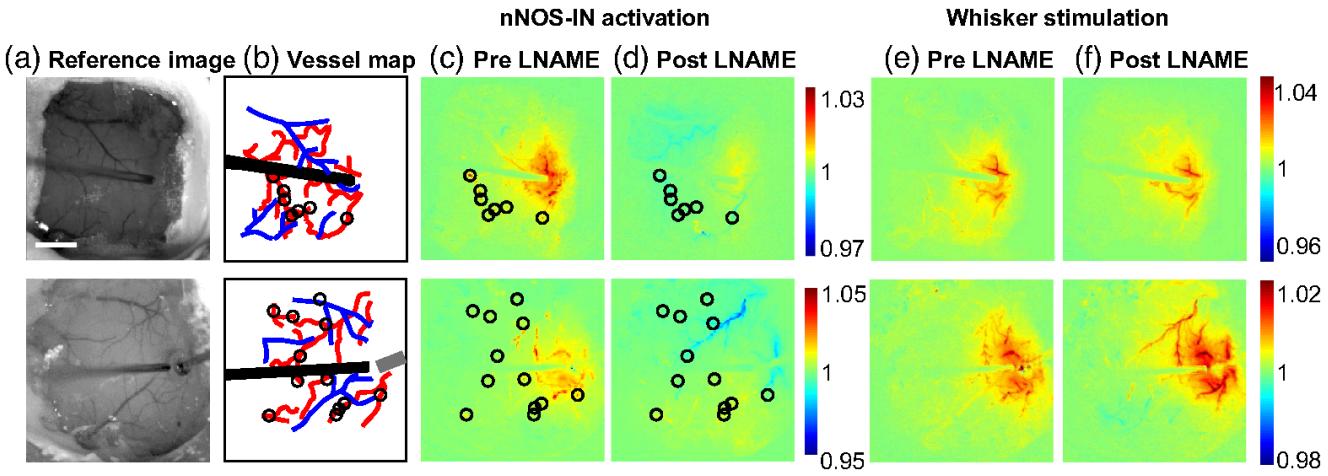

Figure 4.8: Optogenetic nNOS-IN stimulation produces non-conducted increases in Hbt across the arterial vascular network. (a) Reference images from 2 representative animals. Scalebar represents 1mm. **(b)** Vessel map diagram and location of optical probe (black rectangle) and recording electrode (grey rectangle). **(c-f)** Average Hbt image taken 2-5s after the start of optogenetic nNOS-IN stimulation **(c-d)** or whisker stimulation **(e-f)**, pre **(c,e)** and post **(d,f)** injection of LNAME. Colour bars represent fractional change as compared to baseline. Black circles indicate local, non-conducted blood volume increases.

4.6 Discussion

Combining *in vivo* 2D-OIS, electrophysiology, optogenetics and pharmacology, we investigated the role of NO in nNOS IN driven and sensory-evoked neurovascular coupling in the somatosensory cortex of mice. We demonstrated that: first, localised nNOS IN driven haemodynamic changes are mediated by NO; second, initiation of the haemodynamic response to short duration sensory stimulation is not dependent on NO; and third, NOS blockade causes the emergence of vasomotion in anaesthetised mice.

By inhibiting NO synthesis with LNAME, we demonstrated the key role that NO plays in the haemodynamic response to nNOS IN activation (Fig 4.1). Inhibiting production of NO by NOS revealed a larger initial decrease in Hbt in response to nNOS IN activation, which was attenuated when production of NO and 20-HETE were inhibited simultaneously. However, following initiation of the haemodynamic response, the successive increase in Hbt was unaltered by NOS inhibition. These data suggest that the initial vasodilatory response elicited by nNOS IN activation is mediated by NO, at least in part by inhibition of constriction by 20-HETE, while a later vasodilation involves a NO-independent mechanism. These findings extend previous work in cortical slices suggesting that type II nNOS INs evoke vasodilation by NO release[68]. A likely candidate for the delayed vasodilation is GABA[69,70], which is released by active nNOS INs and may act either indirectly via astrocytes to elicit haemodynamic changes[71,72] or can open chloride ion channels in smooth muscle cells, causing direct dilation of arterioles[70].

Our demonstration of a nNOS IN-elicited vasoconstriction (which was increased when NOS was inhibited) further supports the idea that arteriolar constrictions may be evoked by INs, rather than by excitatory neurons[3]. The observed increase in Hbr elicited by nNOS IN activation (Fig 4.1f) is analogous to the negative BOLD signal, further linking IN activity to negative BOLD fMRI responses[7,73,74]. An initial nNOS IN-evoked Hbt minima was not reported in our previous study[7]. This is likely due, in part, to the choice of ROI from which data were analysed. Analysing our previously acquired data using an arterial ROI (Supplementary Figure S4.3) revealed haemodynamic responses which display a similar profile to those reported in the current study (Fig 4.1f).

Whilst NO was found to mediate nNOS IN driven changes in cerebral blood volume, the neurovascular coupling response to short duration sensory stimulation was largely unaltered when NO production was reduced (Fig 4.1). A lack of effect on stimulation-evoked neural activity (Fig 4.3) confirmed that sensory-evoked neurovascular coupling was unaffected by treatment with LNAME. Although nNOS- and eNOS-derived NO have been suggested to play a key role in sensory-evoked neurovascular coupling[22,34,36,75,76] our results call into question

both the involvement of nNOS INs in sensory-evoked functional hyperemia[21] and that NO release is an important mediator of sensory-evoked haemodynamic responses[22]. Our findings are supported by previous studies which have also reported a limited effect of NOS inhibition[4,57,77,78] or genetic deletion of nNOS[29,37] on sensory-evoked functional hyperemia. Prior experimental[79] and modelling studies[80] have suggested potassium release by active neurons as an alternative driver of sensory-evoked functional hyperemia.

Discrepancies in the reported effects of LNAME in the literature may be due to differences in experimental approaches. First, the effect of LNAME may be affected by the application route chosen. Here we used i.p. injection of LNAME to reduce NOS activity throughout the brain[47,52], as compared to topical application which may result in effects being restricted to the superficial cortical layers, or intracortical injection which may limit the effect on pial arterioles[4] - the vascular component most affected by NO[21,81]. Second, stimulation duration may dictate the effect of NOS inhibition on the evoked haemodynamic response, with opposing effects being previously reported for long (60s) and short (4s) duration sensory stimulation[31]. Therefore, the discrepancy between our results and those of Liu et al. (2008) who used a similar pharmacological approach to report a significant involvement of NO (via inhibition of 20-HETE production) in the haemodynamic response to sensory stimulation in rats, may be at least partly explained by the use of short (2s, here) and long (60s[29]) duration stimulations. This is further supported by a recent report that pharmacological ablation of Type I nNOS INs reduces Hbt responses to prolonged, but not brief, whisker stimulation[82].

While we found no evidence for the involvement of NO in the initiation of sensory-evoked functional hyperemia, following inhibition of NO production we observed an oscillation in Hbt, Hbo and Hbr on return to baseline at stimulation offset in both the photostimulation and whisker stimulation experiments (Fig 4.1f). The shape of the haemodynamic response indicates that the haemodynamic return to baseline following stimulation is underdamped, suggesting that NO acts to dampen vasoconstriction after stimulation ends[80,83]. A similar arteriolar constriction, sometimes seen following sensory stimulation, has been shown to be mediated by NPY[3]. Future work could elucidate whether NO attenuates the vasoconstrictive actions of NPY release from nNOS INs following sensory stimulation.

In the current study, a common occurrence following nNOS optogenetic stimulation was a non-conducted blood volume increase at specific points along the surface arterial tree (Fig 4.8c, black circles). This observation suggests nNOS IN stimulation caused local non-conducted dilations in the arterial network, potentially due to local release of NO in close proximity to the vessels. This is supported by a study by Kurjiaka and Segal (1995)[84], who showed that when a distal portion of the anesthetised rat cremaster muscle arterial network is stimulated by acetylcholine a rapid retrograde wave of dilation occurred. However, in the same

preparation the addition of the NO donor sodium nitroprusside elicited only dilation local to the application area. In our experiments, after the addition of LNAME these specific regions of nNOS IN-evoked Hbt increase were not present (Fig 4.8d) suggesting the inhibition of NO release from nNOS neurons at those specific points along the surface arterial tree. The same analysis of the Hbt spatial response following sensory whisker stimulation (Fig 4.8e,f) fails to show the same effect. There were no local, non-conducted, increases in Hbt following whisker stimulation prior to and after LNAME injection. This further supports the argument against the role of nNOS INs or NO in at least the main retrograde dilation of the surface arteries, which is a major component of the neurovascular response function[79,85,86].

In agreement with previous studies[31,66,67] we demonstrated a role for NO in suppressing vasomotion. When NO production was attenuated with LNAME, we observed an increase in the power of low frequency haemodynamic oscillations centred at ~0.1Hz, compared to before injection of LNAME (Fig. 4.7). LNAME may lead to the emergence of vasomotion via the inhibition of eNOS-derived NO, which has previously been suggested to inhibit voltage gated calcium channels in arterial smooth muscle cells and, thereby, vasomotion[87].

Our study is not without limitations. Due to the use of a non-specific NOS inhibitor, it is not possible for us to dissect the involvement of eNOS and nNOS-associated vasoactive mechanisms in the vascular responses we observed. As both the cellular specificity of NOS isoform expression and the isoform-specificity of pharmacological agents have recently been questioned[21], designing experiments that allow specific cellular or isoform dissection is difficult.

Systemic injection of LNAME (75mg/kg, i.p) can evoke increases in blood pressure in anaesthetised mouse[88]. As changes in arterial blood pressure may confound the observed changes in haemodynamic low frequency oscillations[89], future work should aim to clearly distinguish the effects of inhibition of nNOS activity from those associated with arterial blood pressure changes. Topical application of NOS inhibitors (previously shown to induce vasomotion[78] could avoid the potential confound of increased arterial blood pressure.

2D-OIS, used in this study to investigate cortical haemodynamics, predominantly reflects changes in haemoglobin concentration in superficial blood vessels. Although previous studies have suggested that NO is preferentially involved in the regulation of pial arterial, as opposed to capillary, diameter[21,81], and penetrating arteries and capillaries display NO-independent whisker pad stimulation-evoked neurovascular coupling[57], further studies using approaches such as 2-photon microscopy would allow assessment of whether nNOS INs can evoke capillary dilation. To evoke vasodilation, NO released by nNOS INs must diffuse to the vessels[90], therefore regulation of CBF by nNOS INs may depend on their proximity to the vasculature (although recent evidence argues against this[91]). Future assessment of the spatial

distribution of nNOS INs in relation to different cerebral vessels (pial arterioles, penetrating arterioles, capillaries) may reveal a potential for nNOS INs to be differentially involved in blood flow control at different points in the vascular tree[19], as previously suggested for other cell types[92]. For example, locomotion-evoked vasodilation has been suggested to be NOS-dependent in pial arteries, but not penetrating arterioles[21].

Anaesthesia allows the involvement of NO in the regulation of CBF to be assessed in the absence of behaviours such as locomotion, which has been shown to evoke NO-dependent vasodilation[21] and can significantly alter sensory stimulus-evoked haemodynamic responses[55]. Furthermore, the prolonged temporal nature of the experimental paradigm used in this study makes it difficult to perform in awake animals. However, anaesthesia may confound neurovascular coupling[93,94] and may affect the recruitment of INs to sensory stimulation[4], thereby potentially altering the reliance of functional hyperemia on NO or nNOS INs[91]. To minimise the confound of anaesthesia we used an anaesthetic regime under which haemodynamic responses are similar to those observed in the awake mouse[43]. Furthermore, to compensate for some side effects of anaesthesia, mice breathed supplemental oxygen (100%) which likely resulted in hyperoxic conditions[95]. Since hyperoxia can influence NOS activity[96], future experiments should explore the oxygen-dependence of the role of nNOS in sensory-evoked functional hyperemia.

Understanding how, and when, nNOS INs, and NO, regulate CBF may highlight novel therapeutic strategies for neurodegenerative diseases. CBF deficits are observed early in AD[11] and are linked to cognitive decline[97,98]. Therefore, targeting nNOS INs, or increasing NO bioavailability[90], to reverse CBF deficits may prove to be a beneficial strategy for preventing cognitive decline.

4.7 Code and Data Availability

Data files generated and analysed during the current study are available in the DRYAD repository: https://doi.org/10.5061/dryad.jdfn2z3d9

4.8 Acknowledgements

C.H. was funded by a Sir Henry Dale Fellowship jointly funded by the Wellcome Trust and the Royal Society. This research was funded in whole, or in part, by the Wellcome Trust

[Grant number 105586/Z/14/Z]. For the purpose of Open Access, the author has applied a Creative Commons Attribution (CC BY) public copyright licence to any Author Accepted Manuscript version arising from this submission. This work was funded in part by a Medical Research Council UK grant awarded to J.B. and L.W.B [Grant number MR/M013553/1] and a Medical Research Council UK grant awarded to J.B. and C.H. [Grant number MR/X003418/1]. We would like to thank Michael Port for building and maintaining the whisker stimulation device and 2D-OIS imaging equipment, and Rachel Sandy for her assistance with tail vein injections. A preprint version of this manuscript is available on biorxiv (https://doi.org/10.1101/2022.05.24.493260).

4.9 Author Contributions

All authors contributed to the study's conception and design. L.L., E.G., C.H. performed material preparation. L.L., J.B. and C.H. performed data collection and analysis. L.W.B. and C.S. performed data analysis. The first draft of the manuscript was written by L.L. and C.H.; and L.W.B., E.G., C.S., J.B. provided critical review, commentary and revisions on all versions of the manuscript. C.H. and J.B. provided resources and administered the project. All authors read and approved the final version of the manuscript.

4.10 References

1. Attwell D, Buchan AM, Charpak S, Lauritzen M, Macvicar BA, Newman EA. Glial and neuronal control of brain blood flow. *Nature*. Nov 2010;468(7321):232-43. doi:10.1038/nature09613

2. Anenberg E, Chan AW, Xie Y, LeDue JM, Murphy TH. Optogenetic stimulation of GABA neurons can decrease local neuronal activity while increasing cortical blood flow. *J Cereb Blood Flow Metab*. Oct 2015;35(10):1579-86. doi:10.1038/jcbfm.2015.140

3. Uhlirova H, Kılıç K, Tian P, et al. Cell type specificity of neurovascular coupling in cerebral cortex. *Elife*. 05 2016;5doi:10.7554/eLife.14315

4. Vazquez AL, Fukuda M, Kim SG. Inhibitory Neuron Activity Contributions to Hemodynamic Responses and Metabolic Load Examined Using an Inhibitory Optogenetic Mouse Model. *Cereb Cortex*. Nov 2018;28(11):4105-4119. doi:10.1093/cercor/bhy225

5. Cauli B, Tong XK, Rancillac A, et al. Cortical GABA interneurons in neurovascular coupling: relays for subcortical vasoactive pathways. *J Neurosci*. Oct 2004;24(41):8940-9. doi:10.1523/JNEUROSCI.3065-04.2004

6. Dahlqvist MK, Thomsen KJ, Postnov DD, Lauritzen MJ. Modification of oxygen consumption and blood flow in mouse somatosensory cortex by cell-type-specific neuronal activity. *J Cereb Blood Flow Metab*. Oct 2020;40(10):2010-2025. doi:10.1177/0271678X19882787

7. Lee L, Boorman L, Glendenning E, et al. Key Aspects of Neurovascular Control Mediated by Specific Populations of Inhibitory Cortical Interneurons. *Cereb Cortex*. Apr 14 2020;30(4):2452-2464. doi:10.1093/cercor/bhz251

8. Krawchuk MB, Ruff CF, Yang X, Ross SE, Vazquez AL. Optogenetic assessment of VIP, PV, SOM and NOS inhibitory neuron activity and cerebral blood flow regulation in mouse somato-sensory cortex. *J Cereb Blood Flow Metab*. Jul 2020;40(7):1427-1440. doi:10.1177/0271678X19870105

9. Lee J, Stile CL, Bice AR, et al. Opposed hemodynamic responses following increased excitation and parvalbumin-based inhibition. *J Cereb Blood Flow Metab*. Apr 2021;41(4):841-856. doi:10.1177/0271678X20930831

10. Howarth C, Mishra A, Hall CN. More than just summed neuronal activity: how multiple cell types shape the BOLD response. *Philos Trans R Soc Lond B Biol Sci*. Jan 04 2021;376(1815):20190630. doi:10.1098/rstb.2019.0630

11. Iturria-Medina Y, Sotero RC, Toussaint PJ, Mateos-Pérez JM, Evans AC, Initiative AsDN. Early role of vascular dysregulation on late-onset Alzheimer's disease based on multifactorial data-driven analysis. *Nat Commun*. 06 2016;7:11934. doi:10.1038/ncomms11934

12. Palop JJ, Mucke L. Network abnormalities and interneuron dysfunction in Alzheimer disease. *Nat Rev Neurosci*. 12 2016;17(12):777-792. doi:10.1038/nrn.2016.141

13. Verret L, Mann EO, Hang GB, et al. Inhibitory interneuron deficit links altered network activity and cognitive dysfunction in Alzheimer model. *Cell*. Apr 2012;149(3):708-21. doi:10.1016/j.cell.2012.02.046

14. Dudek FE. Loss of GABAergic Interneurons in Seizure-Induced Epileptogenesis-Two Decades Later and in a More Complex World. *Epilepsy Curr*. 2020;20(6_suppl):70S-72S. doi:10.1177/1535759720960464

15. Harris S, Bruyns-Haylett M, Kennerley A, et al. The effects of focal epileptic activity on regional sensory-evoked neurovascular coupling and postictal modulation of bilateral sensory processing. *J Cereb Blood Flow Metab*. Oct 2013;33(10):1595-604. doi:10.1038/jcbfm.2013.115

16. Beishon L, Clough RH, Kadicheeni M, et al. Vascular and haemodynamic issues of brain ageing. *Pflugers Arch*. May 2021;473(5):735-751. doi:10.1007/s00424-020-02508-9

17. Miettinen R, Sirviö J, Riekkinen P, Laakso MP, Riekkinen M. Neocortical, hippocampal and septal parvalbumin- and somatostatin-containing neurons in young and aged rats: correlation with passive avoidance and water maze performance. *Neuroscience*. Mar 1993;53(2):367-78. doi:10.1016/0306-4522(93)90201-p

18. Förstermann U, Sessa WC. Nitric oxide synthases: regulation and function. *Eur Heart J*. Apr 2012;33(7):829-37, 837a-837d. doi:10.1093/eurheartj/ehr304

19. Shaw K, Boyd K, Anderle S, et al. Gradual Not Sudden Change: Multiple Sites of Functional Transition Across the Microvascular Bed. *Front Aging Neurosci*. 2021;13:779823. doi:10.3389/fnagi.2021.779823

20. Vlasenko OV, Dovgan' AV, Maisky VA, Maznychenko AV, Pilyavskii AI. NADPH-Diaphorase reactivity and neurovascular coupling in the basal forebrain and motor cortex. *Neurophysiology*. 2007;39(4):355-357. doi:10.1007/s11062-007-0056-z

21. Echagarruga CT, Gheres KW, Norwood JN, Drew PJ. nNOS-expressing interneurons control basal and behaviorally evoked arterial dilation in somatosensory cortex of mice. *Elife*. 10 2020;9doi:10.7554/eLife.60533

22. Hosford PS, Gourine AV. What is the key mediator of the neurovascular coupling response? *Neurosci Biobehav Rev*. Jan 2019;96:174-181. doi:10.1016/j.neubiorev.2018.11.011

23. Faraci FM, Brian JE. Nitric oxide and the cerebral circulation. *Stroke*. Mar 1994;25(3):692-703. doi:10.1161/01.str.25.3.692

24. Oyekan AO, Youseff T, Fulton D, Quilley J, McGiff JC. Renal cytochrome P450 omega-hydroxylase and epoxygenase activity are differentially modified by nitric oxide and sodium chloride. *J Clin Invest*. Oct 1999;104(8):1131-7. doi:10.1172/JCI6786

25. Gebremedhin D, Lange AR, Lowry TF, et al. Production of 20-HETE and its role in autoregulation of cerebral blood flow. *Circ Res*. Jul 07 2000;87(1):60-5. doi:10.1161/01.res.87.1.60

26. Harder DR, Narayanan J, Gebremedhin D. Pressure-induced myogenic tone and role of 20-HETE in mediating autoregulation of cerebral blood flow. *Am J Physiol Heart Circ Physiol*. May 2011;300(5):H1557-65. doi:10.1152/ajpheart.01097.2010

27. Imig JD, Zou AP, Stec DE, Harder DR, Falck JR, Roman RJ. Formation and actions of 20-hydroxyeicosatetraenoic acid in rat renal arterioles. *Am J Physiol*. Jan 1996;270(1 Pt 2):R217-27. doi:10.1152/ajpregu.1996.270.1.R217

28. Alonso-Galicia M, Hudetz AG, Shen H, Harder DR, Roman RJ. Contribution of 20-HETE to vasodilator actions of nitric oxide in the cerebral microcirculation. *Stroke*. Dec 1999;30(12):2727-34; discussion 2734. doi:10.1161/01.str.30.12.2727

29. Liu X, Li C, Falck JR, Roman RJ, Harder DR, Koehler RC. Interaction of nitric oxide, 20-HETE, and EETs during functional hyperemia in whisker barrel cortex. *Am J Physiol Heart Circ Physiol*. Aug 2008;295(2):H619-31. doi:10.1152/ajpheart.01211.2007

30. Sun CW, Alonso-Galicia M, Taheri MR, Falck JR, Harder DR, Roman RJ. Nitric oxide-20-hydroxyeicosatetraenoic acid interaction in the regulation of K+ channel activity and vascular tone in renal arterioles. *Circ Res*. Nov 30 1998;83(11):1069-79. doi:10.1161/01.res.83.11.1069

31. Ances BM, Greenberg JH, Detre JA. Interaction between nitric oxide synthase inhibitor induced oscillations and the activation flow coupling response. *Brain Res*. Jan 14 2010;1309:19-28. doi:10.1016/j.brainres.2009.09.119

32. Hoiland RL, Caldwell HG, Howe CA, et al. Nitric oxide is fundamental to neurovascular coupling in humans. *J Physiol*. Nov 2020;598(21):4927-4939. doi:10.1113/JP280162

33. Stefanovic B, Schwindt W, Hoehn M, Silva AC. Functional uncoupling of hemodynamic from neuronal response by inhibition of neuronal nitric oxide synthase. *J Cereb Blood Flow Metab*. Apr 2007;27(4):741-54. doi:10.1038/sj.jcbfm.9600377

34. Toth P, Tarantini S, Davila A, et al. Purinergic glio-endothelial coupling during neuronal activity: role of P2Y1 receptors and eNOS in functional hyperemia in the mouse somatosensory cortex. *Am J Physiol Heart Circ Physiol*. Dec 01 2015;309(11):H1837-45. doi:10.1152/ajpheart.00463.2015

35. Hariharan A, Jing Y, Collie ND, Zhang H, Liu P. Altered neurovascular coupling and brain arginine metabolism in endothelial nitric oxide synthase deficient mice. *Nitric Oxide*. Jun 01 2019;87:60-72. doi:10.1016/j.niox.2019.03.006

36. Ayata C, Ma J, Meng W, Huang P, Moskowitz MA. L-NA-sensitive rCBF augmentation during vibrissal stimulation in type III nitric oxide synthase mutant mice. *J Cereb Blood Flow Metab*. Jul 1996;16(4):539-41. doi:10.1097/00004647-199607000-00002

37. Ma J, Ayata C, Huang PL, Fishman MC, Moskowitz MA. Regional cerebral blood flow response to vibrissal stimulation in mice lacking type I NOS gene expression. *Am J Physiol*. Mar 1996;270(3 Pt 2):H1085-90. doi:10.1152/ajpheart.1996.270.3.H1085

38. Wang Q, Kjaer T, Jørgensen MB, et al. Nitric oxide does not act as a mediator coupling cerebral blood flow to neural activity following somatosensory stimuli in rats. *Neurol Res*. Feb 1993;15(1):33-6. doi:10.1080/01616412.1993.11740103

39. White RP, Hindley C, Bloomfield PM, et al. The effect of the nitric oxide synthase inhibitor L-NMMA on basal CBF and vasoneuronal coupling in man: a PET study. *J Cereb Blood Flow Metab*. Jun 1999;19(6):673-8. doi:10.1097/00004647-199906000-00011

40. Percie du Sert N, Hurst V, Ahluwalia A, et al. The ARRIVE guidelines 2.0: Updated guidelines for reporting animal research. *PLoS Biol*. Jul 2020;18(7):e3000410. doi:10.1371/journal.pbio.3000410

41. Taniguchi H, He M, Wu P, et al. A resource of Cre driver lines for genetic targeting of GABAergic neurons in cerebral cortex. *Neuron*. Sep 22 2011;71(6):995-1013. doi:10.1016/j.neuron.2011.07.026

42. Madisen L, Mao T, Koch H, et al. A toolbox of Cre-dependent optogenetic transgenic mice for light-induced activation and silencing. *Nat Neurosci*. Mar 25 2012;15(5):793-802. doi:10.1038/nn.3078

43. Sharp PS, Shaw K, Boorman L, et al. Comparison of stimulus-evoked cerebral hemodynamics in the awake mouse and under a novel anesthetic regime. *Sci Rep*. Jul 2015;5:12621. doi:10.1038/srep12621

44. Langford DJ, Bailey AL, Chanda ML, et al. Coding of facial expressions of pain in the laboratory mouse. *Nat Methods*. Jun 2010;7(6):447-9. doi:10.1038/nmeth.1455

45. Berwick J, Johnston D, Jones M, et al. Neurovascular coupling investigated with two-dimensional optical imaging spectroscopy in rat whisker barrel cortex. *Eur J Neurosci*. Oct 2005;22(7):1655-66. doi:10.1111/j.1460-9568.2005.04347.x

46. Mayhew J, Zheng Y, Hou Y, et al. Spectroscopic analysis of changes in remitted illumination: the response to increased neural activity in brain. *Neuroimage*. Sep 1999;10(3 Pt 1):304-26. doi:10.1006/nimg.1999.0460

47. Bannerman DM, Chapman PF, Kelly PA, Butcher SP, Morris RG. Inhibition of nitric oxide synthase does not prevent the induction of long-term potentiation in vivo. *J Neurosci*. Dec 1994;14(12):7415-25. doi:10.1523/JNEUROSCI.14-12-07415.1994

48. Miyata N, Taniguchi K, Seki T, et al. HET0016, a potent and selective inhibitor of 20-HETE synthesizing enzyme. *Br J Pharmacol*. Jun 2001;133(3):325-9. doi:10.1038/sj.bjp.0704101

49. Poloyac SM, Zhang Y, Bies RR, Kochanek PM, Graham SH. Protective effect of the 20-HETE inhibitor HET0016 on brain damage after temporary focal ischemia. *J Cereb Blood Flow Metab*. Dec 2006;26(12):1551-61. doi:10.1038/sj.jcbfm.9600309

50. Singh H, Cheng J, Deng H, et al. Vascular cytochrome P450 4A expression and 20-hydroxyeicosatetraenoic acid synthesis contribute to endothelial dysfunction in androgen-induced hypertension. *Hypertension*. Jul 2007;50(1):123-9. doi:10.1161/HYPERTENSIONAHA.107.089599

51. Chang JC, Shook LL, Biag J, et al. Biphasic direct current shift, haemoglobin desaturation and neurovascular uncoupling in cortical spreading depression. *Brain*. Apr 2010;133(Pt 4):996-1012. doi:10.1093/brain/awp338

52. Salter M, Duffy C, Garthwaite J, Strijbos PJ. Substantial regional and hemispheric differences in brain nitric oxide synthase (NOS) inhibition following intracerebroventricular administration of N omega-nitro-L-arginine (L-NA) and its methyl ester (L-NAME). *Neuropharmacology*. Jun 1995;34(6):639-49. doi:10.1016/0028-3908(95)00036-6

53. Shonat RD, Wachman ES, Niu W, Koretsky AP, Farkas DL. Near-simultaneous hemoglobin saturation and oxygen tension maps in mouse brain using an AOTF microscope. *Biophys J*. Sep 1997;73(3):1223-31. doi:10.1016/S0006-3495(97)78155-4

54. Aydin AK, Verdier C, Chaigneau E, Charpak S. The oxygen initial dip in the brain of anesthetized and awake mice. *Proc Natl Acad Sci U S A*. Apr 05 2022;119(14):e2200205119. doi:10.1073/pnas.2200205119

55. Eyre B, Shaw K, Sharp P, et al. The effects of locomotion on sensory-evoked haemodynamic responses in the cortex of awake mice. *Sci Rep*. Apr 14 2022;12(1):6236. doi:10.1038/s41598-022-10195-y

56. Mayhew J, Johnston D, Berwick J, Jones M, Coffey P, Zheng Y. Spectroscopic analysis of neural activity in brain: increased oxygen consumption following activation of barrel cortex. *Neuroimage*. Dec 2000;12(6):664-75. doi:10.1006/nimg.2000.0656

57. Zambach SA, Cai C, Helms HCC, et al. Precapillary sphincters and pericytes at first-order capillaries as key regulators for brain capillary perfusion. *Proc Natl Acad Sci U S A*. Jun 29 2021;118(26)doi:10.1073/pnas.2023749118

58. Kaley G, Koller A, Rodenburg JM, Messina EJ, Wolin MS. Regulation of arteriolar tone and responses via L-arginine pathway in skeletal muscle. *Am J Physiol*. Apr 1992;262(4 Pt 2):H987-92. doi:10.1152/ajpheart.1992.262.4.H987

59. Sharp PS, Ameen-Ali KE, Boorman L, et al. Neurovascular coupling preserved in a chronic mouse model of Alzheimer's disease: Methodology is critical. *J Cereb Blood Flow Metab*. Nov 2020;40(11):2289-2303. doi:10.1177/0271678X19890830

60. Shabir O, Pendry B, Lee L, et al. Assessment of neurovascular coupling and cortical spreading depression in mixed mouse models of atherosclerosis and Alzheimer's disease. *Elife*. Jan 11 2022;11doi:10.7554/eLife.68242

61. Orshal JM, Khalil RA. Gender, sex hormones, and vascular tone. *Am J Physiol Regul Integr Comp Physiol*. Feb 2004;286(2):R233-49. doi:10.1152/ajpregu.00338.2003

62. Alonso-Galicia M, Drummond HA, Reddy KK, Falck JR, Roman RJ. Inhibition of 20-HETE production contributes to the vascular responses to nitric oxide. *Hypertension*. Jan 1997;29(1 Pt 2):320-5. doi:10.1161/01.hyp.29.1.320

63. Mulligan SJ, MacVicar BA. Calcium transients in astrocyte endfeet cause cerebrovascular constrictions. *Nature*. Sep 2004;431(7005):195-9. doi:10.1038/nature02827

64. Drew PJ, Shih AY, Kleinfeld D. Fluctuating and sensory-induced vasodynamics in rodent cortex extend arteriole capacity. *Proc Natl Acad Sci U S A*. May 17 2011;108(20):8473-8. doi:10.1073/pnas.1100428108

65. Mayhew JE, Askew S, Zheng Y, et al. Cerebral vasomotion: a 0.1-Hz oscillation in reflected light imaging of neural activity. *Neuroimage*. Dec 1996;4(3 Pt 1):183-93. doi:10.1006/nimg.1996.0069

66. Dirnagl U, Lindauer U, Villringer A. Nitric oxide synthase blockade enhances vasomotion in the cerebral microcirculation of anesthetized rats. *Microvasc Res*. May 1993;45(3):318-23. doi:10.1006/mvre.1993.1028

67. Biswal BB, Hudetz AG. Synchronous oscillations in cerebrocortical capillary red blood cell velocity after nitric oxide synthase inhibition. *Microvasc Res*. Jul 1996;52(1):1-12. doi:10.1006/mvre.1996.0039

68. Perrenoud Q, Rossier J, Férézou I, et al. Activation of cortical 5-HT(3) receptor-expressing interneurons induces NO mediated vasodilatations and NPY mediated vasoconstrictions. *Front Neural Circuits*. 2012;6:50. doi:10.3389/fncir.2012.00050

69. Fergus A, Lee KS. GABAergic regulation of cerebral microvascular tone in the rat. *J Cereb Blood Flow Metab*. Sep 1997;17(9):992-1003. doi:10.1097/00004647-199709000-00009

70. David T, Morillo R, Howarth C, Berwick J, Lee L. The Reversal Characteristics of GABAergic Neurons: A Neurovascular Model. *J Biomech Eng*. Mar 01 2023;145(3)doi:10.1115/1.4056336

71. Cauli B, Hamel E. Revisiting the role of neurons in neurovascular coupling. *Front Neuroenergetics*. 2010;2:9. doi:10.3389/fnene.2010.00009

72. Lecrux C, Hamel E. Neuronal networks and mediators of cortical neurovascular coupling responses in normal and altered brain states. *Philos Trans R Soc Lond B Biol Sci*. Oct 05 2016;371(1705)doi:10.1098/rstb.2015.0350

73. Boorman L, Kennerley AJ, Johnston D, et al. Negative blood oxygen level dependence in the rat: a model for investigating the role of suppression in neurovascular coupling. *J Neurosci*. Mar 24 2010;30(12):4285-94. doi:10.1523/jneurosci.6063-09.2010

74. Boorman L, Harris S, Bruyns-Haylett M, et al. Long-latency reductions in gamma power predict hemodynamic changes that underlie the negative BOLD signal. *J Neurosci*. Mar 2015;35(11):4641-56. doi:10.1523/JNEUROSCI.2339-14.2015

75. Chow BW, Nuñez V, Kaplan L, et al. Caveolae in CNS arterioles mediate neurovascular coupling. *Nature*. Mar 2020;579(7797):106-110. doi:10.1038/s41586-020-2026-1

76. Dirnagl U, Lindauer U, Villringer A. Role of nitric oxide in the coupling of cerebral blood flow to neuronal activation in rats. *Neurosci Lett*. Jan 04 1993;149(1):43-6. doi:10.1016/0304-3940(93)90343-j

77. Adachi K, Takahashi S, Melzer P, et al. Increases in local cerebral blood flow associated with somatosensory activation are not mediated by NO. *Am J Physiol*. Dec 1994;267(6 Pt 2):H2155-62. doi:10.1152/ajpheart.1994.267.6.H2155

78. Lindauer U, Megow D, Matsuda H, Dirnagl U. Nitric oxide: a modulator, but not a mediator, of neurovascular coupling in rat somatosensory cortex. *Am J Physiol*. Aug 1999;277(2 Pt 2):H799-811.

79. Longden TA, Dabertrand F, Koide M, et al. Capillary K(+)-sensing initiates retrograde hyperpolarization to increase local cerebral blood flow. *Nat Neurosci*. May 2017;20(5):717-726.

80. Kenny A, Plank MJ, David T. The role of astrocytic calcium and TRPV4 channels in neurovascular coupling. *J Comput Neurosci*. 02 2018;44(1):97-114. doi:10.1007/s10827-017-0671-7

81. Mishra A, Reynolds JP, Chen Y, Gourine AV, Rusakov DA, Attwell D. Astrocytes mediate neurovascular signaling to capillary pericytes but not to arterioles. *Nat Neurosci*. 12 2016;19(12):1619-1627. doi:10.1038/nn.4428

82. Turner KL, Brockway DF, Hossain MS, et al. Type-I nNOS neurons orchestrate cortical neural activity and vasomotion. eLife Sciences Publications, Ltd; 2025.

83. Dormanns K, Brown RG, David T. The role of nitric oxide in neurovascular coupling. *J Theor Biol*. Apr 7 2016;394:1-17. doi:10.1016/j.jtbi.2016.01.009

84. Kurjiaka DT, Segal SS. Interaction between conducted vasodilation and sympathetic nerve activation in arterioles of hamster striated muscle. *Circ Res*. May 1995;76(5):885-91. doi:10.1161/01.res.76.5.885

85. Chen BR, Kozberg MG, Bouchard MB, Shaik MA, Hillman EM. A critical role for the vascular endothelium in functional neurovascular coupling in the brain. *J Am Heart Assoc*. Jun 12 2014;3(3):e000787. doi:10.1161/JAHA.114.000787

86. Thakore P, Alvarado MG, Ali S, et al. Brain endothelial cell TRPA1 channels initiate neurovascular coupling. *Elife*. Feb 26 2021;10doi:10.7554/eLife.63040

87. Yuill KH, McNeish AJ, Kansui Y, Garland CJ, Dora KA. Nitric oxide suppresses cerebral vasomotion by sGC-independent effects on ryanodine receptors and voltage-gated calcium channels. *J Vasc Res*. 2010;47(2):93-107. doi:10.1159/000235964

88. Moore PK, Oluyomi AO, Babbedge RC, Wallace P, Hart SL. L-NG-nitro arginine methyl ester exhibits antinociceptive activity in the mouse. *Br J Pharmacol*. Jan 1991;102(1):198-202. doi:10.1111/j.1476-5381.1991.tb12153.x

89. Hudetz AG, Roman RJ, Harder DR. Spontaneous flow oscillations in the cerebral cortex during acute changes in mean arterial pressure. *J Cereb Blood Flow Metab*. May 1992;12(3):491-9. doi:10.1038/jcbfm.1992.67

90. Lourenço CF, Laranjinha J. Nitric Oxide Pathways in Neurovascular Coupling Under Normal and Stress Conditions in the Brain: Strategies to Rescue Aberrant Coupling and Improve Cerebral Blood Flow. *Front Physiol*. 2021;12:729201. doi:10.3389/fphys.2021.729201

91. Ahn SJ, Anfray A, Anrather J, Iadecola C. Calcium transients in nNOS neurons underlie distinct phases of the neurovascular response to barrel cortex activation in awake mice. *J Cereb Blood Flow Metab*. Oct 2023;43(10):1633-1647. doi:10.1177/0271678X231173175

92. Hatakeyama N, Unekawa M, Murata J, et al. Differential pial and penetrating arterial responses examined by optogenetic activation of astrocytes and neurons. *J Cereb Blood Flow Metab*. Oct 2021;41(10):2676-2689. doi:10.1177/0271678X211010355

93. Gao YR, Ma Y, Zhang Q, et al. Time to wake up: Studying neurovascular coupling and brain-wide circuit function in the un-anesthetized animal. *Neuroimage*. Jun 2017;153:382-398. doi:10.1016/j.neuroimage.2016.11.069

94. Guo J, Ran M, Gao Z, et al. Cell-type-specific imaging of neurotransmission reveals a disrupted excitatory-inhibitory cortical network in isoflurane anaesthesia. *EBioMedicine*. Mar 2021;65:103272. doi:10.1016/j.ebiom.2021.103272

95. Ivanov KP, Sokolova IB, Vovenko EP. Oxygen transport in the rat brain cortex at normobaric hyperoxia. *Eur J Appl Physiol Occup Physiol*. 1999;80(6):582-7. doi:10.1007/s004210050637

96. Yeh DY, Kao SJ, Feng NH, Chen HI, Wang D. Increased nitric oxide production accompanies blunted hypoxic pulmonary vasoconstriction in hyperoxic rat lung. *Chin J Physiol*. Dec 31 2006;49(6):305-12.

97. Hays CC, Zlatar ZZ, Wierenga CE. The Utility of Cerebral Blood Flow as a Biomarker of Preclinical Alzheimer's Disease. *Cell Mol Neurobiol*. Mar 2016;36(2):167-79. doi:10.1007/s10571-015-0261-z

98. Leijenaar JF, van Maurik IS, Kuijer JPA, et al. Lower cerebral blood flow in subjects with Alzheimer's dementia, mild cognitive impairment, and subjective cognitive decline using two-dimensional phase-contrast magnetic resonance imaging. *Alzheimers Dement (Amst)*. 2017;9:76-83. doi:10.1016/j.dadm.2017.10.001

4.12 Supplementary Materials

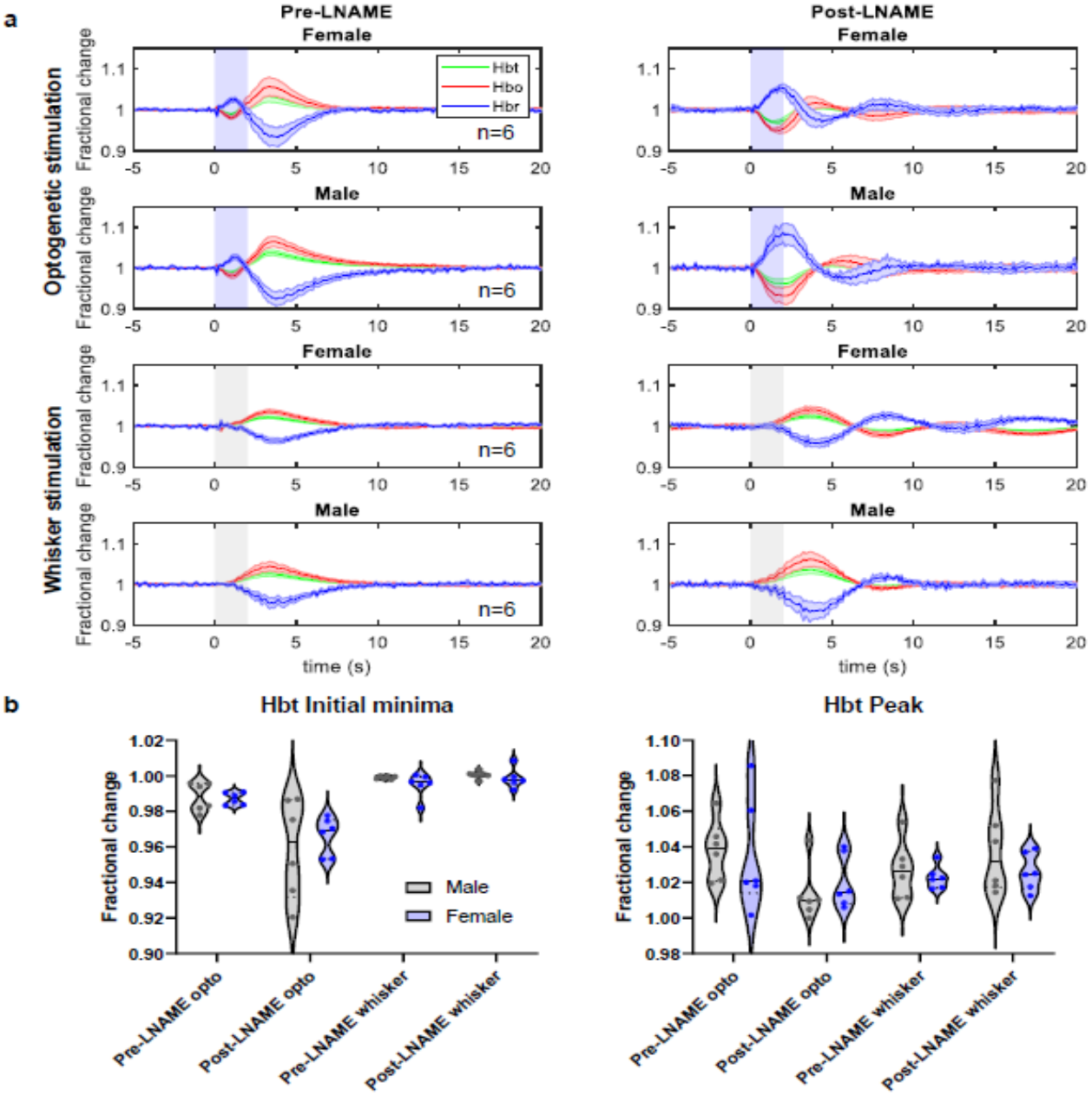

Figure S4.1: No sex-dependent differences in NOS-dependence of haemodynamic responses evoked by 2s nNOS-IN activation or whisker stimulation. Group data (n=6 female mice and 6 male mice). **(a)** Mean fractional change in Hbt, Hbo and Hbr in arteriolar ROI in response to 2s optogenetic activation of nNOS-INs (top two rows) or 2s whisker stimulation (bottom two rows) before (left) and after (right) LNAME injection. Responses shown for female (higher plots) and male (lower plots) mice. Blue shading indicates photostimulation period (top rows), grey shading indicates whisker stimulation period (bottom rows). Data: mean ± SEM, n represents number of mice. **(b):** Initial fractional change ('initial minima') in Hbt **(Left)** and maximum fractional change in Hbt ('peak', **Right**) evoked by optogenetic and whisker stimulation, before and after LNAME. Solid black line indicates median, dashed black line indicates quartiles. Individual data points are shown. Note: these data are combined in Figure 4.1.

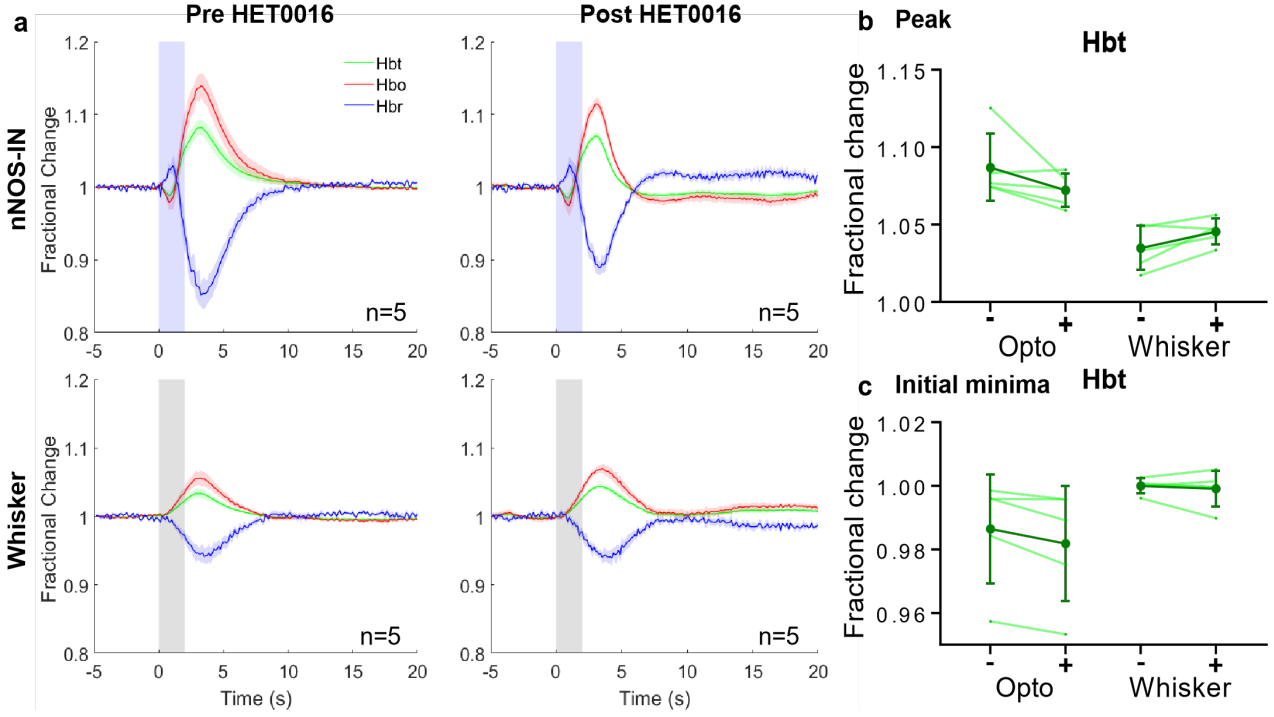

Figure S4.2: Haemodynamic responses during inhibition of 20-HETE synthesis. (a-c): Group data (n=5 mice). **(a)** Mean fractional change in Hbt, Hbo and Hbr in arteriolar ROI in response to 2s optogenetic activation of nNOS-INs (top row) or 2s whisker stimulation (bottom row) before (left) and after (right) HET0016 injection. Blue shading indicates photostimulation period (top row), grey shading indicates whisker stimulation period (bottom row). Data: mean ± SEM, n represents number of mice. **(b-c):** Darker lines represent group mean ± SD, lighter lines indicate trial-averaged mean for individual animals. **(b):** Maximum fractional change in Hbt ('peak') evoked by optogenetic and whisker stimulation, with (+) and without (-) HET0016. **(c):** Initial fractional change ('initial minima') in Hbt in response to optogenetic and whisker stimulation, with (+) and without (-) HET0016.

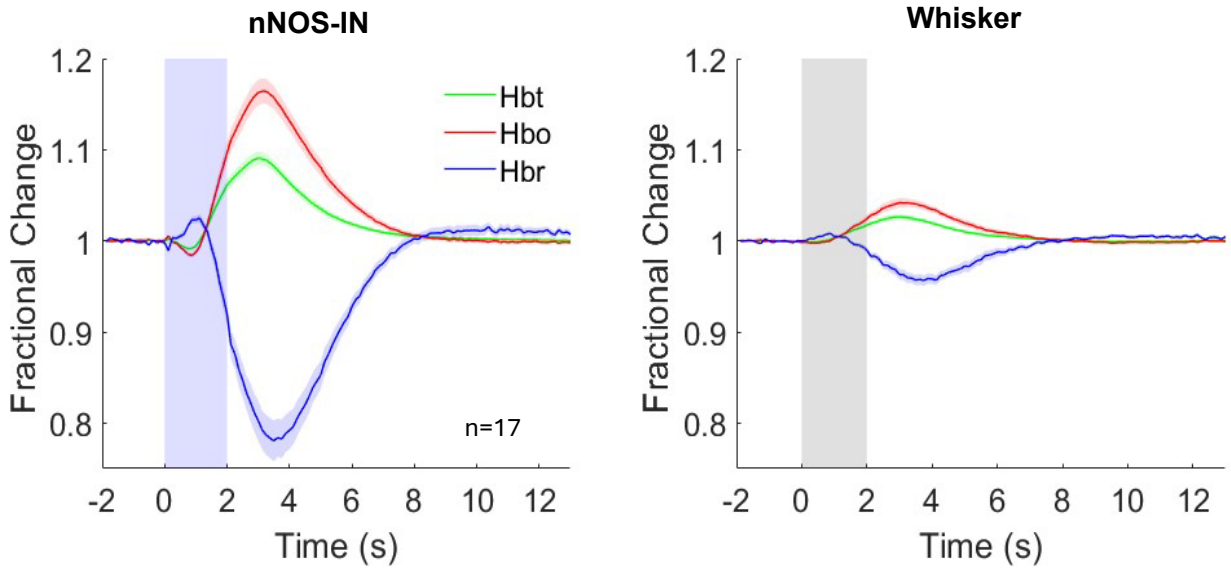

Figure S4.3: Previously collected[7] haemodynamic responses show biphasic response to photostimulation of nNOS-INs. Mean fractional change in Hbt, Hbo and Hbr in artery ROI in response to 2s, 99Hz optogenetic activation of nNOS-INs (left) or 2s whisker stimulation (right). Blue shading indicates photostimulation period, grey shading indicates whisker stimulation period. Data are mean ± SEM, n represents number of mice. Data are taken from imaging only experiments (i.e. no electrode implantation).

Table S4.1: Baseline assumptions for artery ROI for spectral analysis of post-pharmacological intervention data were amended for each mouse. Group mean ± SEM are reported. Assumption for "pre" time point is provided for comparison. Hbt: total haemoglobin.

Pharmacological Intervention	Hbt Concentration (μM)	Oxygen Saturation (%)	n (mice)
"Pre" timepoint	100	80	
LNAME	100.534±0.773	79.16±0.006	12
LNAME + HET0016	101.775±1.207	79.23±0.007	6
HET0016	100.836±1.602	80.76±0.005	5
No Inhibitor	100.264±0.729	79.58±0.004	8

Table S4.2: Pairwise comparisons of total haemoglobin (Hbt) initial minima evoked by nNOS interneuron activation at different time points relative to LNAME injection (Bonferroni adjusted p values reported). (n= 12 mice) *p<0.05, **p<0.01, ***p<0.001

Pairwise comparison	p
Pre-LNAME vs 0mins	0.016*
Pre-LNAME vs 60-70mins	0.0005***
0mins vs 60-70mins	0.009**

Table S4.3: Temporal characteristics of whisker stimulation-evoked haemodynamic response (total haemoglobin, Hbt), before and after LNAME injection.

Parameter	Pre-LNAME [mean ± s.d]	Post-LNAME [mean ± s.d]	Paired t-test	n (mice)
Rise time (s)	1.76 ± 0.29	1.88 ± 0.35	t(11) = -0.87, p = 0.403	12
Time to peak (s)	2.63 ± 0.32	3.01 ± 0.63	t(11) = -1.92, p = 0.082	12
Onset time (s)	0.63 ± 0.21	0.77 ± 0.60	t(11) = -0.77, p =0.461	12

Table S4.4: Effect of LNAME on haemodynamic response – Initial minima: 3-way mixed ANOVA results. Bonferroni correction for multiple comparisons was applied, to account for three different haemodynamic profiles (total haemoglobin: Hbt, oxyhaemoglobin: Hbo, and deoxyhaemoglobin: Hbr). (n= 12 mice) *p<0.017, **p<0.003, *** p<0.0003. Significant interactions were followed up using simple effects tests (*p<0.025, **p<0.005, ***p<0.0005, following Bonferroni correction for multiple comparisons).

Variable	Factor	F(1,10)		
		F	P	η^2
Hbt response in initial minima period	Electrode	1.208	0.297	0.108
	Stim	31.075	0.000***	0.757
	Stim*Electrode	0.572	0.467	0.054
	Drug	21.2	0.001**	0.679
	Drug*Electrode	0.001	0.982	0.000
	Stim*Drug	25.563	0.000**	0.719
	Stim*Drug*Electrode	0.137	0.719	0.014
Hbo response in initial minima period	Electrode	0.897	0.366	0.082
	Stim	31.342	0.000***	0.758
	Stim*Electrode	0.383	0.55	0.037
	Drug	17.618	0.002**	0.638
	Drug*Electrode	0.000	0.994	0.000
	Stim*Drug	22.81	0.001**	0.695
	Stim*Drug*Electrode	0.024	0.881	0.002
Hbr response in initial minima period	Electrode	0.282	0.607	0.027
	Stim	27.526	0.000**	0.734
	Stim*Electrode	0.014	0.908	0.001
	Drug	13.484	0.004*	0.574
	Drug*Electrode	0.018	0.896	0.002
	Stim*Drug	16.223	0.002**	0.619
	Stim*Drug*Electrode	0.036	0.853	0.004

Simple effects tests: LNAME (2s whisker stimulation)	p
Hbt response in initial minima period	0.159
Hbo response in initial minima period	0.201
Hbr response in initial minima period	0.434

Table S4.5: Effect of LNAME on haemodynamic response – Peak: 3-way mixed ANOVA results. Bonferroni correction for multiple comparisons was applied, to account for three different haemodynamic profiles (total haemoglobin: Hbt, oxyhaemoglobin: Hbo, and deoxyhaemoglobin: Hbr). (n= 12 mice) *p<0.017, **p<0.003, *** p<0.0003. Significant interactions were followed up using simple effects tests (*p<0.025, **p<0.005, ***p<0.0005, following Bonferroni correction for multiple comparisons).

Variable	Factor	F(1,10)		
		F	P	η^2
Peak Hbt response	Electrode	2.058	0.182	0.171
	Stim	0.085	0.776	0.008
	Stim*Electrode	0.010	0.924	0.001
	Drug	3.058	0.111	0.234
	Drug*Electrode	2.851	0.122	0.222
	Stim*Drug	9.229	0.013*	0.48
	Stim*Drug*Electrode	1.450	0.256	0.127
Peak Hbo response	Electrode	1.966	0.191	0.164
	Stim	0.008	0.931	0.001
	Stim*Electrode	0.015	0.905	0.001
	Drug	2.287	0.161	0.186
	Drug*Electrode	2.533	0.143	0.202
	Stim*Drug	8.795	0.014*	0.468
	Stim*Drug*Electrode	1.433	0.259	0.125
Peak Hbr response	Electrode	2.079	0.180	0.172
	Stim	0.312	0.589	0.030
	Stim*Electrode	0.090	0.77	0.009
	Drug	0.981	0.345	0.089
	Drug*Electrode	1.641	0.229	0.141
	Stim*Drug	8.551	0.015*	0.461
	Stim*Drug*Electrode	1.744	0.216	0.149
Simple effects tests: LNAME (2s whisker stimulation)			p	
Peak Hbt response			0.129	
Peak Hbo response			0.124	
Peak Hbr response			0.127	

Table S4.6: Effect of LNAME on haemodynamic response – peak-to-peak amplitude: 3-way mixed ANOVA results. Bonferroni correction for multiple comparisons was applied, to account for three different haemodynamic profiles (total haemoglobin: Hbt, oxyhaemoglobin: Hbo, and deoxyhaemoglobin: Hbr). (n=12 mice) *p<0.017, **p<0.003, ***p<0.0003.

Variable	Factor	F(1,10)		
		F	p	η_2
Peak-to-peak amplitude: Hbt	Electrode	2.118	0.176	0.175
	Stim	12.499	0.005*	0.556
	Stim*Electrode	0.408	0.537	0.039
	Drug	1.489	0.25	0.13
	Drug*Electrode	1.296	0.281	0.115
	Stim*Drug	0.079	0.784	0.008
	Stim*Drug*Electrode	0.943	0.354	0.086
Peak-to-peak amplitude: Hbo	Electrode	1.805	0.209	0.153
	Stim	15.061	0.003*	0.601
	Stim*Electrode	0.334	0.576	0.032
	Drug	1.784	0.211	0.151
	Drug*Electrode	1.06	0.327	0.096
	Stim*Drug	0.114	0.743	0.011
	Stim*Drug*Electrode	1.253	0.289	0.111
Peak-to-peak amplitude: Hbr	Electrode	1.334	0.275	0.118
	Stim	19.48	0.001**	0.661
	Stim*Electrode	0.163	0.695	0.016
	Drug	2.181	0.171	0.179
	Drug*Electrode	0.749	0.407	0.07
	Stim*Drug	0.234	0.639	0.023
	Stim*Drug*Electrode	2.321	0.159	0.188

Table S4.7: Results of 2-way repeated measures ANOVA comparing haemodynamic responses (total haemoglobin: Hbt) in no inhibitor condition (n=8 mice, *p<0.05, **p<0.01, ***p<0.001), and simple effects tests (following Bonferroni correction for multiple comparisons, *p<0.025, **p<0.005, ***p<0.0005).

Variable	Factor	F(1,7)		
		F	p	η^2
Hbt response in initial minima period	Stim	106.469	0.000017***	0.938
	Timepoint	0.791	0.403	0.102
	Stim*Timepoint	7.450	0.029*	0.516
Peak Hbt response	Stim	2.895	0.133	0.293
	Timepoint	1.946	0.206	0.218
	Stim*Timepoint	1.133	0.322	0.139
Peak-to-peak amplitude: Hbt	Stim	14.348	0.007**	0.672
	Timepoint	1.866	0.214	0.21
	Stim*Timepoint	0.113	0.747	0.016
Simple effects tests (Hbt response in initial minima period)			p	
Whisker stimulation	'Pre' vs 'Post'		0.183	
Optogenetic stimulation	'Pre' vs 'Post'		0.074	

Table S4.8: Effect of sex on haemodynamic response (total haemoglobin, Hbt) to nNOS IN activation or whisker stimulation, before and after LNAME injection. (n = 12 mice).

Parameter	Group	Male n=6 [mean ± s.d.]	Female n=6 [mean ± s.d.]	Independent samples t-test
Hbt initial minima	Pre-LNAME optogenetic stimulation	0.988 ± 0.008	0.987 ± 0.003	t(6.786) = 0.274, p = 0.792
	Post-LNAME optogenetic stimulation	0.959 ± 0.028	0.966 ± 0.011	t(6.417) = -0.578, p = 0.583
	Post-LNAME whisker stimulation	1.001 ± 0.002	0.999 ± 0.006	t(10) = 0.799, p = 0.221
Hbt peak	Pre-LNAME optogenetic stimulation	1.038 ± 0.017	1.034 ± 0.032	t(10) = 0.242, p = 0.814
	Pre-LNAME whisker stimulation	1.027 ± 0.016	1.023 ± 0.006	t(10) = 0.596, p = 0.564
	Post-LNAME whisker stimulation	1.038 ± 0.025	1.026 ± 0.011	t(6.775) = 1.080, p = 0.317
Parameter	Group	Male n=6 Median	Female n=6 Median	Mann-Whitney U test
Hbt initial minima	Pre-LNAME whisker stimulation	0.999	0.996	U = 9, z = -1.441, p = 0.150
Hbt peak	Post-LNAME optogenetic stimulation	1.010	1.014	U = 24, z = 0.961, p = 0.337

Table S4.9: Results of 2-way repeated measures ANOVA for stimulation-evoked multi-unit activity (MUA) in absence and presence of LNAME (n=4 mice).

Variable	Factor	F(1,3)		
		F	p	η^2
MUA Peak	Stim	5.361	0.104	0.641
	Drug	0.032	0.869	0.011
	Drug*Stim	0.245	0.655	0.075
Mean MUA	Stim	3.865	0.144	0.563
	Drug	0.003	0.958	0.001
	Drug*Stim	0.007	0.939	0.002

Table S4.10: Effect of LNAME and HET0016 on haemodynamic response – Initial minima: 2-way repeated measures ANOVA results (n=6 mice, *p<0.05, **p<0.01, ***p<0.001), and simple effects tests (following Bonferroni correction for multiple comparisons, *p<0.025, **p<0.005, ***p<0.0005). Hbt: total haemoglobin.

Variable	Factor	F(1,5)		
		F	p	η^2
Hbt response in initial minima period	Stim	7.549	0.04*	0.602
	Inhibitor	2.697	0.161	0.350
	Stim*Inhibitor	18.809	0.007**	0.790
Simple effects tests				
Whisker stimulation	'Pre' vs 'Post'		0.785	
Optogenetic stimulation	'Pre' vs 'Post'		0.050	

Table S4.11: Effect of LNAME and HET0016 on haemodynamic response – Peak: 2-way repeated measures ANOVA results (n=6 mice, *p<0.05, **p<0.01, ***p<0.001), and simple effects tests (following Bonferroni correction for multiple comparisons, *p<0.025, **p<0.005, ***p<0.0005). Hbt: total haemoglobin.

Variable	Factor	F(1,5)		
		F	p	η^2
Peak Hbt response	Stim	2.776	0.157	0.357
	Drug	0.548	0.492	0.099
	Stim*Drug	23.137	0.005**	0.822
Simple effects tests			p	
Whisker stimulation	'Pre' vs 'Post'		0.013*	
Optogenetic stimulation	'Pre' vs 'Post'		0.052	

Table S4.12: Effect of HET0016, results of 2-way repeated measures ANOVA comparing haemodynamic responses (n=5 mice), *p<0.05, **p<0.01, ***p<0.001, and simple effects tests (following Bonferroni correction for multiple comparisons, *p<0.025, **p<0.005, ***p<0.0005). Hbt: total haemoglobin.

Variable	Factor	F(1,4)		
		F	p	η^2
Hbt response in initial minima period	Stim	4.220	0.109	0.513
	Drug	3.336	0.142	0.455
	Stim*Drug	28.469	0.006**	0.877
Peak Hbt response	Stim	30.061	0.005**	0.883
	Drug	0.225	0.660	0.053
	Stim*Drug	5.911	0.072	0.596
Hbt minima: Simple effects tests			p	
Optogenetic stimulation	'Pre' vs 'Post'		0.043	
Whisker stimulation	'Pre' vs 'Post'		0.587	

Table S4.13: Descriptive statistics of power in low frequency arteriole oscillations (Area under curve (AUC), 0.09-0.11Hz).

Variable		Mean	SEM	n (mice)
AUC (0.09-0.11Hz) LNAME	Pre	2.42	0.24	12
	Post	9.80	1.62	
AUC (0.09-0.11Hz) No Inhibitor	Pre	2.70	0.35	8
	Post	3.82	0.54	

Table S4.14: Statistical analysis of power in low frequency arteriole oscillations: 2 way mixed ANOVA (*p<0.05, **p<0.01, ***p<0.001) and simple effects tests (following Bonferroni correction for multiple comparisons, *p<0.0125, **p<0.0025, ***p<0.00025). AUC: Area under curve.

Variable	Factor	F(1,18)		
		F	p	η2
AUC (0.09-0.11Hz)	Time	14.265	0.001**	0.442
	Drug	8.948	0.008**	0.332
	Drug*Time	7.765	0.012*	0.301
Simple effects tests			p	
LNAME	Post vs Pre		0.000062***	
No Inhibitor	Post vs Pre		0.531	
Pre timepoint	LNAME vs No Inhibitor		0.497	
Post timepoint	LNAME vs No Inhibitor		0.009*	

Chapter 5: Discussion

5.1 Abstract

Through the studies detailed in this PhD I aimed to uncover the roles of two specific subtypes of interneuron in neurovascular coupling, using two-dimensional optical imaging spectroscopy (2D-OIS), optogenetics and electrophysiology. I also investigated the role NO plays in both nNOS interneuron-driven and sensory stimulation-driven neurovascular coupling. In this final chapter, I will bring together the main findings of these studies and discuss their implications within the field of neurovascular research.

5.2 The Role of Cortical Interneurons in Neurovascular Coupling

In this thesis, I have demonstrated that optogenetically activating nNOS and SST INs leads to large, robust, localised increases in blood volume and saturation. This finding shows that the activity of interneurons can dynamically drive local, cerebral haemodynamics, supporting the idea that they could play a role in linking neural activity to vascular responses in neurovascular coupling.

5.2.1 SST Interneurons

Optogenetically activating SST INs causes a localised increase in cerebral blood volume. This finding is supported by other optogenetic studies in the field (Krawchuk et al., 2020; Vo et al., 2025). But these data are in contrast with slice studies, where activation of SSTs was shown to induce vasoconstriction, and thus would lead to a reduction in CBF (Cauli et al., 2004; Mohamed et al., 2024). There are many potential reasons for this difference in findings. For instance, in these studies, they look at the activity of individual SST INs on singular blood vessels in *ex vivo* brain slices, whereas I investigated a much larger population of both INs and vessels in the cortex. As the SST IN population is very diverse in its expression of neurotransmitters, it could be that when this larger population is activated, there is a greater variety of transmitters released, leading to this difference in response. An example of this is that it is estimated that up to 40% of SST-INs co-express nNOS (Yavorska and Wehr., 2016), so when the cortex is activated in the SST mice, there will not only be a release of SST but also of NO, which is a potent vasodilator, causing this localised increase in blood volume. To explore the cause of the localised increase in blood volume in response to SST IN activation, in future studies, one could use a pharmaceutical agent to block the neurotransmitters that SST INs are known to co-transmit and then optogenetically activate the SST INs and measure the haemodynamic response. For example, one could use L-NAME to block NOS activity (as was done in the fourth chapter of this thesis), and if a reduction or total blockade of the

increase in blood volume with photoactivation of SST INs is observed, then we can assume that NO release from SST INs is causing the positive haemodynamic responses. Another, perhaps more elegant, way of investigating this would be to cross the SST-ChR2 strain of mice with one expressing the promoter to selectively express halorhodopsin in nNOS-expressing interneurons alongside the ChR2 in the SST INs. As halorhodopsin suppresses the activity of the cells it is expressed in when yellow light is shone upon it, this mouse line would allow for precise spatial and temporal control of activation of SST INs and suppression of nNOS INs. Hence, by shining a blue and yellow light simultaneously on the cortex of these mice while measuring haemodynamic activity, it would be possible to parse out the differing contributions of these cell types to the total SST IN haemodynamic response. Another potential reason for the difference in results could be related to the use of different stimulation paradigms. Mohamed et al. (2024) observed, in *ex vivo* brain slices, that SST INs can elicit vasoconstrictions or vasodilations, dependent on the frequency of activation; showing that low-frequency (2Hz) optostimulation of SST INs triggers vasodilation and high-frequency (20Hz) induces vasoconstriction. While I performed a small number of experiments recording the haemodynamic responses to different frequencies of light stimulation, future studies could look at this in a full set of experiments, doing a full sweep of frequencies, to uncover whether SST INs differ in their activity on the vasculature *in vivo*.

When the SST INs were stimulated for a longer duration, 16 seconds, in some of the experiments, a large increase in blood volume and saturation was observed in the central region, after cessation of the stimulation. Given the delayed nature of this response, after the optogenetic stimulation had finished, it is unlikely to be caused by any direct action of the SST INs on the vessels. Instead, this positive, post-stimulus haemodynamic response is more likely to be caused by the activation of a secondary pathway. As the response is large and slow, a potential candidate for this response could be astrocytes, which can work slower to enact haemodynamic changes (Howarth, 2014). It has been shown that SST INs can induce Ca^{2+} elevations in astrocytes through SST receptors on astrocyte processes (Mariotti et al., 2018; Henriques et al., 2022; Vo et al., 2025). Interestingly, in these studies, the Ca^{2+} elevations were found to be larger and more robust with sustained SST IN activation, potentially explaining why this post-stimulus haemodynamic response is observed after the 16 second stimulation but not the 2 second stimulation. As Ca^{2+} elevations in astrocytes are known to cause slow, positive haemodynamic responses (Institoris et al., 2022), it could be that the SST IN stimulation leads to the release of SST onto the astrocytic process, activating the astrocytes. The importance of this potential alternate pathway for NVC, with its slow, prolonged haemodynamic response, is that it could provide an extended, increased blood supply to a metabolically expensive cortical area- be it through a high density of neural activity or due to

protracted activation. If this were the case, then it appears the SST INs could play a key role in controlling the haemodynamic innervation to these areas.

The 16 second SST IN stimulation experiments in which the positive, post-stimulus haemodynamic response (discussed in the previous paragraph) occurred, also displayed a negative surround haemodynamic response around the central activated region. A possible cause for this negative surround response could be lateral inhibition- where the projections from activated SST INs cause inhibition in adjacent cortical areas, leading to a reduction in blood flow and thus a negative neural and haemodynamic response around the activated region. Lateral inhibition has been previously shown to occur from SST INs (Karani et al., 2016). The importance of understanding this response is that it could contribute to the negative BOLD response seen in fMRI imaging, the cause of which is yet to be elucidated. In these studies, a decrease in deep-layer MUA activity is shown to correlate with the negative BOLD response (Boorman, 2010), as we see with the experiments showing the negative surround (Figure 3.5B). The negative BOLD response could thus be caused by the activity of SST INs, under certain conditions. The result of this response is a more precise allocation of blood to the active area, with less blood perfusing the surrounding regions, so it could again be showing a 'top-down control' role of SST INs diverting the cortex's blood resources to areas which require it most. If this is indeed one of the roles of SST INs, then it could be taken advantage of for medical use in conditions such as stroke or traumatic brain injury (Girouard and Iadecola, 2006; Whitehead et al., 2024), where a lack of blood perfusion in specific areas causes or exacerbates damage to the brain. By stimulating SST INs in the areas affected by these conditions, blood could be redirected to these regions, limiting the damage.

5.2.2 nNOS Interneurons

The finding that direct activation of nNOS INs drives a positive, localised haemodynamic response without evoking a detectable neural correlate (Figure 3.3) sheds light on the potential role of nNOS INs within NVC. This potential role is in detecting neural activity through projections stretching through the depth of the cortex, and translating it into localised CBF increases, through the release of the potent vasodilator NO. This potential pathway of nNOS-IN mediated NVC is supported in the field, with others also finding that nNOS-IN activation causes robust vasodilations (Krawchuk et al., 2020; Echagarruga et al., 2020; Chow et al., 2020), and ablation of nNOS INs causes decreases in the haemodynamic response to sensory stimulation (Turner et al., 2025). Further support comes from a 2-photon study using awake mice with GCaMP expressed in nNOS INs, in which nNOS INs were shown to exhibit diverse patterns of activity during whisker puff-induced local arteriolar dilations (Ahn et al., 2023). The calcium transients in these active nNOS INs were shown to correlate with various parts of the dilation, with some active immediately prior to the dilation, and others activated gradually after

the dilation. This diversity in activity highlights the complex dynamics by which nNOS INs contribute to NVC. The proximity of nNOS INs to microvessels in the brain adds to this theory of nNOS mediated NVC, allowing for the rapid diffusion of NO to precisely modulate blood flow in highly localised regions, which would allow for the spatial and temporal specificity we see in NVC responses (Perrenoud et al., 2012).

Given the support for this potential pathway and the results of the optogenetic activation in Chapter 3 (Figures 3.3 and 3.5), it was surprising that we didn't see a reduction in the haemodynamic response to whisker stimulation when NO was blocked with L-NAME (Figure 4.1). This calls into question the involvement of nNOS INs in somatosensory-NVC, especially given that the NO blockade was found to decrease the initial vasodilation caused by direct activation of nNOS INs (Figure 4.1). While this finding contradicts the idea of nNOS INs directly linking neural activity and haemodynamic responses in NVC, through the release of NO, it doesn't rule out the possibility of them playing a role in the response; this role could just be more nuanced. This pathway could instead be involved in different kinds of NVC, originating from different sources of neural activity. For example, it has been shown that blocking NO does have an effect on the haemodynamic response elicited by locomotion (Echagarruga et al., 2020). There is already precedent for the idea that different functional brain regions employ differing pathways for NVC (Rungta et al., 2018; Shaw et al., 2022), so it could be that the nNOS IN pathway is involved in NVC in regions other than the whisker barrel cortex. These regions could potentially be in subcortical structures, such as the hippocampus and striatum, where nNOS INs have been shown to be expressed (Christenson Wick et al., 2019). To test this idea, a future study could look at screening various stimulation types (i.e. motor, visual, behavioural…etc) and assess whether NO inhibition affects the haemodynamic response to these stimulations, hopefully leading to a better idea of which brain regions incorporate nNOS INs into NVC.

There are other potential explanations for the finding that the initiation of the sensory-evoked NVC response was largely unaltered during NOS inhibition. During the experiments in Chapter 4, only short (2 second) stimulations were assessed, so it could be that nNOS INs are only recruited into sensory evoked-NVC during more prolonged periods of neural activity. There is precedent for INs behaving this way in NVC, for example SST INs (Mariotti et al., 2018; Krogsgaard et al., 2023; Vo et al., 2025). A future study could test this theory using a range of stimulation durations and quantifying the effect of NO inhibition on NVC.

As discussed in the introduction chapter of this thesis, multiple pathways and cell types have been shown to be involved in driving the NVC response. So, it is likely that rather than any one of these being the single pathway driving NVC, they work in tandem to ensure the precise

direction of blood flow to areas of neural activity. If this is the case, then it could be that these multiple pathways have evolved to act as redundancies for each other, ensuring NVC still occurs even when one or more of the other pathways isn't functioning, or is being recruited for a different purpose. In this situation, it could be that, by inhibiting the nNOS IN pathway, the haemodynamic response wasn't observed to be altered because the other pathways were still able to translate the whisker stimulation to a localised haemodynamic response. As NVC is such an important mechanism within the brain, it provides a strong evolutionary incentive for these redundancies to exist, and looking at past pharmacology studies within the field would explain why it takes numerous inhibitory agents, used in tandem, to lower the NVC response to 70% (Hosford and Gourine, 2019). This suggests that nNOS INs could have a role in driving NVC through the release of NO, but that mechanism is protected by redundancies.

5.2.2.1 NO does drive the nNOS-IN haemodynamic response

The importance of the release of NO by nNOS INs to drive dilation in proximal vessels has been established previously (Iadecola et al., 1993; Kitaura et al., 2007; Stefanovic et al., 2007). However, the findings in this thesis reveal a more complex role of NO in this mechanism than previously hypothesised. Inhibition of NO synthesis with L-NAME unveiled a significant initial vasoconstriction that was otherwise counteracted by NO's vasodilatory action (Figure 4.1). This underlying constrictive force was attenuated when both NO and 20-HETE production were blocked, identifying 20-HETE as a key mediator of this effect. This suggests a pathway for nNOS-IN-driven dilations, whereby in usual conditions NO not only causes dilation through the cGMP pathway, but also by blocking the constriction of 20-HETE.

5.3 nNOS Interneurons in Disease

The finding that nNOS INs are capable of driving localised haemodynamics, albeit in a potentially more nuanced manner than through a direct link in NVC, could help further understanding of how NVC becomes dysfunctional in disease. It has been shown that nNOS INs are both lost and driven to dysfunction in AD (Miettinen et al., 1993; Thorns et al., 1998; Necchi et al., 2002; Duchemin et al., 2012; Choi et al., 2018). As this thesis shows that the activity of nNOS INs drives cerebral haemodynamics, it follows that this reduction in nNOS INs could be contributing to the breakdown of NVC in AD. One could explore this idea by assessing the correlation of the decrease in nNOS INs, using histochemical assays at different time points in disease progression, with the breakdown of NVC. If this were found to be strongly correlated, then that suggests that targeting preservation of nNOS IN numbers and

function could be a suitable therapeutic target for AD research. Future studies could investigate whether preserving nNOS INs could limit the breakdown of NVC in AD and improve the prognosis of the disease.

5.3.1 Targeting nNOS INs for Treatment

The ability of nNOS INs to drive localised increases in blood volume in the brain without affecting neural activity could be utilised for therapeutic purposes. In AD, CBF is reduced (Hays et al., 2016), which leads to less oxygenated blood and glucose supplying the brain, reducing its ability to clear amyloid-beta and tau, reducing neural activity and starving cells in the brain of oxygen, eventually causing neural death (Kisler et al., 2017). Using a treatment strategy that activates nNOS INs in the brain would lead to increased perfusion of blood, potentially alleviating these problems and slowing down or even stopping the progression of the disease. Importantly, this treatment strategy, according to the findings in this thesis (Figure 3.4), wouldn't cause large, global changes in neural activity, meaning the metabolic load in the brain wouldn't be significantly increased, making this treatment more effective for patients' brains already experiencing metabolic stress due to NVC breakdown. This treatment strategy could be used across the whole brain or even be more targeted to specific areas that are shown, by using BOLD-fMRI, to be more affected by the CBF reduction. The form of this treatment need not be optogenetic activation of the nNOS-INs (this would be very difficult to do in humans), but could either be through pharmacological activation of the nNOS- INs or even by using designer receptors exclusively activated by designer drugs (DREADDs), which allow for targeted activation of specific cell types and have the potential to be translational to humans (Urban and Roth, 2015). Whichever form this potential treatment was to take, a future study could test its efficacy by crossing nNOS optogenetic mice with an AD model mouse strain, then carrying out a treatment regimen of light activation of nNOS-INs on these mice and assessing whether the treatment works to reduce the pathology.

5.6 Conclusion

In conclusion, the work presented in this thesis provides a refined and more nuanced understanding of the roles of SST and nNOS INs in NVC than had previously been observed. By using *in vivo* optogenetics, this research has demonstrated that activating SST INs drives a net increase in local blood volume, a finding that contrasts with their previously established vasoconstrictive role and points towards complex interactions involving co-released vasodilators or secondary pathways. Furthermore, this thesis challenges the prevailing model of the nNOS/NO pathway as a primary driver of sensory-evoked NVC. While I showed direct

activation of nNOS INs elicits an NO-dependent vasodilation that opposes a 20-HETE-mediated constriction, this mechanism appears non-essential for the initial response to whisker stimulation. Taken together, these findings show that IN control of CBF is highly complex, context-dependent and protected by significant redundancy. This work underscores that a complete understanding of NVC will require elucidating the dynamic interplay between multiple, parallel signalling pathways that ensure blood flow in the brain is robustly maintained.

5.7 References

Ahn, S. J., Anfray, A., Anrather, J., & Iadecola, C. (2023). Calcium transients in nNOS neurons underlie distinct phases of the neurovascular response to barrel cortex activation in awake mice. *Journal of Cerebral Blood Flow & Metabolism, 43*(10), 1633–1647.

Boorman, L., Kennerley, A. J., Johnston, D., Jones, M., Zheng, Y., Redgrave, P., & Berwick, J. (2010). Negative Blood Oxygen Level Dependence in the Rat:A Model for Investigating the Role of Suppression in Neurovascular Coupling. *Journal of Neuroscience*, 30(12), 4285–4294.

Cauli, B., Tong, X.-K., Rancillac, A., Serluca, N., Lambolez, B., Rossier, J., & Hamel, E. (2004). Cortical GABA Interneurons in Neurovascular Coupling: Relays for Subcortical Vasoactive Pathways. *The Journal of Neuroscience, 24*(41), 8940–8949.

Christenson Wick, Z., Tetzlaff, M. R., & Krook-Magnuson, E. (2019). Novel long-range inhibitory nNOS-expressing hippocampal cells. *eLife, 8*, e46816.

Choi, S., Won, J.-S., Carroll, S. L., Annamalai, B., Singh, I., & Singh, A. K. (2018). Pathology of nNOS expressing GABAergic neurons in mouse model of Alzheimer's disease. *Neuroscience, 384,* 41–53.

Chow, B. W., Nuñez, V., Kaplan, L., Granger, A. J., Bistrong, K., Zucker, H. L., Kumar, P., Sabatini, B. L., & Gu, C. (2020). Caveolae in CNS arterioles mediate neurovascular coupling. *Nature, 579*(7797), 106–110.

Duchemin, S., Boily, M., Sadekova, N., & Girouard, H. (2012). The complex contribution of NOS interneurons in the physiology of cerebrovascular regulation. *Frontiers in Neural Circuits, 6*, 51.

Echagarruga, C. T., Gheres, K. W., Norwood, J. N., & Drew, P. J. (n.d.). nNOS-expressing interneurons control basal and behaviorally evoked arterial dilation in somatosensory cortex of mice. *eLife, 9*, e60533.

Girouard, H., & Iadecola, C. (2006). Neurovascular coupling in the normal brain and in hypertension, stroke, and Alzheimer disease. *Journal of Applied Physiology*, *100*(1), 328–335.

Hays, C. C., Zlatar, Z. Z., & Wierenga, C. E. (2016). The utility of cerebral blood flow as a biomarker of preclinical Alzheimer's Disease. *Cellular and Molecular Neurobiology*, 36(2), 167-179.

Henriques, V. J., Chiavegato, A., Carmignoto, G., & Gómez-Gonzalo, M. (2022). Astrocytes Modulate Somatostatin Interneuron Signaling in the Visual Cortex. *Cells, 11*(9), 1400.

Hosford, P. S., & Gourine, A. V. (2019). What is the key mediator of the neurovascular coupling response? *Neuroscience and Biobehavioral Reviews, 96*, 174–181.

Howarth, C. (2014). The contribution of astrocytes to the regulation of cerebral blood flow. *Frontiers in Neuroscience*, *8*, 103.

Iadecola, C., Zhang, F., & Xu, X. (1993). Role of nitric oxide synthase-containing vascular nerves in cerebrovasodilation elicited from cerebellum. *The American Journal of Physiology, 264*(4 Pt 2), R738-746.

Institoris, A., Vandal, M., Peringod, G., Catalano, C., Tran, C. H., Yu, X., Visser, F., Breiteneder, C., Molina, L., Khakh, B. S., Nguyen, M. D., Thompson, R. J., & Gordon, G. R. (2022). Astrocytes amplify neurovascular coupling to sustained activation of neocortex in awake mice*. Nature Communications, 13*(1), 7872

Karnani, M. M., Jackson, J., Ayzenshtat, I., Tucciarone, J., Manoocheri, K., Snider, W. G., & Yuste, R. (2016). Cooperative networks of cortical inhibitory interneurons. *Neuron*, *91*(5), 1104–1119.

Kisler, K., Nelson, A. R., Montagne, A., & Zlokovic, B. V. (2017). Cerebral blood flow regulation and neurovascular dysfunction in Alzheimer's disease. *Nature Reviews Neuroscience*, *18*(7), 419–434.

Kitaura, H., Uozumi, N., Tohmi, M., Yamazaki, M., Sakimura, K., Kudoh, M., Shimizu, T., & Shibuki, K. (2007). Roles of nitric oxide as a vasodilator in neurovascular coupling of mouse somatosensory cortex. *Neuroscience Research, 59*(2), 160–171.

Krawchuk, M. B., Ruff, C. F., Yang, X., Ross, S. E., & Vazquez, A. L. (2020). Optogenetic assessment of VIP, PV, SOM and NOS inhibitory neuron activity and cerebral blood flow regulation in mouse somato-sensory cortex. *Journal of Cerebral Blood Flow & Metabolism, 40*(7), 1427–1440.

Krogsgaard, A. R., Lønstrup, M., & Lauritzen, M. (2023). Somatostatin-expressing interneurons are unlikely drivers of functional hyperemia in neocortex. *Cerebral Cortex*, *33*(6), 2824–2838.

Mariotti, L., Losi, G., Sessolo, M., Melone, M., Chiavegato, A., & Carmignoto, G. (2018). The inhibitory tone of somatostatin-positive interneurons modulates sensory-evoked responses in the primary somatosensory cortex. *Cerebral Cortex*, *28*(4), 1461–1476.

Miettinen, R., Sirviö, J., Riekkinen, P., Laakso, M. P., Riekkinen, M., & Riekkinen, P. (1993). Neocortical, hippocampal and septal parvalbumin- and somatostatin-containing neurons in young and aged rats: Correlation with passive avoidance and water maze performance. *Neuroscience, 53*(2), 367–378.

Mohamed, B., O'Reilly, J., Picaud, S., Gac, B. L., Belzic, E., Castro, L. R. V., Soula, H., Dusart, I., Li, D., & Cauli, B. (2024). Bidirectional control of neurovascular coupling by cortical somatostatin interneurons *(p. 2024.11.06.622247). bioRxiv.*

Necchi, D., Virgili, M., Monti, B., Contestabile, A., & Scherini, E. (2002). Regional alterations of the NO/NOS system in the aging brain: A biochemical, histochemical and immunochemical study in the rat. *Brain Research, 933*(1), 31–41.

Perrenoud, Q., Geoffroy, H., Gauthier, B., Rancillac, A., Alfonsi, F., Kessaris, N., Rossier, J., Vitalis, T., & Gallopin, T. (2012). Characterization of Type I and Type II nNOS-Expressing Interneurons in the Barrel Cortex of Mouse. *Frontiers in Neural Circuits, 6*, 36.

Rungta, R. L., Chaigneau, E., Osmanski, B.-F., & Charpak, S. (2018). Vascular Compartmentalization of Functional Hyperemia from the Synapse to the Pia. *Neuron, 99*(2), 362-375.

Shaw, K., Howarth, C., & Sharp, P. S. (2022). A finite element model of neurovascular coupling in the olfactory bulb. *Frontiers in Neuroscience*, *16*, 888462.

Shaw, K., Boyd, K., Anderle, S., Hammond-Haley, M., Amin, D., Bonnar, O., & Hall, C. N. (2022). Gradual Not Sudden Change: Multiple Sites of Functional Transition Across the Microvascular Bed. *Frontiers in Aging Neuroscience, 13*, 779823.

Stefanovic, B., Schwindt, W., Hoehn, M., & Silva, A. C. (2007). Functional Uncoupling of Hemodynamic from Neuronal Response by Inhibition of Neuronal Nitric Oxide Synthase. *Journal of Cerebral Blood Flow & Metabolism, 27*(4), 741–754.

Thorns, V., Hansen, L., & Masliah, E. (1998). nNOS expressing neurons in the entorhinal cortex and hippocampus are affected in patients with Alzheimer's disease. *Experimental Neurology, 150*(1), 14–20.

Turner, K., Brockway, D., Hossain, M. S., Griffith, K., Greenawalt, D., Zhang, Q., Gheres, K., Crowley, N., & Drew, P. J. (2025). Type-I nNOS neurons orchestrate cortical neural activity and vasomotion. *eLife, 14*, RP105649.

Urban, D. J., & Roth, B. L. (2015). DREADDs (designer receptors exclusively activated by designer drugs): Chemogenetic tools with therapeutic utility. *Annual Review of Pharmacology and Toxicology, 55,* 399–417.

Vo, T. T., Jung, W. B., Jin, T., Im, G. H., Lee, S., & Kim, S.-G. (2025). Somatostatin-expressing interneurons induce early NO-driven and late specific astrocyte-mediated vasodilation. *Nature Communications, 16*(1), 6606.

Whitehead, B., Corbin, D., Meadows, E., Zhang, N., Hollander, J. M., Karelina, K., & Weil, Z. M. (2024). Cerebral hypoperfusion exacerbates vascular dysfunction after traumatic brain injury. *Experimental Neurology, 380,* 114907.

Yavorska, I., & Wehr, M. (2016). Somatostatin-Expressing Inhibitory Interneurons in Cortical Circuits. *Frontiers in Neural Circuits, 10*, 76.